Isolation of HepG2-derived extracellular vesicles spiked in human blood serum using magnetic beads and click chemistry.

Lieke Geraets

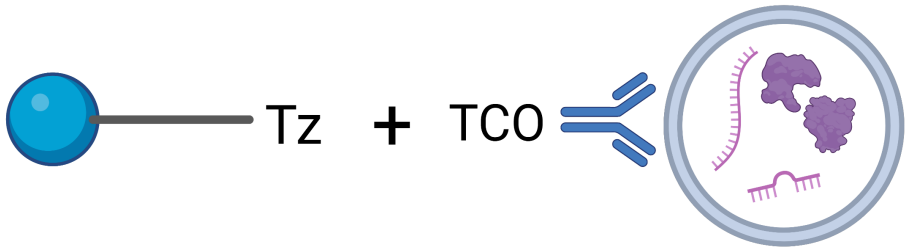

Research group
MCBP

Date
4-7-2023

Under supervision of
R. Bansal PhD and drs. R.S. Booijink MSc

External member
prof.dr.ir. P. Jonkheijm

1 Samenvatting

Hepatocellulair carcinoom (HCC) levert een grote bijdrage aan sterfte cijfers gerelateerd aan kanker. De grootste uitdaging rondom HCC binnen de westerse wereld is de vaak dat de diagnose pas in een laat stadium wordt gesteld. Volgens onderzoekers kan een diagnose in een vroeg stadium van de ziekte overlevingskansen van patienten verbeteren. Er is dus een vernieuwende diagnose- en screening tool nodig.

Extracellulaire vesicles (EVs) bestaan uit een lipide dubbellaag en zijn verdeeld in apoptotische lichamen (1-5 μm), microblaasjes (100-1000 nm) en exosomen (30-120 nm). Deze EVs vertegenwoordigen de cellen waar ze vandaan komen en vertegenwoordigen het stadium van bijvoorbeeld HCC. EVs zijn toegankelijk en representatief voor het weefsel vergeleken met huidige diagnose technieken. Toch blijft het lastig om EVs te isoleren uit een biopt door verontreinigingen in de samples.

Het doel van dit onderzoek is om the immunoisolatie van HepG2-EVs uit verrijkte bloed serum samples te testen aan de hand van een klikchemie reactie tussen magnetische deeltjes en antilichamen. Dit wordt gedaan met de stoffen tetrazine (Tz) en trans-cycloocteen (TCO).

De aanwezigheid van het epitheel cell adhesie molecuul (EpCAM) is bevestigd op het membraan van de cellen en de EVs door middel van fluorescentie microscopie.

Na het optimaliseren van the conjugatie methode van het EpCAM antilichaam aan de TCO en de magnetische deeltjes aan orthopyridyl sulfide (OPSS) en Tz, is 19,9% van de magnetische deeltjes positief geschat voor een EV. Hierna is het systeem gestest op humaan bloed serum. PBS en serum samples zijn verrijkt met Calceine-AM gekleurde HepG2-EVs. Meerdere incubatie protocollen zijn getest.

Aan de hand van flowcytometrie is de populatie van de magnetische deeltjes geschat die positief was voor een EV. Voor het meest efficiente protocol was dit 21,3%, 9,5% en 5.4% voor sample met EV-verrijkt PBS, 50% serum in PBS en 100% serum.

Daarnaast is de hoeveelheid vrije thiol groepen gekwantificeerd met een ellman's experiment. Magnetische deeltjes hebben ongeveer 0,400-0,651 mmol vrije thiol groepen per 100 μg deeltjes. Na de conjugatie aan OPSS(-Tz), is ongeveer 20,29-25,27% van de thiol groupen aan OPSS gebonden.

Kortom, de verontreinigingen in het serum veroorzaken een verlaagde efficientie van de isolatie van HepG2-EVs aan de hand van een klikchemie reactie. De efficientie van het systeem zal moeten worden verbeterd maar de immunoisolatie van de EVs uit bloed serum samples is een mogelijkheid die in de toekomst een snelle en veilige diagnostische- and screening marker kan vormen voor mogelijke HCC-patiënten in een vroeg stadium.

2 Abstract

Hepatocellular carcinoma (HCC) is a top contributor to cancer-related deaths. In the Western world, the biggest issue regarding this disease is the late stage at diagnosis. Research has shown how early diagnosis of HCC can improve survival chances, however, current surveillance techniques have proven to be inadequate for such an early stage. A new diagnostic and surveillance technique is therefore desired.

Extracellular vesicles (EVs) are lipid bilayers categorised into apoptotic bodies (1-5 μm), microvesicles (100-1000 nm) and exosomes (30-120 nm). These EVs represent the cells from which they are derived and they are representative of the stage of for instance HCC. EVs are more accessible and representative of the tissue than current diagnostic methods. However, it remains challenging to isolate EVs from biopsies, due to contaminants. Immuno-affinity-based isolation techniques can separate the targeted subpopulations of EVs from contaminants.

The aim of this research is to test the immuno-based isolation of HepG2-derived EVs from spiked serum samples using a click chemistry reaction between magnetic beads and antibodies. This is achieved by using a tetrazine (Tz) and trans-cyclooctene (TCO) reaction.

Epithelium cell adhesion molecule (EpCAM) was confirmed on the cell and EV surface using fluorescence microscopy.

After optimizing the method of conjugating the EpCAM antibody to TCO and magnetic beads to an orthopyridyl disulfide (OPSS) and Tz, 19.9% of the beads were estimated to be positive for an EV. Thereafter, the system was tested in human blood serum samples. HepG2-derived EVs were stained using Calcein-AM and spiked in PBS and serum samples. Multiple incubation protocols were tested.

Using flow cytometry, the population of magnetic beads that were positive for a Calcein-AM stained EV was estimated. For the most efficient protocol, this population was 21.3%, 9.5% and 5.4% for samples of EV-spiked PBS, 50% serum in PBS and 100% serum.

In addition, the amount of free thiol groups on the magnetic beads was quantified using an Ellman's assay. Empty beads were estimated to contain 0.400-0.651 mmol free thiol groups per 100 μg of beads. After conjugation to OPSS(-Tz), it was estimated that 20.29-25.27% of the thiol groups have bound to OPSS.

To conclude, the contaminants in serum cause a decreased capture efficiency of the click chemistry beads while capturing HepG2-derived EVs. Improvements will have to be made to increase the capture efficiency but the immuno-based isolation of EVs from blood serum samples holds a promising future as a quick, low-risk diagnostic and surveillance marker for the early-stage diagnosis of HCC in patients.

Contents

3 List of abbreviations

HCC Hepatocellular carcinoma
BCLC Barcelona Clinic Liver Cancer
AASLD American Association for the Study of Liver Diseases
HBV Hepatitis B virus
HCV Hepatitis C virus
NAFLD Non-alcoholic fatty liver disease
TACE Transarterial chemoembolization
TARE Transarterial radioembolization
RT Radiotherapy
ERK Extracellular signal-related kinase
LR Liver resection
LT Liver transplant
AFP Alpha fetoprotein
US Ultrasound
CT Computed tomography
MRI Magnetic resonance imaging
EV Extracellular vesicle
MVB Multivesicular body
sEV Small extracellular vesicle
HDL High-density lipoprotein
LDL Low-density lipoprotein
IDL Intermediate-density lipoprotein
VLDL Very low-density lipoprotein
Lp(a) Lipoprotein a
PCR Polymerase chain reaction
UC Ultracentrifugation
UF Ultrafiltration
TFF Tangential flow filtration
SEC Size exclusion chromatography
DLS Dynamic light scattering
TCO trans-cyclooctene
OPSS Orthopyridyl disulfide
Tz Tetrazine
iEDDA Inverse electron demand Diels-Alder cycloaddition
PEG Polyethylene glycol
ASGR1 Asianoglycoprotein receptor
EpCAM Epithelial cell adhesion molecule
CD9 Cluster of differentiation 9
FACS Fluorescence-activated cell sorting
FSC Forward scatter
SSC side scatter
DTNB 5,5-dithio-bis(2-nitrobenzioc acid), Ellman's reagent
TNB 2-nitro-5-thionbenzoat
DMEM Dulbecco's modified eagle medium
FBS Fetal bovine serum
DMSO Dimethyl sulfoxide
BSA Bovine serum albumin
TBS Tris-buffered saline
TBST Tris-buffered saline containing 0.1% Tween-20 detergent
DTT 1,4-dithiothreitol

4 Introduction

4.1 Hepatocellular carcinoma treatment, surveillance and diagnosis

Hepatocellular carcinoma (HCC) is a common type of cancer and a top 3 contributor to cancer-related deaths[1–3]. Diagnosis at an early stage is crucial for survival rate. Patients diagnosed at an early stage with a single tumour and no vascular invasion, have a 3-year disease-specific survival rate of 92.23%, whereas for patients with vascular invasion or multiple small (< 5cm) tumours, this decreases to 79% [4]. This shows that a diagnosis at a later stage in the disease is associated with a significantly higher risk of recurrence. However, the lack of specific symptoms makes HCC difficult to diagnose early [5]. According to estimations, the incidence of HCC is increasing rapidly and will continue to rise, partly due to unhealthy lifestyles [3].

The best system for staging HCC is the Barcelona Clinic Liver Cancer (BCLC) system, according to the American Association for the Study of Liver Diseases (AASLD) [6]. It claims to provide the best assessment of HCC score since it considers liver function and the disease's burden on the patient. The BCLC system is visualized in figure 1. As described in the figure, the early stages of the BCLC system include patients with tumours under 2 or 3 cm while still preserving their liver function. The more advanced and terminal stages include patients with tumours that have spread or invaded blood vessels or have metastasized while also having a deteriorating liver function [7].

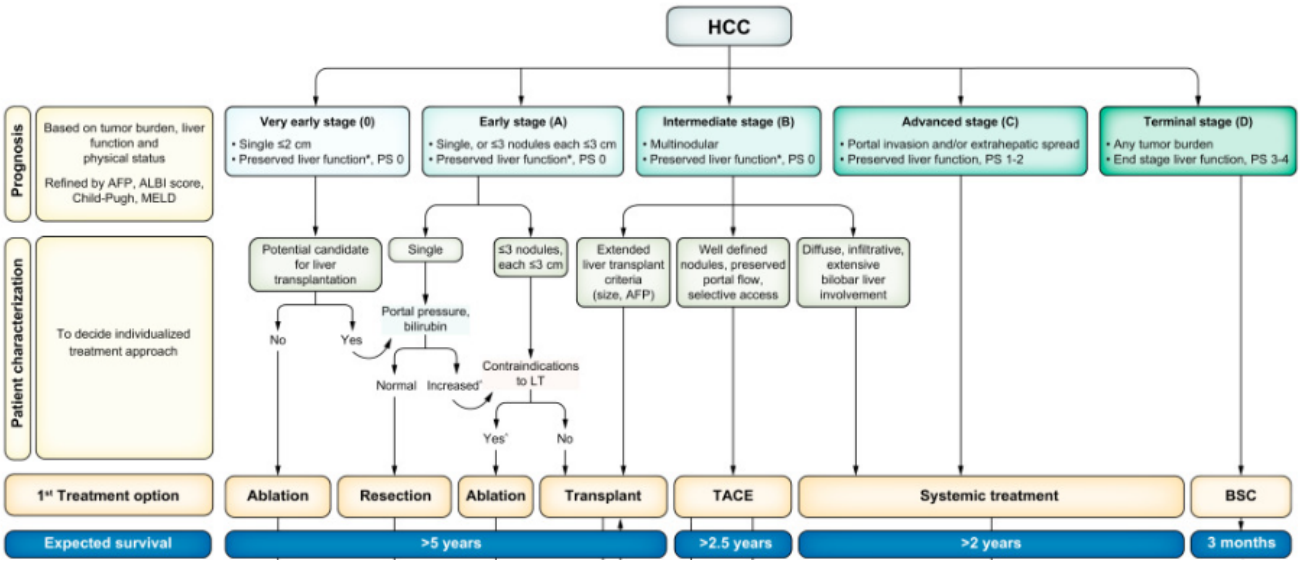

Figure 1: *Barcelona Clinic Liver Cancer (BCLC) staging system of HCC. [7]*

Risk factors for developing HCC include any factors that could lead to liver cirrhosis. These include Hepatitis B virus (HBV), Hepatitis C virus (HCV), alcohol consumption and nonalcoholic fatty liver disease (NAFLD). Due to rising numbers of obesity, it is expected that the numbers of HCC development due to NAFLD will rise as well [8].

Often, the aforementioned conditions are pro-inflammatory and can lead to fibrosis and cirrhosis. This leads to a change in the microenvironment that encourages hepatocytes to transform. Anti-apoptotic pathways are activated and immune surveillance is decreased. The increased proliferation of the hepatocytes and decreasing telomeres cause an increase in chromosomal instability and therefore a higher chance of development of a tumour [9]. These risk factors and causes of HCC are summarized in figure 2.

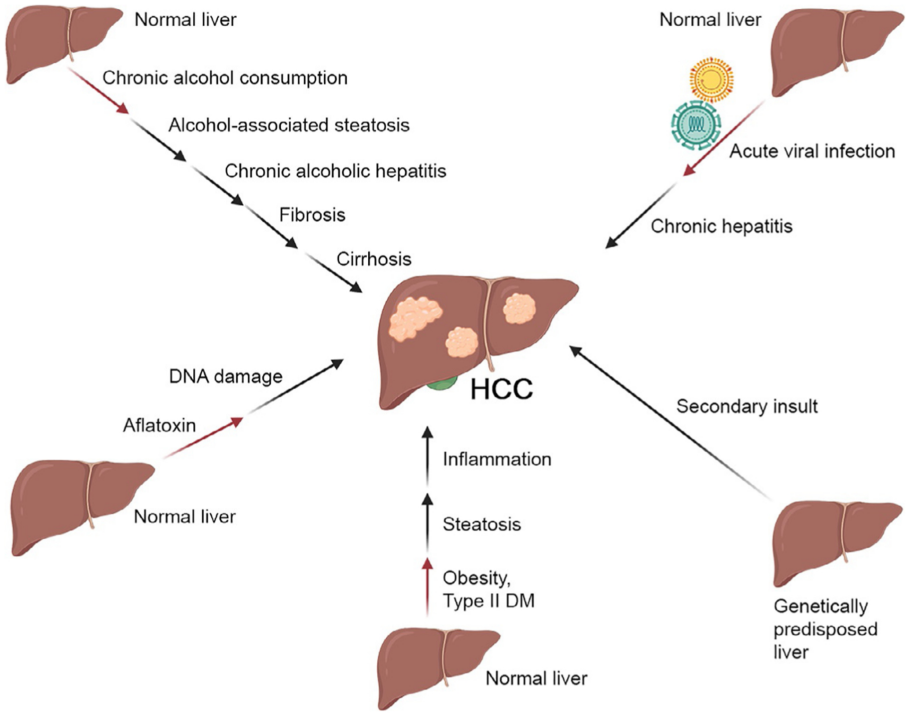

Figure 2: *Risk factors and causes of the development of hepatocellular cancer [10].*

Currently, HCC treatment consists of curative methods such as surgical resection, liver transplants and ablative techniques (e.g. thermal ablation)[11]. The risk of recurrence after liver resection is up to 70% within 5 years [12]. Although liver transplants are highly effective with a recurrence rate of only 11-18%, the allograft shortage and need for lifelong immunosuppression are limitations to this treatment option [13].

Noncurative treatments prolong survival by slowing tumour growth. Chemotherapies have little benefit for HCC patients due to their systemic toxicity and short survival benefits [11]. The standard of palliative care for patients with an intermediate stage of HCC is transarterial chemoembolization (TACE). This technique uses the cytotoxicity from therapeutic agents such as doxorubicin to induce tumour necrosis. However, TACE is associated with side effects, including post-embolization syndrome, fevers and nausea [11]. Another palliative therapy is transarterial radioembolization (TARE). Radioactive microspheres are injected to induce tumour necrosis. This therapy includes an angiogram and coil embolization to avoid damage to non-HCC tissue. Compared to TACE, TARE has shown equivalent survival rates but causes fewer side effects [11]. Patients with portal vein tumour invasion or metastases can undergo external beam radiation therapy (RT). This therapy has proven to alleviate pain from metastatic lesions [11]. For more advanced stages of HCC, sorafenib is also a treatment option. It is a multikinase inhibitor that targets several pathways including the RAF/MAPK/extra-cellular signal-related kinase (ERK) pathway. By inhibiting pathways like these, the drug obstructs the stimulation of cell growth, survival and angiogenesis. Compared to other molecular therapies such as sunitinib and brivanib, sorafenib has proven to be superior when comparing survival rates. Drugs that are currently being studied and have promising effects are ramucirumab and cabozantinib [11]. Survival rates of the discussed treatment options are found in table 1.

Table 1: *Survival rates of patients undergoing HCC treatments [11].*

Treatment	Stage (BCLC)	Survival rate
Liver resection (LR)	O, A	5 year survival rate: 62-94%
Liver transplant (LT)	O, A	5 year survival rate: 25-55%
Chemotherapy	C	8.1-11 months
Transarterial chemoembolization (TACE)	B	2 year survival rate: 63%
Transarterial radioembolization (TARE)	B	14 months vs. 8 months (control)
Radiation therapy (RT)	C	2 year survival rate: 21-69%
Sorafenib	C	10.7 months vs. 7.9 months(control)
Sunitinib	C	7.9 months
Brivanib	C	9.5 months
Ramucirumab	C	Equivalent to placebo
Cabozantinib	C	10.2 months vs. 8 months (control)

As discussed, early diagnosis and treatment of HCC are crucial for the survival chances of patients. Currently, surveillance techniques are used for patients with an increased risk of developing HCC. These consist of patients with cirrhosis and patients with chronic liver disease without cirrhosis [14]. Surveillance has proven to increase longevity by approximately 3 months for the incidence of HCC of 1.5%/year. Meaning, if 1.5% of the research population is diagnosed with HCC in 1 year, the surveillance can provide an extra 3 months of longevity. When the incidence in the researched population is higher, such as 6% per year, surveillance can increase longevity up to 9 months [15]. Surveillance techniques include the use of Alpha fetoprotein (AFP) and ultrasound (US). The optimal and recommended interval of surveillance ranges from 4 to 8 months [6].

As described by Marrero et al.[6], these surveillance methods are often classified as inadequate for diagnosing HCC in the early stages of the disease. Diagnosis using US is challenging due to the unclear distinction between benign and malignant lesions especially if they are small. In addition, patients with NASH are often obese which makes US measurements more difficult [16]. AFP is estimated to provide only a 25% positive predictive value for HCC [6]. Computed tomography (CT) and magnetic resonance imaging (MRI) techniques are not recommended for HCC surveillance due to their poor cost-effectiveness. However, studies do show that MRI is more effective than US [6]. A diagnosis can be made using for instance multiphase CT or multiphase MRI. Biopsies are often used for inconclusive nodules that are found using imaging techniques. However, risks include bleeding, tumour seeding, and a failure of obtaining representative tissue [6]. AFP is considered the most useful biomarker for HCC but is still positive in only 60-80% of cases. Also, false positives are not uncommon. Among others, non-malignant conditions can also cause elevated AFP levels [5]. Since these surveillance and diagnostic methods are inadequate, there is a need for a new method to diagnose HCC earlier than is currently possible, to increase survival rates among patients.

The discussed surveillance techniques are summarized in table 2 including their approximate sensitivity and specificity.

Table 2: *Overview of HCC surveillance techniques [6, 17–19].*

Surveillance technique	Considered positive for HCC	Advantages	Limitations	Sensitivity	Specificity
Alfa fetoprotein (AFP)	Blood level >20ng/mL	- Most used biomarker for HCC. - Non-invasive blood biopsy.	- Other liver diseases also have raised AFP levels. - Only 25% positive predictive value.	60%	90%
Ultrasound (US)	Lesions >10mm	- Relatively quick procedure. - Relatively cheap. - Non-invasive.	- Difficult to distinguish between malignant and benign lesions. - Not reliable enough for lesions <10mm.	65-80%	90%
Magnetic resonance imaging (MRI)	- Lesions >2cm show a typical vascular pattern.	- Better diagnostic ability compared to US. - Less false positives compared to US.	- Poor cost-effectiveness.	80-90%	91-98%
Computed tomography (CT)	- Lesions >2cm show a typical vascular pattern.	- Comparable results to MRI	- Poor cost-effectiveness. - Radiation exposure.	71.4%	97.5%
Tissue biopsy	- Architectural and cytological features of HCC are found in biopsy.	- Used for definite diagnosis of HCC. - False positives are rare	- Invasive. - Not representative for the entire liver. - Risk of bleeding, tumour seeding etc.	90%	100%

4.2 Extracellular vesicles and their function in hepatocellular carcinoma surveillance

As discussed, a new method of HCC surveillance and diagnosis is desired. Extracellular vesicles (EVs) could prove useful in creating such a method.

EVs are lipid-enclosed vesicles that are released by almost every cell and found in bodily fluids such as blood [20, 21]. They are categorized into subtypes: exosomes, microvesicles/microparticles and apoptotic bodies. Apoptotic bodies are the largest subtype of EVs. The formation of apoptotic bodies occurs by blebbing from apoptotic cells. They are about 1-5 μm in size. Microvesicles are generated from the outward budding of the cell membrane and are 100-1000 nm in size. Exosomes are the smallest EV subtype and are about 30-120 nm. They are generated by intraluminal buds that fuse with the cell membrane. Multivesicular bodies (MVBs) are formed which usually encapsulate multiple exosomes. These MVBs either fuse with lysosomes or will release their contents into the extracellular space. Exosomes and microvesicles overlap in size and density which makes them difficult to separate with current techniques. Collectively they are called small EVs (sEVs). Their contents usually consist of lipids, proteins, RNAs or DNA fragments. They can be useful for diagnostic or surveillance purposes since their contents are related to the cell from which they are derived [21].

In healthy people, EVs play an important role in liver cell communication. Normal EVs are modulators of normal liver function and promote liver regeneration and repair. Especially hepatocyte-derived EVs have been shown to stimulate the regrowth of liver mass through the delivery of sphingolipids and enzymes [22, 23]. It can be assumed that in the case of liver disease, the EVs excreted from diseased cells, will differ from their healthy counterparts. For instance, due to the important signalling role of EVs, and the fact that their contents reflect the status of the cells from which they are derived [21].

Liquid biopsies that contain tumour-derived EVs, circulating tumour cells or tumour-derived cell-free DNA can prove to be a useful tool in HCC and other cancer surveillance. Tumour-derived cell-free DNA concentrations, however, have proven to be very low in some early-stage tumours [24]. An advantage of EVs is that the EV lipid bilayer encapsulates the DNA or RNA contents and protects it whereas cell-free DNA is directly exposed. Researchers theorize that the lipid bilayer protects the contents during for instance freeze-thaw and transport oscillations [24]. When looking at circulating tumour cells in patients with HCC, the concentration is also low. Research has shown numbers between 1 and 5 circulating tumour cells for a 7.5mL blood sample. Although the low concentration of circulating tumour cells makes HCC distinguishable from healthy control samples, it is speculated that HCC-derived EV concentrations in the blood are higher [25].

Tumour-derived EVs reflect the evolving tumour at all stages of the disease. They play a role in modifying the tumour environment and can promote tumour progression. They can for instance stimulate angiogenesis and cause vascular growth, vascular leakage and immune regulation. Overall, EVs play a role in remodelling the extracellular matrix and in intercellular communication [21].

A characteristic of EVs excreted by tumours is that they are abnormally large. These so-called oncosomes are typically between 100 and 400nm. Researchers speculate that these vesicles are produced in a non-apoptotic way, through plasma membrane blebbing, by silencing of the cytoskeletal regulator Diaphanous-related formin-3. Research has also shown how large oncosomes are only derived from tumour cells at a quantifiable rate, not from other cells. In addition, the number of vesicles that are found is directly related to the aggressiveness of the cancer [26]. In hepatitis patients, EVs have been proven to actively contribute to the progression of the disease. Vesicles isolated from both HBV and HCV patients, contain viral material which enables these EVs to further spread the virus to healthy cells. The lipid bilayer of the vesicle provides protection against antibodies that neutralize these viruses [27]. Research has also shown that, in response to saturated fatty acids often involved in fatty liver disease, hepatocytes increase their excretion of EVs [28].

4.3 Extracellular vesicle analysis in blood samples

Blood samples are a minimally invasive way to obtain a patient sample, especially compared to other tissue biopsies. Therefore it could be an ideal method of obtaining body fluid containing EVs to use for surveillance or diagnostic purposes. However, blood is also a very complex fluid, containing many molecules such as non-physiological EVs, protein aggregates, lipoproteins and viruses that share many biophysical properties with EVs. Therefore isolating a specific subpopulation of EVs from the blood can be challenging [29].

Blood plasma has an estimated EV concentration of 10^{10} EVs/mL [30]. However, this total amount of EVs found in blood samples is not limited to EVs that are released from pathological tissue. The blood cells themselves also release a substantial amount of EVs. Research has shown that roughly 30% of all EVs in the blood are erythrocyte-derived, 20% are leukocyte-derived and 50-90% are platelet-derived EVs [31].

Proteins are the most common non-EV contaminants found while isolating a subpopulation of EVs from blood samples. Blood plasma contains about 60-80 mg/ml of protein with the most abundant proteins being albumins, globulins, coagulation factors, lipoproteins and iron-binding/transferring proteins. These can aggregate and obtain properties similar to those of EVs in terms of size, charge and buoyant density [32].

The protein corona of EVs found in the blood typically consist of immunoglobulins, complement proteins, coagulation factors, cytokines, enzymes, DNA and RNAs. This may affect the physiological roles of the EVs and influence their mobility and interactions with surroundings and target surfaces. It is therefore important to remove unbound proteins from the blood sample before EV isolation [33, 34].

A very common contaminant found while isolating specific EVs are lipoproteins. These are spherical particles that can transport lipids in the bloodstream. They can be categorized into high-density lipoproteins (HDL), low-density lipoproteins (LDL), intermediate-density lipoproteins (IDL), very low-density lipoproteins (VLDL), lipoproteins a (Lp(a)), chylomicrons and chylomicron remnants. They can have similar sizes or densities as EVs but lipoprotein concentrations in blood are much higher than the EV concentrations. Therefore it is important to remove the lipoproteins before performing EV analysis on a blood sample [29]. This is difficult however, density and size-based isolation techniques will not provide adequate removal of the contaminants. Immunochemistry could therefore be a way to differentiate between the EVs and contaminants such as lipoproteins. Viral particles also create difficulties while isolating EVs since EVs can provide an envelope making it difficult to separate the virion from the host EV [34, 35].

In addition, bacterial and fungal EVs have been found in human blood plasma samples. The microbial contaminant in a blood sample can be evaluated by checking for genetic material using a polymerase chain reaction (PCR) [36, 37].

Table 3 shows an overview of nanoparticles present in blood samples according to previous research [34].

Table 3: *Nanoparticles present in the blood [34]. * Numbers can change significantly wih prandial status and diet. ** Numbers of particles calculated from reported mass concentrations from plasma. *** Most present post-prandially. ****Numbers of particles calculated from reported mass concentrations of their specific protein in plasma.*

Blood-plasma nanoparticle	Subgroup	Diameter (nm)	Density (g/cm^3)	Concentration in blood plasma (particles/mL)
Extracellular vesicles (EVs)	All plasma EVs	40-1 000	1.08-1.21	10^8-10^{13} on average, 10^{10}
	Platelet-derived EVs			10^8-10^{13}
Lipoproteins	High density	5-12	1.063-1.210	10^{16*}
	Low density	18-25	1.019-1.063	10^{15*}
	Intermediate density	25-35	1.006-1.019	$10^{12*,**}$
	Lipoprotein (a)	12-500	1.048-1.086	10^{12**}
	Very low density	30-80	0.930-1.006	$10^{12*,**}$
	Chylomicrons	75-1 200	<0.930	$10^{13*,***}$
	Chylomicron remnants	30-80	0.950-1.006	10^{12}* - $10^{13*,***,****}$
Protein aggregates		<1-15 000	1.4 (dense packing)	10^{17**} of albumin 10^{16**} of globulins
Viruses		30-300	1.16-1.18 (most retroviruses)	Depends on infection status

4.4 Isolation of extracellular vesicles

In order to use EVs for HCC surveillance, they first have to be isolated from the sample. Factors that are important in the isolation of EVs are rapidity, isolation and retrieval efficiency, purity, affordability and lastly, throughput [21].

Currently, ultracentrifugation (UC) is a widely used method for EV isolation and is considered the gold standard. This technique depends on density-based isolation and uses the size and density of EVs to separate them. It consists of an initial low speed centrifugation to deplete intact cells which is followed by high speed centrifugation for several hours to precipitate EVs. It produces a moderate yield of EVs without the use of damaging chemicals. The disadvantages of UC are that it takes a long time to complete and the large ultracentrifuges which are needed, are costly and may not be available in a clinical setting [21]. In addition, the use of UC on the EV samples can cause aggregation of the EVs, which makes single EV separation more difficult. An example of a UC technique to isolate EVs is shown in figure 3.

Using UC on blood samples to isolate EVs can lead to a low yield due to the binding of EVs to protein aggregates. So by removing the protein aggregates, a portion of the EVs in the blood is also removed [34, 38]. In addition, research shows that albumin and HDLs are common contaminants after performing UC [38].

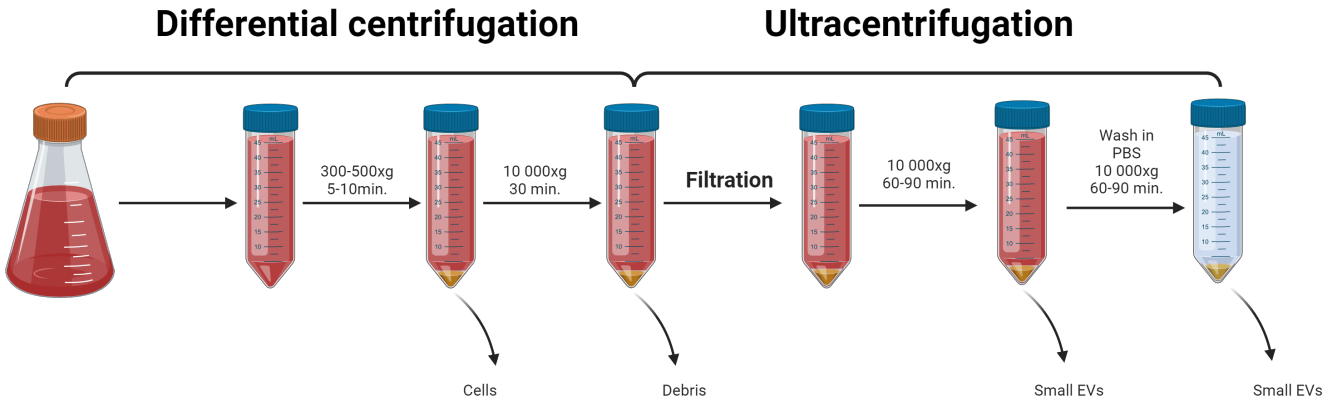

Figure 3: *Ultracentrifugation method for isolation of EVs. Created with BioRender.com, based on research by Doyle et al. [39]*

Ultrafiltration (UF) is a size-based isolation technique. EVs can be isolated by using a specific membrane as a filter with an appropriate pore size. By filtering the sample, larger particle sizes can be filtered out and EVs can be separated by size. Problems with this method arise due to proteins that are similar in size compared to the EVs and potential clogging of the filter [21]. A variation of UF, tangential flow filtration (TFF), is often used to adjust the concentration of the blood sample. During this technique, the sample does not flow through the membrane but across. It is not an efficient isolation technique for blood samples since after performing TFF, blood nanoparticles such as protein aggregates and lipoproteins are still abundantly present in the EV sample due to the size similarities [34]. But in comparison to the perpendicular flow filtration, TFF has shown less clogging of the filter (cake formation) and therefore better particle separation, based on the pore size of the filter. In addition, TFF is more gentle on shear-sensitive molecules due to the tangential flow. For the purpose of isolating EVs from a sample, TFF has been deemed a better method because it provides better particle separation [40]. The two discussed ultrafiltration methods are shown in figure 4, where the left image shows the process of TFF and the right image shows ultrafiltration using a perpendicular flow.

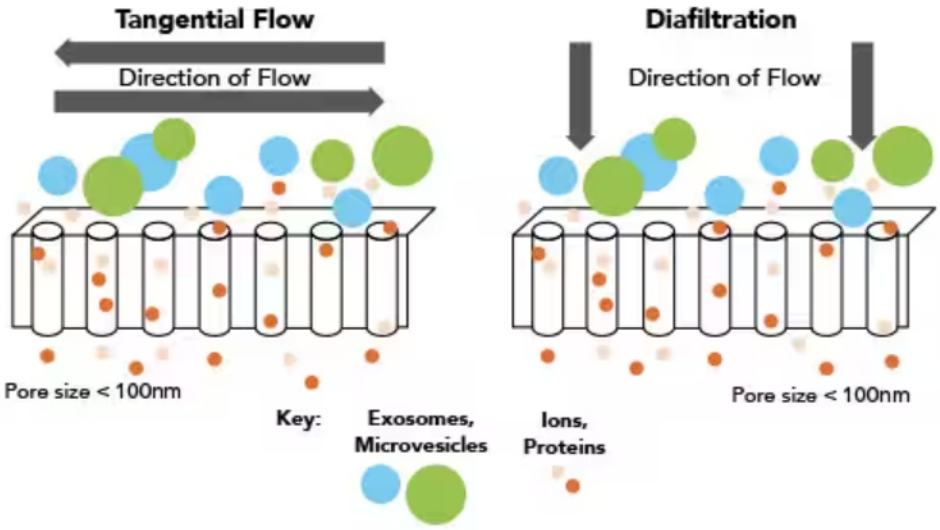

Figure 4: *Ultrafiltration methods for concentration of EV solution. The left shows a tangential flow technique while the right shows a diafiltration (perpendicular) flow technique [41].*

A column separation technique called Size Exclusion Chromatography (SEC) is also based on size difference. Heterogeneous porous beads are placed in a column. The openings and shafts in the beads can trap smaller particles which will cause them to take longer to elute than larger particles. The sizes of the beads and the openings can be adjusted to isolate a specific size of EV. The minimal pressure leads to no damage to the structural integrity of the EVs and the method leads to almost no sample loss compared to UC and UF. However, UC may lead to purer samples, so after completing SEC, UC is often still necessary [21]. An example of EV isolation using SEC is shown in figure 5.

Using SEC for blood samples usually leads to preparations free from significant protein contamination and to a high vesicle yield although still some low levels of albumin contamination have been reported. SEC is one of the most successful techniques in removing HDLs as well as their miRNA cargo [34, 38].

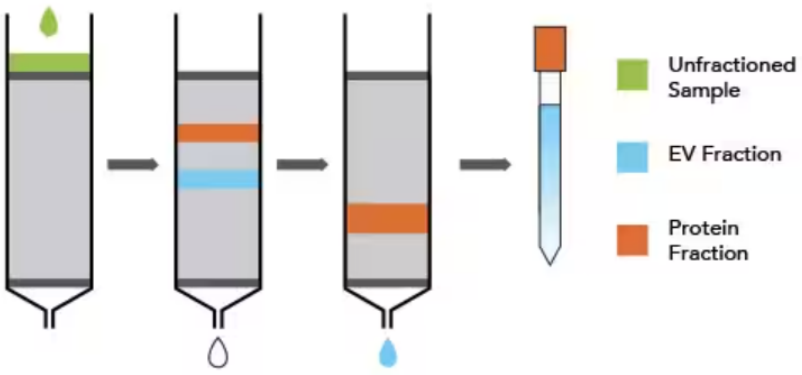

Figure 5: *Size exclusion chromatography (SEC) method for isolation of EVs [41].*

Immuno-based isolation can separate specific sub-populations of EVs which differentiates it from the previously explained methods. It uses an antibody cocktail to bind to specific transmembrane molecules on the EVs. It can lead to higher purity, efficiency and yield. The disadvantage, however, is that EVs can often be damaged while trying to separate them from the antibodies. Also, serum proteins of the blood

interfere with analysis [21]. In blood samples, immuno-based isolation can also be used as a negative selection to remove highly abundant blood proteins and lipoproteins [42].

Table 4: *An overview of methods to isolate extracellular vesicles from blood samples [34].*

Characteristic	**Size exclusion chromatography**	**Ultrafiltration**	**Differential ultracentrifugation**	**Immunoaffinity purification**
Plasma volume (mL)	<0.5, [43]	>3.0, [44]	>3.0, [44]	<1.0, [43]
Time (h)	1.5-2.0, [39]	0.5, [39]	3.0-4.0, [45]	4.0-overnight, [45]
Cost	High	Medium	Low	High
Principal of isolation	Difference in hydrodynamic size and shape	Difference in hydrodynamic size	Difference in sedimentation coefficient (hydrodynamic size and density)	Interaction between specific protein and antibody
Nanoparticles efficiently removed	Soluble proteins, high density lipoproteins [46].	Soluble proteins [47]	None [48]	All particles, except protein of interest
Major contaminants	Lipoproteins which are similar in size as the EVs [49].	Lipoproteins which are similar in size or larger than the EVs, large protein aggregates [50].	Proteins aggregates, aggregates of proteins and cell-free nucleic acids, lipoproteins [51].	Non-specific binding of plasma proteins
Recovery efficiency (%)	100, 65, [34]	80-84, 37, [34]	5-22, 40, 16, [34]	>90, [34]
Functionality of isolated EVs	Good	Medium	Medium	Poor

Table 4 shows several widely used methods of EV isolation and their application characteristics for the isolation of EVs from blood samples. It shows the major contaminants of the sample after each isolation process. The results in the table show how immunoaffinity leads to little contamination compared to the other methods, such as UC [34].

5 Aim and objectives

During this project, immuno-based isolation of EVs will be researched. Through the use of click chemistry, magnetic beads will be conjugated to antibodies enabling the capture of EVs. The aim is to determine if this previously used technique of HCC-derived EV isolation is applicable to blood serum samples. Previous experiments have shown how EVs were captured from culture medium, but it is expected that due to the higher contents of contaminants (such as lipoproteins), the capture of EVs from blood serum will be more difficult and less efficient.

While researching the application of the click chemistry-based immuno-isolation of HepG2-derived EVs in human blood serum, several objectives are formed. First of all, it is crucial to confirm surface antibodies on the surface of the used cell line but also on the HepG2-derived EVs. This ensures that the right antibody will be conjugated to the magnetic beads and EV isolation will be possible. Furthermore, the currently produced protocol for the immuno-based isolation of the EVs from culture medium has to be reproducible before moving on to the isolation from serum samples. In addition, the magnetic beads that are used for this immuno-isolation technique will be researched further. The amount of free thiol groups on the beads will be quantified and an estimation of the decrease of these thiol groups will be made after conjugating the beads. Finally, the capture efficiency of the system will be estimated when isolating the HepG2-derived EVs from human blood serum samples. Several different variations in the incubation of the system will be tested to reach maximum recovery efficiency.

6 Methodology

In this section, the overall methodology, regarding the characterization of the EVs, the immuno-isolation technique using magnetic beads conjugated to antibodies, and the validation of the experiments will be explained.

6.1 Extracellular vesicle characterization

The size of EVs can be estimated using Dynamic Light Scattering (DLS) measurements. This technique uses Brownian motion and can determine particle size distributions. The Brownian motion of individual particles depends on the particle size and influences the intensity at which the particle scatters the laser light. Using these intensity fluctuations, velocity and particle size can be determined according to the Einstein-Stokes relationship [52].

A dot blot is performed to test the affinity of the antibodies to the EVs. The sample is directly blotted onto a nitrocellulose membrane. This is then blocked with a primary antibody before incubation. A consecutive washing step will remove unbound antibodies. After washing, a secondary and later a tertiary horseradish-peroxidase antibody is added to enable detection. Dot blots are often a method that is used to test the binding of an antibody [53]. The horseradish-peroxidase is an enzyme that oxidizes products such as luminol. This reaction results in a fluorescent product which consequently produces light. This light can then be captured by an imaging device. Often, while using horseradish-peroxidase for immunohistochemistry, a peroxide solution and a substrate solution based on luminol, are used [54]. The reaction mechanism of luminol catalysed by horseradish-peroxidase is shown in figure 6.

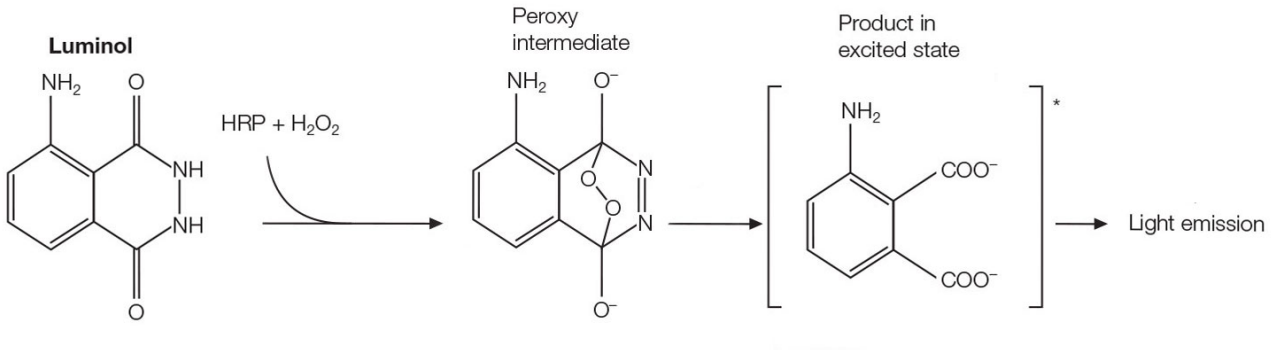

Figure 6: *Chemiluminescence of horseradish-peroxidase (HRP) and luminol [55].*

6.2 Extracellular vesicle isolation

During the performed immuno-isolation, a click chemistry reaction is used to conjugate the magnetic bead to an antibody. Click chemistry reactions are fast and simple in nature. They are usually easy to purify, versatile, regiospecific and produce high product yields [56].

In this project, trans-cyclooctene (TCO) and tetrazine (Tz) will react according to an inverse electron demand Diels-Alder cycloaddition (iEDDA). This will result in fast reaction kinetics and high selectivity while having a non-catalytic nature. This makes the TCO and Tz bond ideal, since usually protein reactions are constrained due to low concentration [57].

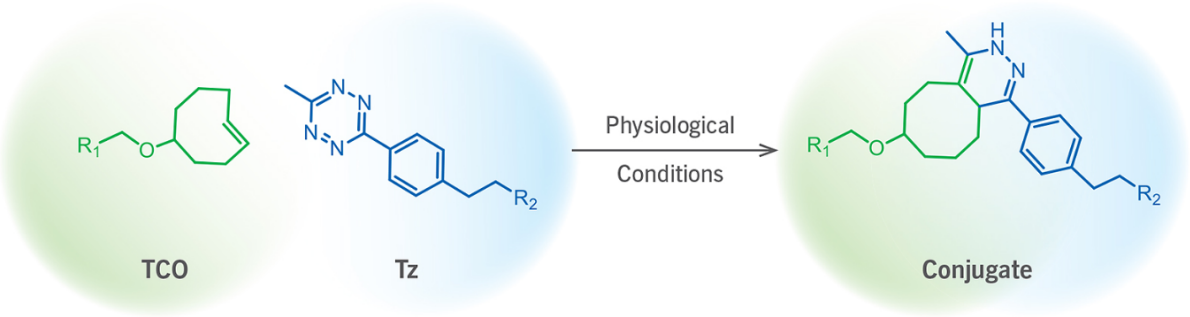

Figure 7: *Click reaction between TCO (trans-cyclooctene) and Tz (tetrazene) [58].*

The reaction is visualized in figure 7.

In this project, magnetic beads are used to bind antibodies to the EVs and therefore isolate a specific subpopulation of HCC-derived EVs.

The magnetic bead is attached to 5 polyethylene glycol (PEG) links which will attach to a Tz - TCO link to, for instance, an asialoglycoprotein receptor (ASGR1) antibody. The PEG spacer is added to decrease steric hindrance to improve the binding of the TCO to the Tz. The bead complex is clarified in figure 8. Several of the antibodies that could be used are: antihuman epithelial cell adhesion molecule (EpCAM), antihuman cluster of differentiation 9 (CD9) and antihuman ASGR1. EpCAM binds tumour-specific antigens, CD9 binds EV-specific antigens while ASGR1 is specific for liver cells (hepatocytes)[21, 29, 59, 60].

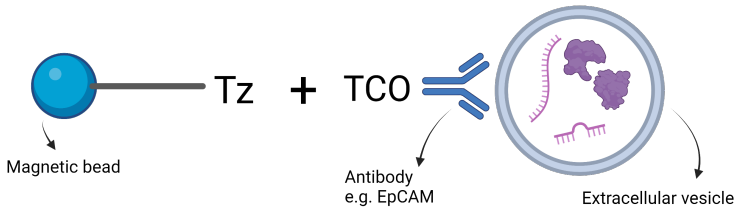

Figure 8: *Magnetic beads bound to an antibody which in turn binds to an appropriate extracellular vesicle. Created with BioRender.com*

First, the magnetic beads are attached to the OPSS-PEG link (step 1 in table 5), then to the Tz (step 2 in table 5). Antibodies are attached to the TCO separately (step 3 in table 5). The antibody-TCO complexes and bead-PEG-Tz complexes are incubated and washed using a magnet (step 5 in table 5).

Table 5: *Steps to undergo magnetic bead conjugation to antibodies and EVs using a trans-cyclooctene (TCO) and tetrazine (Tz) click reaction.*

	Step	
1	Bead is linked to OPSS-PEG5-NH2	
2	Bead-OPSS is linked to 6-methyl-tetrazine(Tz)-PEG5-NHS	
3	Antibody is linked to TCO-PEG4-NHS	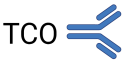
4	TCO and Tz click reaction occurs	
5	Bead-OPSS-Tz + TCO-Antibody complex is created	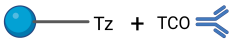
6	EVs bind to the antibody and therefore also the magnetic bead	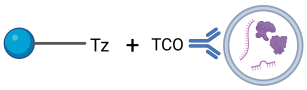

Eventually, the specific subpopulation of EVs that is targeted should bind to the bead-OPSS-TZ+TCO-antibody complex and make EV isolation possible. This is demonstrated in figure 9. Here, the washing steps are shown which enable the isolation of the bead-EV complexes from other contaminants which are found in the sample.

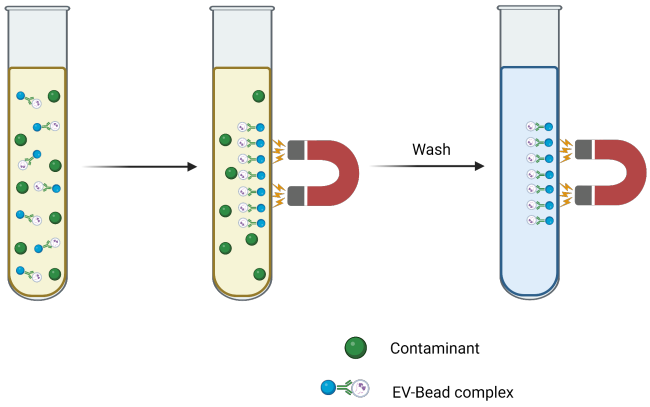

Figure 9: *Magnetic beads bound to an antibody are used to isolate extracellular vesicles from a sample. Created with BioRender.com, based on research by Jiawei et al. [61].*

The EVs that are targeted during the experiments originate from HepG2 cell culture medium. Collected HepG2 medium contains a low EV concentration. To increase this concentration, a tangential flow filter is used (TFF). TFF in comparison to UC is more efficient and will cause less disruption of the structural integrity of the EVs. In comparison to UF, TFF will prevent molecule accumulation and membrane fouling by applying the media parallel instead of perpendicular to the membrane [62].

Fluorescence-activated cell sorting (FACS) is used to determine if the different components are conjugated and if EVs are bound. FACS uses the concept of flow cytometry, which can use the fact that cells or EVs have specific surface markers to which specific antibodies can bind. The absence or presence of a specific antibody on the cell surface can determine the cell's phenotype. FACS uses excitation and detection of fluorescent light signals from for instance fluorescent antibodies or Calcein-AM-stained EVs, and can therefore provide information on the cell's phenotype. The system uses dichroic filters to steer fluorescent light to specific detectors and bandpass filters to determine the wavelengths of light that are read by the detector. Eventually, signals of the detectors are converted into digital signals [63]. After passing the detector, EVs or cells with the same fluorescent signals can be diverted toward a designated

collecting tube based on electrical charge [64]. The laser beam that is used in this technique will be scattered by the particle that passes. This will result in forward scatter which relays information on the size of the particle, and side scatter which relays information on the surface of the particle and its complexity. This is shown in figure 10. Since multiple subpopulations of cells or EVs can be separated at once, FACS is time and reagent efficient [64].

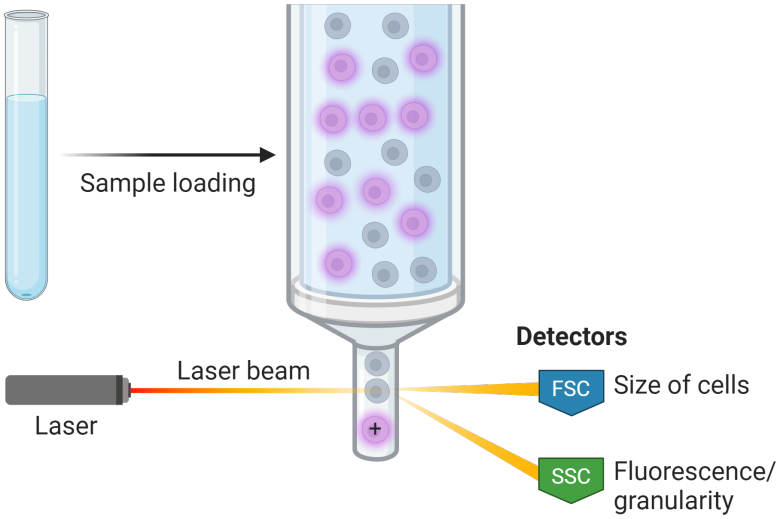

Figure 10: *Fluorescence-activated cell sorting (FACS). Created with BioRender.com*

6.3 Validation

To determine if EVs are captured by the system, they need to be distinctively measured by the flow cytometer. This is achieved by staining the EVs with Calcein-AM. Calcein-AM is a non-fluorescent lipophilic ester that can pass through the cell membrane. Once it has entered the cell, it is cleaved by esterases. A product of this reaction is Calcein, a photoreactive alcohol. In addition, Calcein is hydrophilic and therefore cannot pass through the cell membrane, resulting in the entrapment of Calcein within the cell or EV [65]. Non-living debris and dead cells are not stained by the Calcein-AM since they lack the necessary non-specific esterases. EVs and cells, however, do contain them. Figure 11 shows how the cleavage of the AM from the non-fluorescent Calcein-AM produces the fluorescent Calcein.

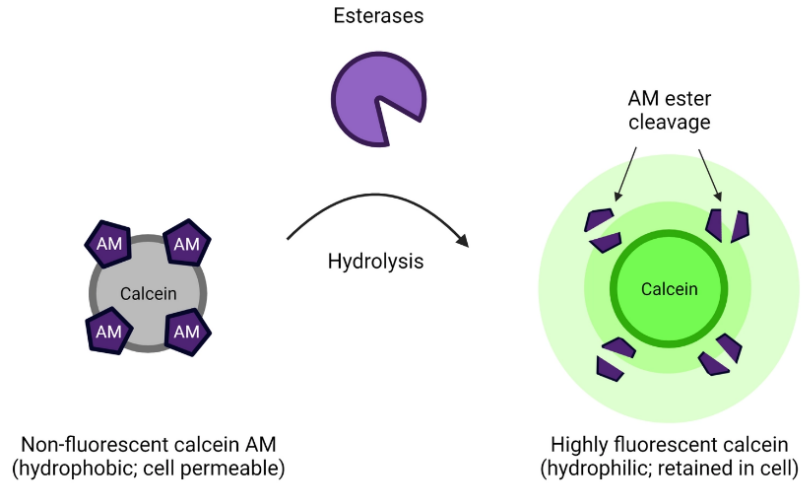

Figure 11: *Cleavage of AM by esterases to produce Calcein [66].*

The magnetic beads that are used during this research contain free thiol groups that will react with Orthopyridyl disulfide (OPSS) to eventually make the conjugation to the Tz group possible, enabling the click reaction. In literature, Ellman's reagent, 5,5-dithio-bis(2-nitrobenzioc acid) or also called DTNB, is used to quantify the free thiol groups present in a certain sample. This is possible due to the reaction of DTNB with the sulfhydryl groups which results in 2-nitro-5-thionbenzoate (TNB). This reaction is shown in figure 12. TNB is a coloured product and absorbs light at 412 nm. By quantifying the amount of generated TNB through colourimetric analysis or UV-vis spectroscopy, the amount of free thiol groups can be calculated [67]. This reaction could be used to quantify the number of magnetic beads that have bound and the amount that is still free to react.

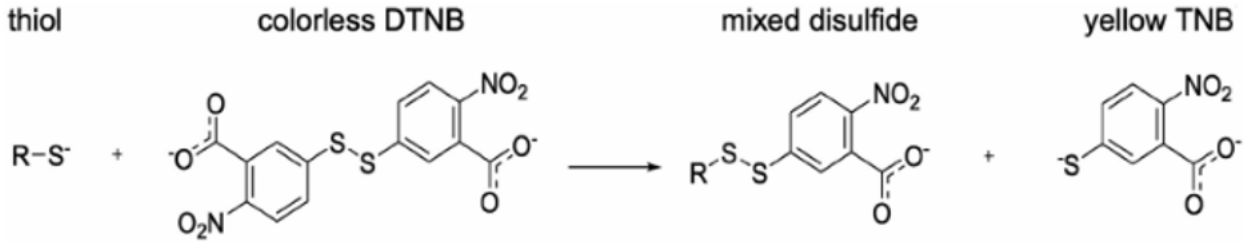

Figure 12: *Ellman's reagent/5,5-dithio-bis(2-nitrobenzioc acid) (DTNB) reacting with a free thiol to produce 2-nitro-5-thionbenzoate (TNB) [68].*

7 Method

7.1 Cell Culture

The used cell line for the experiments is the HepG2 line (ATCC). The cells have an epithelial-like morphology and are isolated from a 15-year-old male with HCC. The cells show key characteristics of hepatocytes [69]. The HepG2 cells were cultured in Dulbecco's Modified Eagle Medium (DMEM) with L-glutamine (Lonza, Walkersville MD, USA) with antibiotics (1% Penicillin and 1% Streptomycin, Sigma, St. Louis, MD, USA) and 10% Fetal Bovine Serum (FBS). Incubation of the cells is done at 5% CO_2 and a temperature of $37°C$. They were seeded in a T175 (175 cm^2) at 15 000 cells/cm^2. Finally, the cells are incubated in starvation medium (medium without FBS) for approximately 48-72 hours to prevent interference from the EVs that are present in FBS. In doing so, it is important to keep in mind that in the absence of FBS, the cells can experience cell stress and can change phenotype as well as show a change in EV cargo. In addition, the amount of EVs that is excreted is increased when the cells are depleted of FBS [70].

7.2 HepG2-derived extracellular vesicle isolation, concentration and analysis

7.2.1 Harvesting cells and extracellular vesicles

The medium of the starved cells was collected and centrifuged at 300xg for 10 minutes to remove any cells that are present. The supernatant was collected, leaving the pellet of dead cells and cell fragments. The supernatant was centrifuged at 2800xg for 10 minutes to remove dead cells and debris. Again, the supernatant was collected, containing the EVs.

The cells left in the T175 were washed twice with PBS. 3mL of 0.05% trypsin-EDTA was used to release the cells from the flask and from each other with an incubation period of 5 minutes at $37°C$. 17 mL of medium was added to the detached cells and the cells were then counted. Thereafter, the cells were centrifuged at 300xg for 5 minutes and the medium was aspirated. The cells were then fixed by incubating them in 2 mL of 4% formaldehyde for 15 minutes at room temperature. Finally, the cells were centrifuged again at 300xg for 5 minutes. They were then resuspended in PBS and 1% bovine serum albumin (BSA) to prevent excessive clumping of the cells.

7.2.2 Tangential flow filtration

The concentrating of the EVs is done using TFF. The TFF device (TFF-easy, HansaBiomed, Tallinn, Estonia) was first washed with PBS before running the sample through. About 1mL of the sample was collected after filtering. After each sample, the filter was washed using PBS and finally MilliQ. The pore size of the filter was 5nm.

7.2.3 Antibody and Calcein stainings

Cells and concentrated EVs were stained with antibodies and Calcein-AM (65-0853-81, Invitrogen, Waltham, Massachusetts, USA). Both fluorescently labelled EpCAM (EpCAM-FITC, SAB 4700424-100TST, Sigma-Aldrich, Saint Louis, Missouri, USA) and fluorescently labelled ASGR1 (ASGR1-FITC, VioBirght REAfinity 130-109411, Miltenyi Biotech, Berisch Gladbach, Germany) antibodies were used. FACS analysis was later performed in the appropriate fluorescence channel. For the stainings, 2 EV samples were used of approximately 100μL. For EpCAM, 2μL was added to reach a 1:50 concentration. The Calcein-AM staining consisted of adding 2μL of working a concentration of 2μM Calcein-AM dissolved in dimethyl sulfoxide (DMSO), to the 100μL EV sample. Stainings were incubated for at least 1 hour at room temperature before proceeding. For the cells, the stainings were performed in similar concentrations and after incubation, they were centrifuged at 300xg and resuspended in PBS + 1% BSA. All samples were stored in aluminium

foil until further analysis, to avoid bleaching. The performed ASGR1 staining was done on two samples. One sample of HepG2 cells was fixed using 4% formaldehyde and one sample was washed and resuspended in 2% FBS + PBS after centrifugation. The samples were then stained with the ASGR1 with a fluorescent label, by adding 2μL antibody to 100μL of sample. This resulted in a concentration of 1:50. Incubation consisted once again of 1 hour at room temperature. Thereafter, 900 μL of 2% FBS + PBS was added and the samples were centrifuged at 300xg for 5 minutes. They were then washed twice by resuspending in 1mL of 2% FBS + PBS and centrifugation at 300xg for 5 minutes.

Finally, the stained cells were run through the flow cytometer, measuring 10 000 events. Measurements included the appropriate fluorescence channel according to the fluorescent label of the used antibody.

Leftover EV samples from the staining, as well as the stained cells, were pipetted into a counting slide at a volume of 10 μL. The effects of the Calcein-AM and EpCAM staining were then observed under the inverted microscope (Nikon eclipse Ti) with the appropriate fluorescence channel.

7.2.4 Dot blot

The affinity of several antibodies to the EVs was tested using a dot blot. A nitrocellulose membrane (GE Healthcare, Chicago, Illinois, USA) was used to immobilize the collected EVs.

A serial dilution of EVs in starvation medium was prepared. The following ratios were used: only EVs, 1:1, 1:2, 1:5, 1:10 ratios of EVs : medium and only medium. 2.5 μL of the sample was spotted onto the membrane and dried until clear. After, the membrane was blocked in 5% powdered milk (Bio-rad, Lunteren, Netherlands) in Tris-Buffered Saline containing 0.1% Tween-20 detergent (TBST) for a duration of 1 hour on the roller mixer. The binding sites were blocked to avoid unspecific binding of the antibodies.

The membrane was then washed 3 times for 5 minutes with TBST on the roller mixer. Afterwards, the membranes were incubated with primary antibodies EpCAM, CD9, CD63 or ASGR1 with a concentration of 0.5 μg/mL (diluted in PBS) overnight at 4 $^{\circ}C$ on the roller mixer. Further information on the used antibodies during the dot blot experiment is found in table 6.

Table 6: *Information on the used primary antibodies during the dot blot.*

Primary antibody			
	Dilution	Manufacturer	Cat. No
EpCAM	0.5 μg/mL	Nalgene, ThermoFisher Waltham, Massachusetts, USA	RS032509-10
CD9	0.5 μg/mL	Hansa Biomed, Talinn, Estonia	HBM-CD63-100
CD63	0.5 μg/mL	Hansa Biomed, Talinn, Estonia	HBM-CD9-100
ASGR1	0.5 μg/mL	Invitrogen, Waltham, Massachusetts, USA	PA5-52885

Table 7: *Information on the used secondary antibodies during the dot blot, with their respective primary antibodies.*

Primary antibody	**Secondary antibody**			
		Dilution	Manufacturer	Cat. No
EpCAM CD9 CD63	Goat anti-mouse	1:100	DAKO, Wiesentheid, Germany	P0447
ASGR1	Goat anti-rabbit	1:100	DAKO, Wiesentheid, Germany	P0448

Table 8: *Information on the used tertiary antibodies during the dot blot, with their respective antibodies.*

Primary antibody	**Tertiary antibody**			
		Dilution	Manufacturer	Cat No.
EpCAM CD9 CD63 ASGR1	Anti-goat	1:100	DAKO, Wiesentheid, Germany	P0449

The host of the used antibodies was mouse for all except the ASGR1 antibody which was produced in rabbit. Therefore, 2 1:100 dilutions were prepared for the secondary antibody in TBS. The secondary antibodies were goat anti-rabbit (table 7) and goat anti-mouse (table 7). 3mL of the appropriate secondary antibody solution was added to each membrane after performing 3 washing steps of 5 minutes with TBST. Afterwards, the membranes were incubated for 1 hour on the roller mixer at room temperature.

Anti-goat (table 8) was used as the tertiary antibody for all membranes. It was prepared in a 1:100 dilution in TBS and after performing 3 washing steps with TBST for 5 minutes, 3 mL of tertiary antibody solution was added to each membrane and this was incubated for 1.5 hours on the roller mixer at room temperature.

Finally, the membranes were washed 3 times with TBST after which 3 mL of TBS was added to each membrane. Pierce ECL Western Blotting Substrate (Thermo Fisher, Waltham, Massachusetts, USA) is used for detection. The strips were taken out of the TBS and ECL substrate was added in a 1:40 dilution of part A and part B. This was incubated for 5 minutes. The membranes were then imaged in a blot imager (blot imager, cell-source, New York, New York, USA). Processing of the images was done using ImageJ software (U.S. National Institutes of Health, Bethesda, Maryland, USA).

7.3 Dynamic light scattering

In these experiments, Dynamic light scattering measurements were used to determine particle sizes in several samples.

Human blood serum samples were prepared at 0%, 1%, 5%, 10%, 50% and 100% in PBS. Each sample was 1mL in total. The EV sample of 700 μL dedicated to the DLS measurement, was supplemented with 300 μL of PBS to form a sample of 1mL total. These samples underwent a DLS (Zetasizer nano-Zs, Malvern, Malvern Panalytical, UK) measurement.

7.4 Magnetic bead conjugation

Conjugation was performed using ortho-pyridyl disulfide (OPSS) functionalized with 5KDa polyethyleneglycol (PEG). The OPSS-PEG5-NH2 was dissolved in dimethylsulfoxide (DMSO) solution with a concentration of 30mg/mL. Thiol magnetic beads of sizes 1-5 μm (PEMSH200701303, Accubead Bioneer, Daejeon

Republic of Korea) were used. 100 μL of 10mg/mL beads was combined with 7.2 μL of OPSS-PEG5-NH2 and 92.8 μL of PBS resulting in a total volume of 200 μL. This solution was left to react for 2 hours on a mixer at room temperature at pH 7.0. After, the beads were washed 5 times with PBS using a strong magnet and resuspended in 100 μL of PBS with a pH of 8.5.

6-Methyl-Tetrazine-PEG5-NHS (cp-6062, Conju-Probe, San Diego, California, USA) was dissolved in DMSO to a concentration of 30mg/mL. 100 μL of beads-OPSS-PEG5-NH2, 7.9 μL of 6-Methyl-Tetrazine-PEG5-NHS and 92.1 μL of PBS with a pH of 8.5 were combined. This was left to react on a mixer for 2 hours at room temperature. Afterwards, the beads were washed 5 times with PBS using a strong magnet. Eventually, the beads are resuspended in 100μL of PBS with 1% BSA.

To conjugate, for instance, the EpCAM (FITC) antibody to the TCO, Trans-cyclooctene-PEG4-NHS was dissolved in DMSO to a concentration of 3mg/mL. 100 μL of PBS and 2μL of EpCAM antibody was combined with 8.6 μL Trans-Cyclooctene-PEG4-NHS and 91.4 μL PBS. This was incubated for 1 hour at room temperature, pH 7.0. Amicon ultra 0.5mL centrifugal filters 10KDa (Millipore, Burlington, Massachusetts, USA) were used to purify the solution. It was centrifuged 3 times at 5000 RPM for 20 minutes while resuspending and adding 100 μL of PBS during each round. The column was spun upside down for 5 minutes at 5000 RPM to retrieve the conjugated antibodies. This resulted in an end volume of over 200 μL. Before storage or FACS analysis, 100 μL of PBS with 1% BSA is added.

The following samples were prepared: EpCAM-TCO, beads, beads-OPSS, beads-OPSS-Tz, HepG2 (EV or cell)-beads-OPSS + TZ-TCO-EpCAM and beads-OPSS-TZ + TCO-EpCAM. The samples contained 10 μL of the EpCAM-TCO, 5μL of beads-OPSS and 50μL of HepG2 cells that were fixed with 4% formaldehyde with a cell count of $8 * 10^6$ cells/mL. The cells/EVs and EpCAM antibodies were left to incubate for 1 hour on the roller bank before adding the beads-OPSS-Tz and incubating for another hour. Next, the solution was washed three times with PBS and a magnet. If necessary, the samples were diluted with PBS + 1% BSA to reach an end volume of at least 250 μL for each sample. FACS was then used to analyse the samples.

Following these experiments, another experiment was performed to test the capture ability of the conjugated magnetic beads to capture the HepG2-derived EVs from blood serum samples. The beads were conjugated to Tz according to the above-mentioned steps. An antibody solution of 10μg/mL EpCAM (Vu1D9 10x, Nalgene ThermoFisher, Waltham, Massachusetts, USA) was prepared to then conjugate it to TCO according to the mentioned steps. While concentrating EVs using the TFF system, the sample was concentrated to about 0.5mL instead of 1mL to avoid diluting the serum and PBS samples while still spiking them with a maximum amount of EVs. The concentrated EV sample was then stained with Calcein-AM (65-0853-81, Invitrogen, Waltham, Massachusetts, USA) using a concentration of 1:50 of 2mM Calcein-AM solution in the EV sample. Incubation lasted for at least 30 minutes, similar to previous experiments. Three different samples were spiked with EVs. For each sample, 25μL of stained EVs was added to 250 μL of solution. The following solutions were spiked: PBS, PBS and serum (1:1) and serum. These amounts are shown in table 9.

Table 9: *Samples of PBS and human blood serum spiked with HepG2-derived EVs.*

Sample	**Amount of stained HepG2-derived EVs (μL)**	**Amount of PBS (μL)**	**Amount of serum (μL)**	**Total volume (μ)**
PBS	25	250	-	275
PBS and serum	25	125	125	275
Serum	25	250	-	275

10μL of conjugated beads was added to each sample in addition to 20μL of EpCAM-TCO solution. Three different protocols for the incubation time were tested to determine the ideal protocol for capturing EVs from serum. These are described in table 10.

Table 10: *Tested incubation protocols for the optimal capture of HepG2-derived EVs from PBS and human blood serum samples.*

Sample	Incubation of EpCAM-TCO in spiked PBS/serum sample	Incubation of beads-OPSS-Tz in spiked PBS/serum sample
Protocol A	Overnight, at $4°C$	Overnight, at $4°C$ *
Protocol B	Overnight, at $4°C$	1 hour, at room temperature
Protocol C	1 hour, at room temperature	1 hour, at room temperature

* Conjugated beads and EpCAM-TCO were incubated at the same time

Finally, the samples were washed in the same manner as before, 3 times in PBS + 1% BSA.

In addition to the magnetic beads, a control experiment using anti-EpCAM ferrofluids (Janssen Diagnostics, LLC, Raritan, NJ, USA) was performed. The same spiked PBS/serum samples were prepared as before to which 4 μL of ferrofluid was added. These samples were incubated at room temperature for 33 minutes, resuspending the solution every 3 minutes. Thereafter the samples were washed 3 times using a strong magnet and PBS + 1% BSA.

7.4.1 Fluorescence-activated cell sorting

FACS measurements (FACSAria ii, BD, Franklin Lakes, New Jersey, USA) were performed to check whether the stainings or conjugation experiments succeeded. All measurements consisted of 10 000 events unless specified. A Pe filter was used with an excitation wavelength of 488 nm and an emission of 585/42 nm. In addition, a FITC filter was used with an excitation wavelength of 488 nm and an emission of 530/30 nm. For all conjugation experiments and stainings, a threshold of 5000 was used for the forward scatter. In the experiment that measured ferrofluids, a threshold of 1000 was used for the forward scatter.

7.5 Ellman's reagent

As discussed, Ellman's reagent/DTNB (Thermo Fisher, Waltham, Massachusetts, USA) is used to quantify the free thiol groups on the beads. First, a 1M Tris-HCl buffer with a pH of 8.0 is prepared by combining 12.11 g of Tris(hydroxymethyl)aminomethane (Acros Organics, ThermoFisher, Waltham, Massachusetts, USA) and 80 mL of MilliQ. Using a pH meter, a pH of 8 was achieved by the addition of HCl to the solution. Once the desired pH was reached, the solution was topped up to 100 mL using MilliQ. The samples that were used in this experiment are the empty magnetic beads, beads conjugated to OPSS and beads conjugated to OPSS and Tz. These were prepared following the conjugation protocol that was described in chapter 7.4. The samples that will be used in this experiment have been adjusted to contain approximately the same amount of (conjugated) beads. First, the PBS in these samples is replaced by the Tris pH 8.0 buffer using the strong magnet. The samples are then diluted at 100% sample (50 μL sample), 50% (25 μL sample + 25 μL Tris buffer) and 20% sample (10 μL sample + 40 μL Tris buffer) Separately, the DTNB was dissolved in Tris pH 8.0 buffer with a concentration of 500μM, preparing a total of 500 μL of DTNB in Tris buffer. Finally, 50 μL of the diluted samples is then combined with 50 μL of DTNB in Tris buffer. This is incubated for 30 minutes at room temperature. After incubation, 300 μL of Tris pH 8.0 buffer is added to each sample, resulting in a total volume of 400 μL of each sample. This volume is divided into 2 to create duplo conditions of each sample in a 96 wells plate. In addition, a duplo control of Tris buffer is used. The absorbance of the samples is measured in an absorbance plate reader (PerkinElmer, multimode plate reader Victor 3, USA) at 405nm.

After analysing the results of the performed experiment according to the described protocol, the method was adjusted. 100 μL of beads of each sample were washed and resuspended in 100 μL of Tris buffer (pH 8.0). Sample dilutions were then prepared of 100% sample (40μL) 50% sample (20 μL sample + 20 μL Tris buffer) and 25% sample (10 μL sample + 30 μL Tris buffer). These sample dilutions were then combined

with 402 μL of Tris buffer and 8 μL of DTNB in Tris buffer (4mg/mL). This was incubated for 15 minutes after which 200 μL of the samples were pipetted in duplo in a 96 wells plate. Finally, the absorbance of the samples is measured in an absorbance plate reader (PerkinElmer, multimode plate reader Victor 3, USA) at 405nm. The obtained results are analysed using GraphPad (GraphPad Software, San Diego, California, USA)

8 Results

8.1 Characterization of HepG2 cells and extracellular vesicles

Before isolation of the EVs using the magnetic beads is possible, it is important to validate the presence of the surface antibodies on the HepG2 cells and the HepG2-derived EVs. This is done using stainings, which are evaluated by fluorescence microscopy and flow cytometry.

8.1.1 Fluorescence microscopy

The cultured HepG2 cells were stained with EpCAM and imaged using an inverted microscope. The results are shown in figure 13. The images clearly show how the cells were successfully stained using EpCAM proving they indeed express EpCAM as a marker. In addition, the EpCAM signal is clearly seen around the edges of the cells showing the expression of EpCAM on the cell surface.

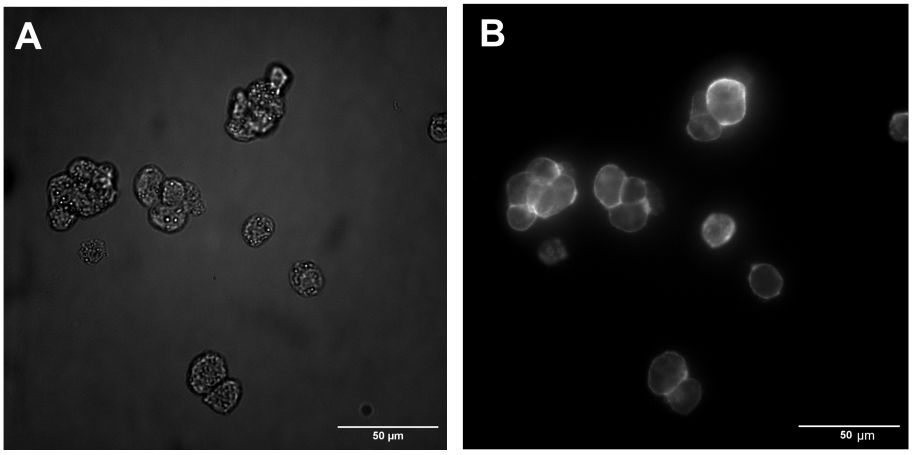

(a) *EpCAM stained HepG2 cells, brightfield, 60x*

(b) *EpCAM stained HepG2 cells, Pe, 60x*

Figure 13: *HepG2 cells stained with EpCAM imaged under brightfield and Pe filter, 60x objective.*

The HepG2-derived EVs were also stained using EpCAM, shown in figure 14, indicated by the red arrows. These images show that besides the cells, the EVs also express the EpCAM marker.

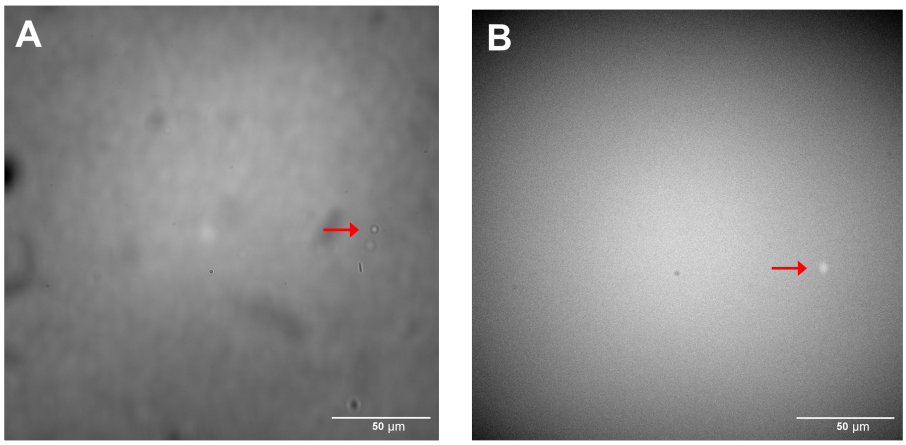

(a) *EpCAM stained HepG2-derived EVs,brightfield, 60x*

(b) *EpCAM stained HepG2-derived EVs, Pe, 60x*

Figure 14: *HepG2-derived EVs stained with EpCAM under brightfield and Pe filter, 60x objective.*

The EVs were also stained with Calcein-AM. The images are shown in figure 15, where stained EVs are indicated by the red arrows. The shown EV is indeed stained. However, it was difficult to image the EVs because of rapid photobleaching.

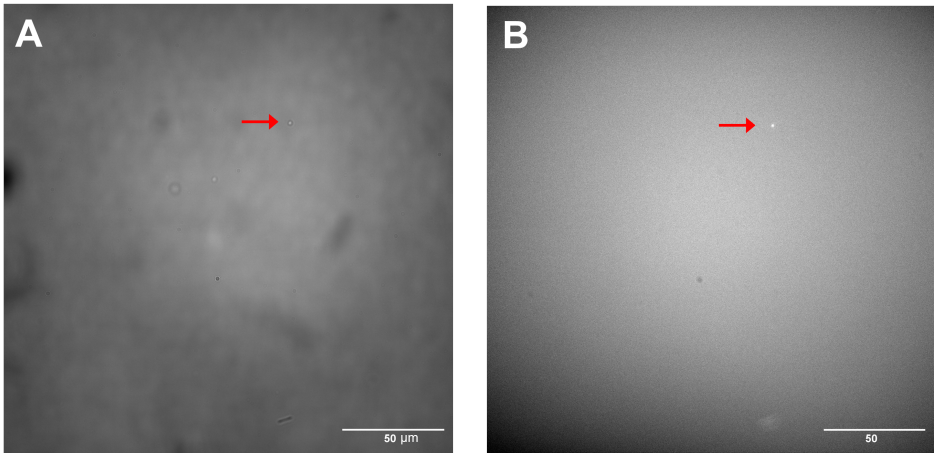

(a) *Calcein-AM stained HepG2-derived EVs, brightfield, 60x* **(b)** *Calcein-AM stained HepG2-derived EVs, FITC, 60x*

Figure 15: *HepG2-derived EVs stained with Calcein-AM under brightfield (A) and FITC filter (B), 60x objective.*

8.1.2 Flow cytometry

FACS measurements performed on the unstained HepG2 cells and the EpCAM stained HepG2 cells show that the cells express the EpCAM marker. Figure 16 shows a shift towards the right in the fluorescent Pe channel, in the stained cells, indicating a positive EpCAM staining. To quantify this, 91.4% of the cells were measured to be positive for EpCAM.

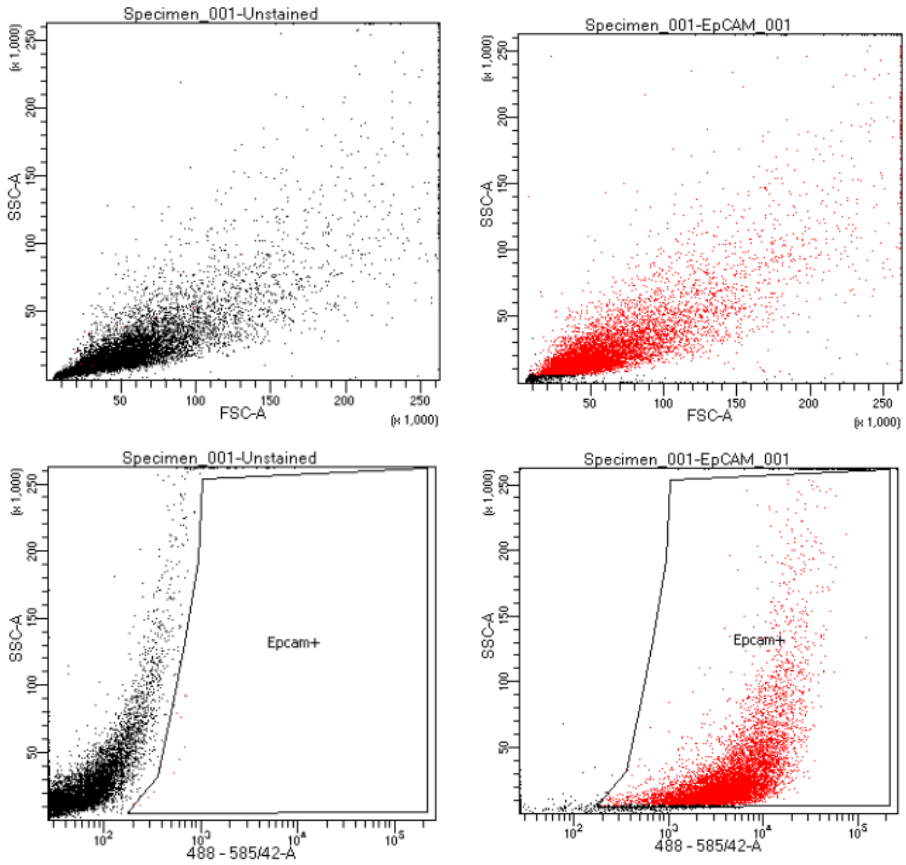

(a) *Unstained, fixated HepG2 cells* **(b)** *EpCAM stained, fixated HepG2 cells*

Figure 16: *FACS analysis of unstained and EpCAM-Pe stained HepG2 cells. The 488-585/42 filter shows the Pe signal. In addition, forward scatter (FSC) informs about the size while side scatter (SSC) informs about the complexity.*

Using a similar protocol to the EpCAM and Calcein-AM staining, fixed and live HepG2 cells were also stained with ASGR1-(FITC). The results of the FACS measurements are shown in figures 17 (unstained cells) and 18 (ASGR1-FITC stained cells). Figure 17 shows that fixation of the cells causes the population to shift slightly in the FITC channel. Also, the side scatter of the cells seems to increase when fixating the cells, changing the complexity of the cells. Figure 18 shows that the HepG2 cells show an expression of ASGR1 in about 43.3% of cases (for live HepG2 cells). However, in fixed cells, this expression is only 15.5%. This is a promising amount although much less than the expression of EpCAM measured in figure 16. The decrease of EpCAM signal in the fixed cells could be due to the 4% formaldehyde which can influence the availability of the surface antibodies and therefore interfere with the staining.

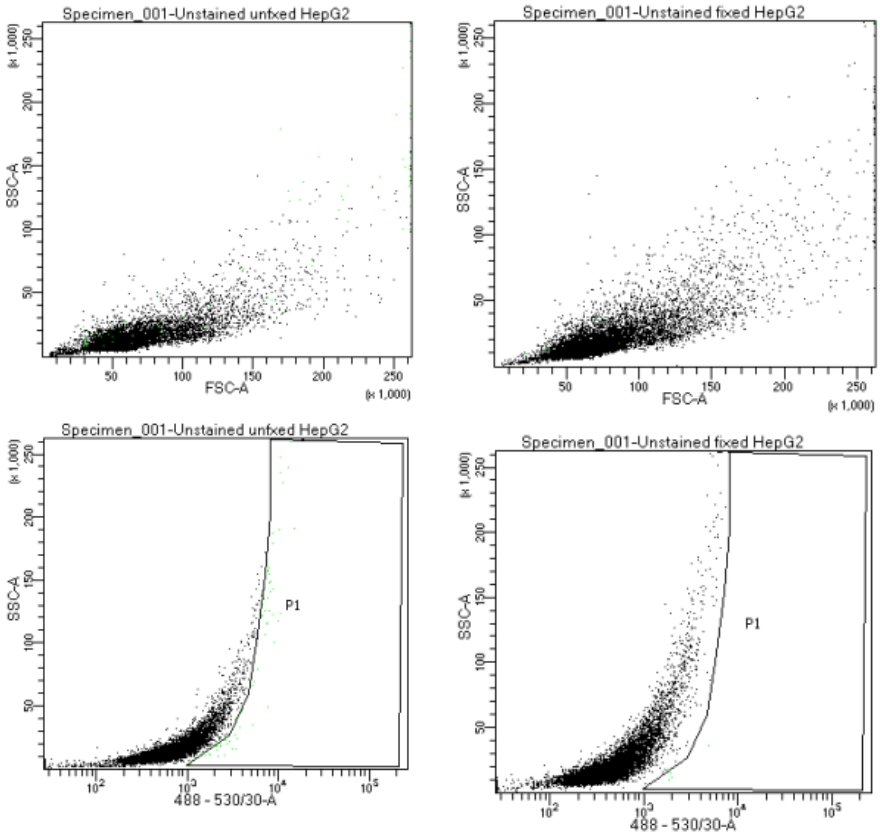

(a) *Unstained, live HepG2 cells* **(b)** *Unstained, fixated HepG2 cells*

Figure 17: *FACS of unstained, live and fixated HepG2 cells. The 488-530/30 channel shows the FITC signal. In addition, forward scatter (FSC) informs about the size while side scatter (SSC) informs about the complexity.*

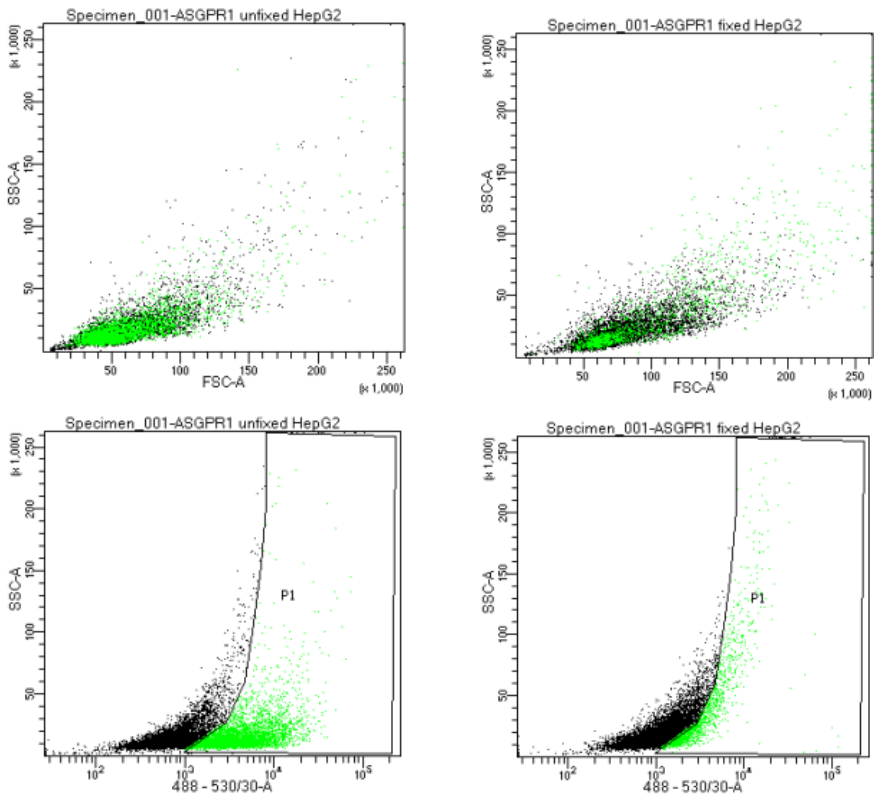

(a) *ASGR1 stained, live HepG2 cells* **(b)** *ASGR1 stained, fixated HepG2 cells*

Figure 18: *FACS analysis of ASGR1 stained, live and fixated HepG2 cells. The 488-530/30 channel shows the FITC signal. In addition, forward scatter (FSC) informs about the size while side scatter (SSC) informs about the complexity.*

8.1.3 Dot Blot HepG2-derived extracellular vesicles

A dot blot was performed to check the expression of CD9, EpCAM, CD63 and ASGR1 on the EVs. EVs were spotted in a serial dilution on the membrane. The chemiluminescent signal was then measured to evaluate the presence of the antibodies on the EVs. Results are shown in figure 19. This was quantified in figure 20 where the average intensities over the diameters of each spot in the images are shown.

The results show that CD9 markers were present in the highest magnitude on the EVs. Also in high abundance was the ASGR1 marker followed by CD63 and EpCAM markers which were slightly less present. Based on these findings, it was concluded that CD9 is an appropriate marker for the isolation of these EVs. According to literature, CD9 is an EV-specific marker[21]. The addition of ASGR1 as a liver-cell-specific marker should be successful based on the dot blot. However, especially the values in figure 20 should be looked at critically. Due to an inconsistent background signal which is visible in figure 19, the intensities can be difficult to compare. This dot blot therefore may not be reliable enough to show relative expression of the EVs but it can be said that all four tested antibodies were expressed by the EVs. Additional profile plots of the intensities of the dot blots are found in appendix 11.1.

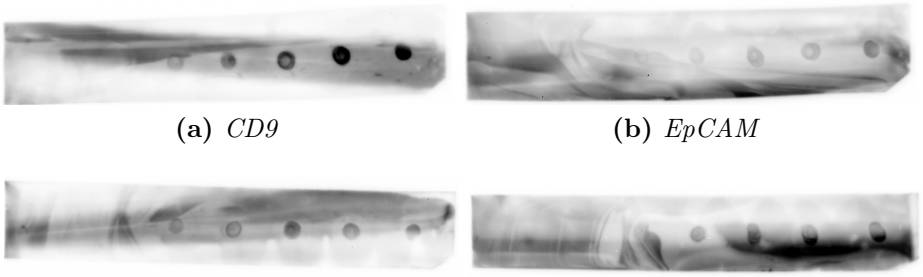

(a) *CD9* **(b)** *EpCAM*

(c) *CD63* **(d)** *ASGR1*

Figure 19: *Dot blot of HepG2-derived EVs using antibodies CD9, EpCAM, CD63 and ASGR1. Dilutions of EV : medium from left to right were: 0:1, 1:10, 1:5, 1:2, 1:1, 1:0.*

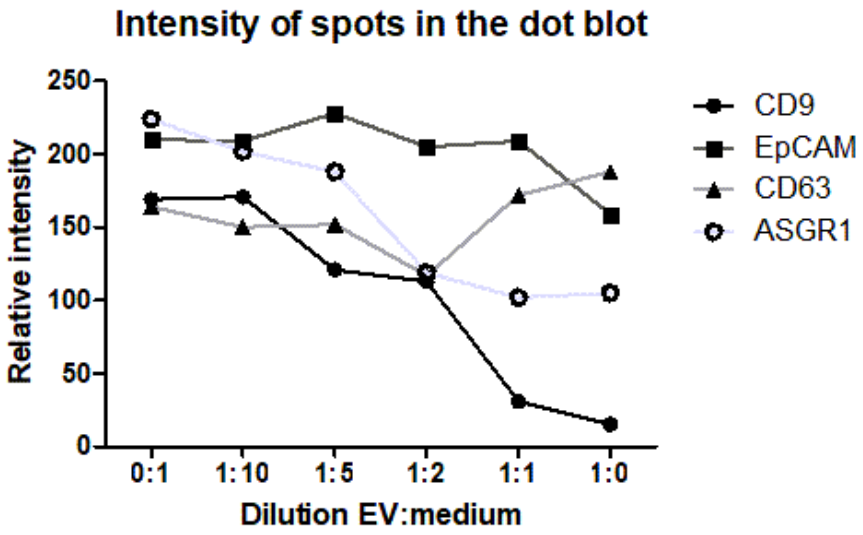

Figure 20: *Pixel intensities of the spots in the dot blot of HepG2-derived EVs using antibodies CD9, EpCAM, CD63 and ASGR1.*

8.2 Dynamic light scattering

8.2.1 Dynamic light scattering measurements on human blood serum

Intensity graphs showing size distributions resulting from the DLS measurement performed on human blood samples are found in figure 21. The DLS measurements resulted in three measurements per sample that gave inconsistent results at times. One measurement per sample is shown in the figure. It seems, the higher the concentration of human blood serum, the higher the intensity peaks are for larger particles. Also, more peaks appear for higher concentrations of human blood serum. This could be due to the change in the viscosity of the sample since the DLS measurements and calculations highly depend on viscosity.

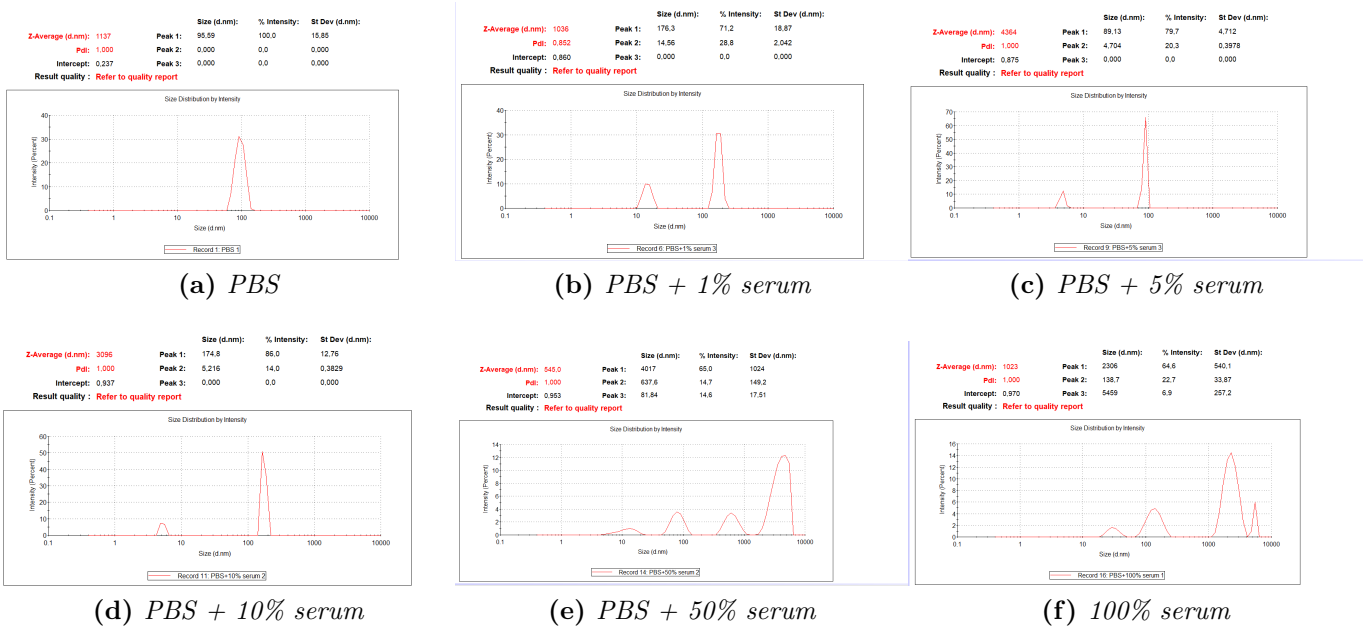

(a) *PBS* (b) *PBS + 1% serum* (c) *PBS + 5% serum*

(d) *PBS + 10% serum* (e) *PBS + 50% serum* (f) *100% serum*

Figure 21: *DLS measurements of human blood serum in PBS in concentrations 0%, 1%, 5%, 10%, 50% and 100%.*

8.2.2 Dynamic light scattering measurements of HepG2-derived extracellular vesicles

The DLS measurement was also performed in HepG2-derived EVs. This was done twice, with EV samples originating from different samples of HepG2 cells. The results are shown in figure 22. The difference in intensity and placement of the peaks shows how the isolated EVs can vary in size and numbers even though they originate from the same cell type. Looking at the peaks, one sample has 141.3 nm, 24.21 nm and 6.776 nm sizes particles whereas the other sample has 343.1 nm and 27.54 nm sizes particles. It is therefore likely that the HepG2-derived EVs have sizes in the range of tens and hundreds of nanometers, even though sizes can vary for each sample.

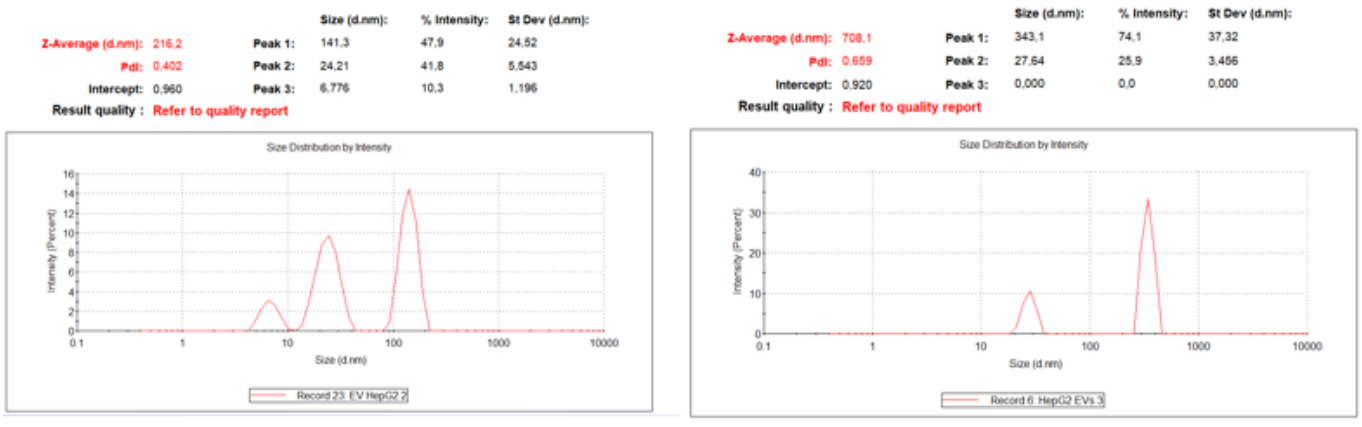

Figure 22: *DLS measurements of HepG2-derived EVs. Two different samples are measured. The samples contain EVs of two different HepG2 samples.*

The results in figure 23 show how the time between DLS measurement and isolation of the EVs has a large influence on the DLS results. Intensity graphs of HepG2 EVs are shown in the top three graphs where the measurement was performed on the same day as the isolation and concentration of the EVs.

The peaks are seen at 202.2-343.1 nm and 13.60-27.64 nm. The bottom three graphs show DLS results from the same EVs after being kept at $4°C$ for 7 days after isolation. The peaks are seen at 4555 nm, and 247.8-360.3 nm. It is suspected that the increase in the particle size is caused by the aggregation of the EVs in the sample with time.

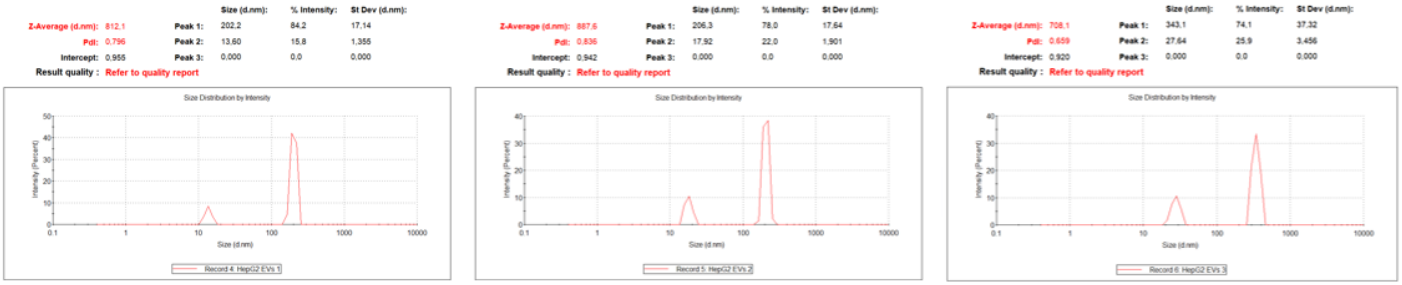

(a) *Day of isolation*

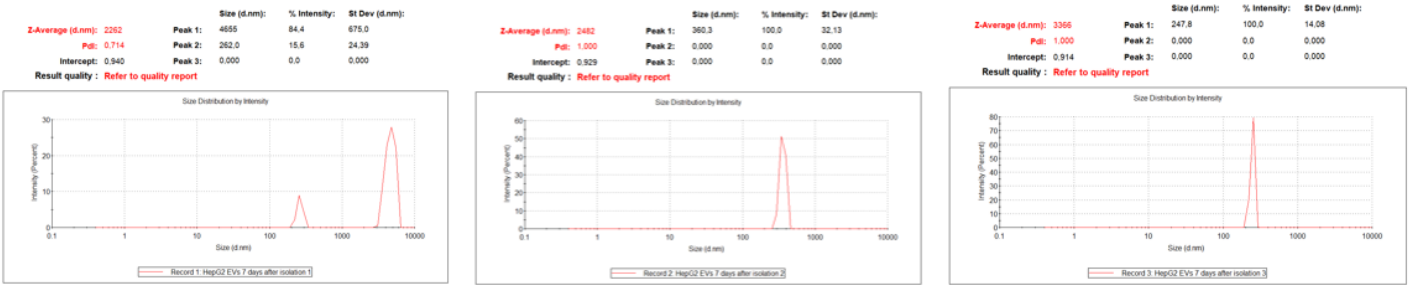

(b) *After 7 days at 4°C.*

Figure 23: *DLS measurements of HepG2-derived EVs. The same sample of EVs was measured, once on the day of isolation and once 7 days after isolation after the sample was kept at 4°C.*

8.3 Magnetic Bead Conjugation

Following the described protocol for the conjugation of the beads, magnetic beads were conjugated to EpCAM-FITC and to HepG2 cells. This conjugation failed, the cells were seemingly not captured by the beads. However, the conjugation of the Tz to the beads was successful with a population of beads of 32.4% positive for Tz. The results are shown in Appendix 11.2.

Following this experiment, an experiment was performed conjugating the beads to EpCAM, ASGR1 and CD9 antibodies without a fluorescent label. Also, the capturing of EVs was attempted instead of HepG2 cells. These EVs were stained with Calcein-AM. Methods similar to those described in chapter 7 were used for the concentration of the EVs using TFF, the Calcein-AM staining of the EVs and the conjugation of the beads to the antibodies. Again, the results were not as expected. The EVs seemed to not have bound to the magnetic bead system. Results are shown in Appendix 11.3.

Due to the failed conjugation results, the conjugation was performed again, but the antibody concentration was increased approximately 20 times. The antibodies that were used were ASGR1 and EpCAM. The results of the FACS analysis following this experiment are shown in Appendix 11.4. The increased antibody did not seem to have a large effect on the conjugation efficiency of the EVs to the magnetic beads. Unfortunately, the used antibody-TCO complexes and EVs were over 48 hours old before FACS analysis, due to time constraints. This could have affected the outcome.

Finally, the conjugation was attempted using EpCAM-TCO which was prepared on the same day as FACS analysis of the magnetic bead-EV complexes. This resulted in capturing of EVs using the magnetic beads. The FACS results are shown in figures 24 and 25.

Figure 24 shows how an estimated 29.6% of the beads were positive for Tz in the Pe channel. The conjugation of the beads to OPSS and Tz was therefore successful.

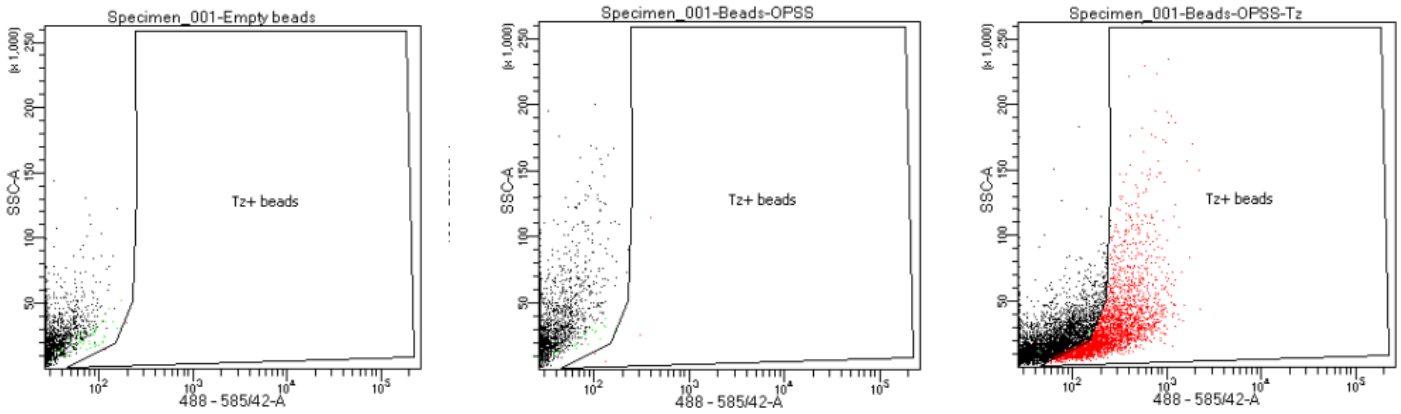

(a) *empty beads* **(b)** *beads-OPSS* **(c)** *beads-OPSS-Tz*

Figure 24: *FACS analysis of empty magnetic beads, beads bound to OPSS and beads conjugated to OPSS and Tz. The positive population (red) of fully conjugated beads is estimated to be 29.6%. The 488-585/42 channel shows the PE signal, in this case indicating the Tz binding. In addition, side scatter (SSC) informs about the complexity of the particles.*

In figure 25, it is visible how both loose EVs were measured by the FACS and also EVs that were positive for both FITC and PE channels and therefore indicating they were attached to the beads (which include the Pe positive Tz).

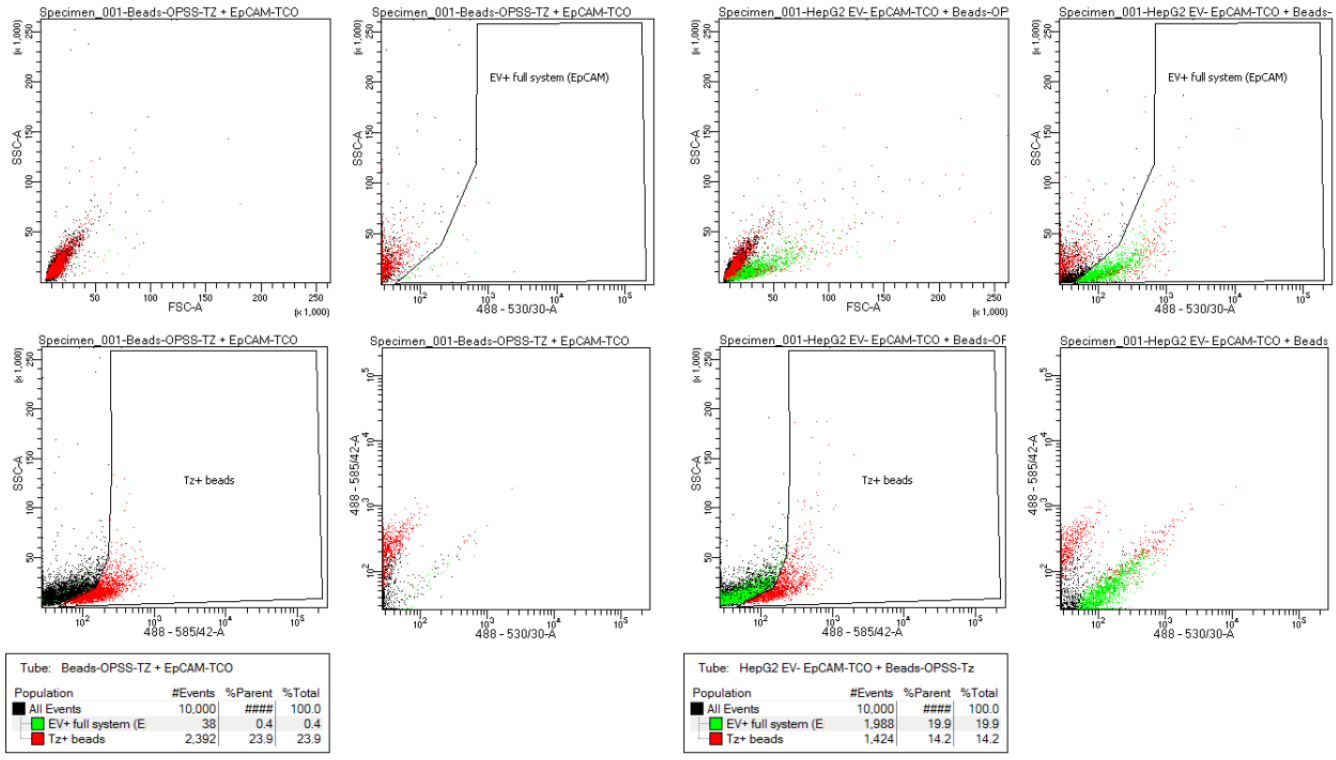

(a) *EpCAM-TCO + Beads-OPSS-Tz* **(b)** *HepG2 EV-EpCAM-TCO + beads-OPSS-Tz*

Figure 25: *EpCAM-TCO + conjugated beads and HepG2-EpCAM-TCO + conjugated beads, analysed using FACS including FITC (488-530/30 nm) and PE (488-585/42 nm) channels. In addition, forward scatter (FSC) informs about the size while side scatter (SSC) informs about the complexity.*

During this experiment, LX2 cells and activated LX2 cells were also tested using the same protocol.

Results are shown in figure 26. It is very clear how the (activated) LX2 EVs did not bind to the EpCAM and conjugated beads. This shows how the system is specific for HepG2-derived EVs among the tested EV populations.

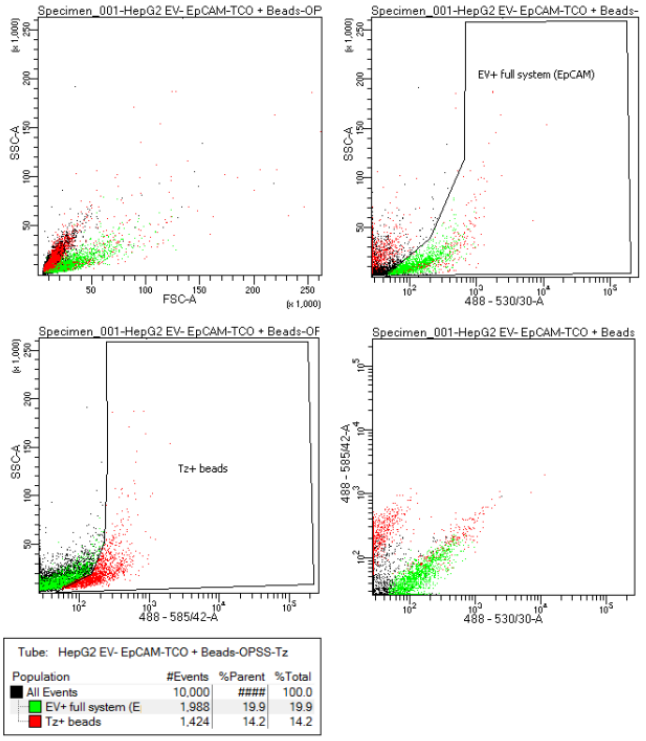

(a) *HepG2 EV + full system*

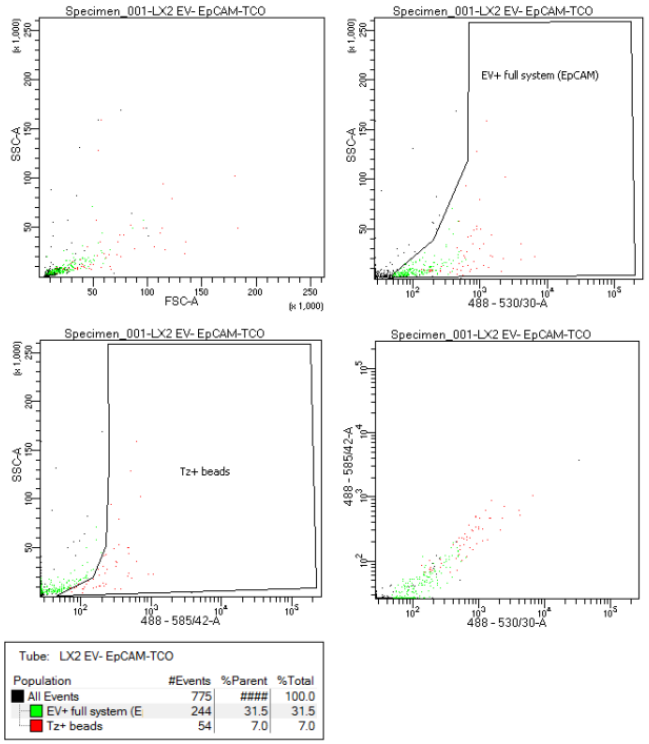

(b) *LX2 EV + full system*

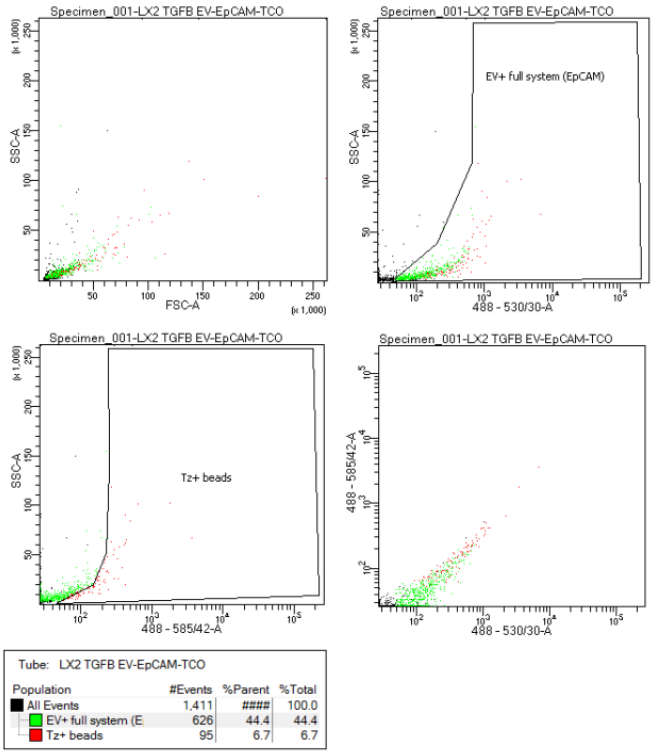

(c) *activated LX2 EV + full system*

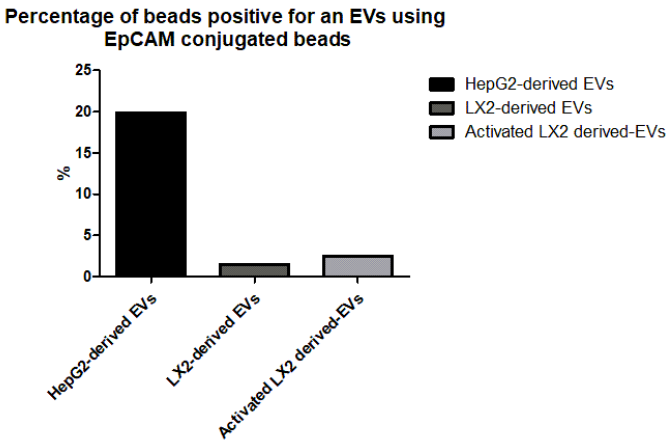

(d) *Histogram of the percentage of beads bound to an EV*

Figure 26: *HepG2, LX2 and activated LX2-derived EVs isolated using EpCAM conjugated beads. The samples were analysed using FACS, including FITC (488-530/30 nm) and PE (488-585/42 nm) channels. In addition, forward scatter (FSC) informs about the size while side scatter (SSC) informs about the complexity.*

The conjugation using the EpCAM antibody was attempted a second time at a concentration of

10μg/mL. The results were similar to the first attempt although the conjugation of EVs to beads was slightly lower, only 9%. The figures are found in Appendix 11.5.

Finally, the percentage of beads scoring positive for Tz declines when looking at the samples of the system. When the beads are bound to EpCAM and EVs, the positive population has dropped to 14.2%. figure 27 shows a comparison between the samples. The decline in Tz signal could be due to contaminants (particles other than the magnetic beads) being measured in the samples where the beads have been conjugated to the antibody and EV. Although these more complex samples have been washed, contaminants may have remained in the sample, lowering the number of measured events which is positive for Tz. Also, it is possible that the reaction between Tz and TCO changes the Tz molecule so that it becomes less fluorescent in the Pe channel.

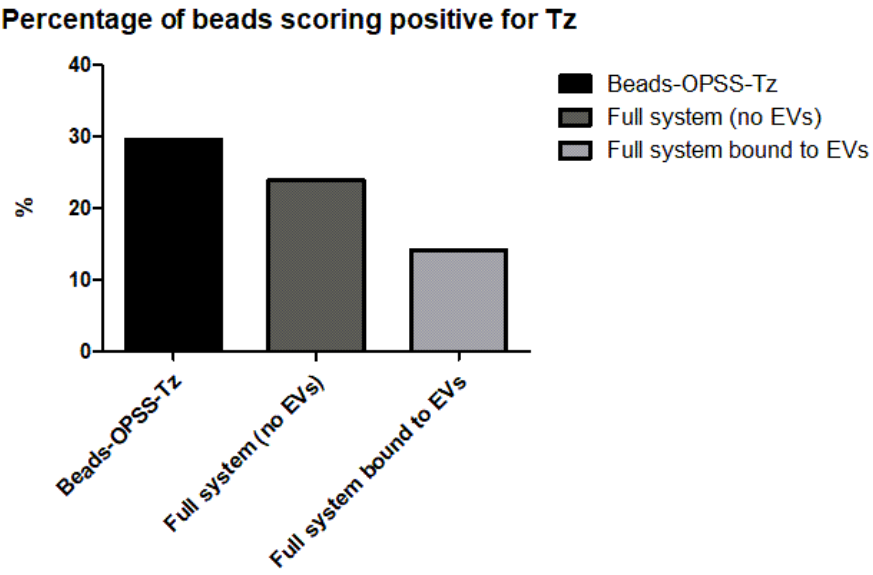

Figure 27: *Percentage of the beads scoring positive for Tz in the different samples of the conjugation of the magnetic beads to EVs. Percentages were obtained through gating of the flow cytometry results.*

8.3.1 HepG2-derived EV isolation from blood serum samples

Conjugation experiments were performed in serum samples spiked with Calcein-AM stained HepG2-derived EVs. These consisted of samples that were conjugated following different incubation protocols to determine the most efficient way to capture the EVs from the serum sample. As a control, anti-EpCAM ferrofluids were used to validate the presence of the EVs in the samples. Results of this validation are shown in figure 28.

The anti-EpCAM ferrofluid was difficult to measure using flow cytometry, only 1 227 events were measured compared to 10 000 for the conditions where supposedly the ferrofluid is bound to EVs (or other structures binding to the anti-EpCAM). It is suspected that the increasing size of the ferrofluid bound to EVs resulted in more measurable events for the flow cytometer. In addition, in the EV spiked conditions (figure 28 b, c and d), an increase in signal in the FITC channel (488-530/30) is seen, possibly due to the capture of Calcein-AM stained EVs. This FITC signal becomes less prominent in the samples with relatively more serum than PBS, possibly indicating that the capture of Calcein-AM stained EVs is less efficient in blood serum than in PBS samples and other particles were captured by the EpCAM.

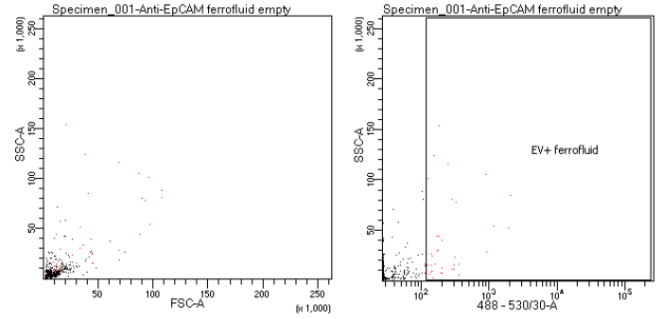

(a) *Anti-EpCAM ferrofluid, 1 227 events measured*

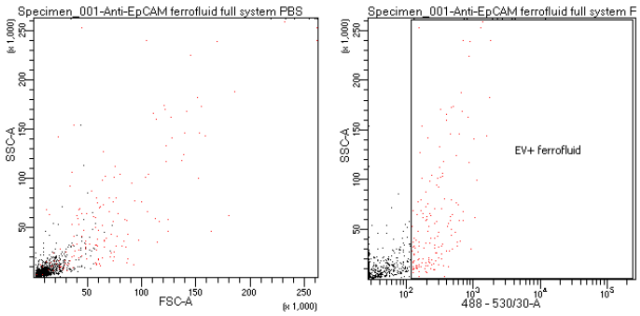

(b) *Anti-EpCAM ferrofluid in EV spiked PBS, 2 177 events measured*

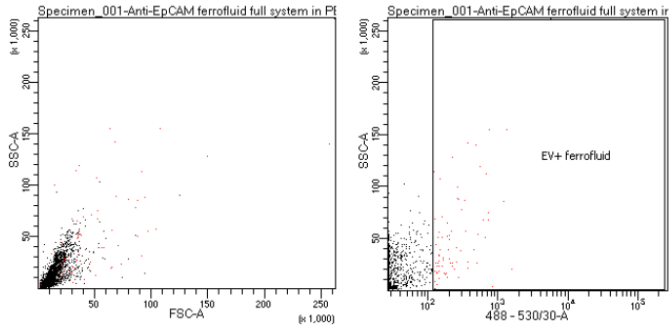

(c) *Anti-EpCAM ferrofluid in EV spiked PBS and serum (1:1), 10 000 events measured*

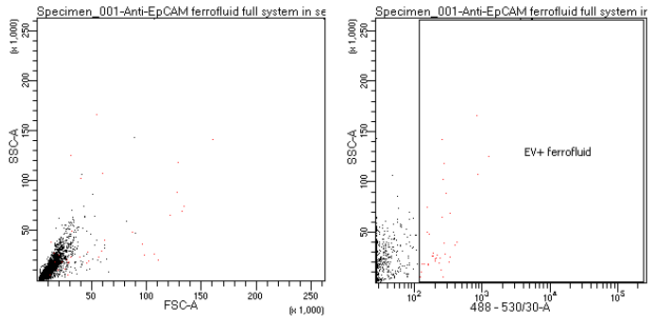

(d) *Anti-EpCAM ferrofluid in EV spiked serum, 10 000 events measured*

Figure 28: *FACS analysis of anti-EpCAM ferrofluids in PBS, EV spiked PBS, EV spiked PBS and serum (1:1) and EV spiked serum. EVs were stained with Calcein-AM resulting in a signal in the FITC (488-530/30) channel. In addition, side scatter (SSC) informs about the complexity of the particles. Gating may have been inaccurate. Empty ferrofluid already scored 2.9% positive for an EV, while ferrofluid in PBS scored 7.2%, ferrofluid in serum and PBS 0.7% and ferrofluid in serum 0.4%.*

To validate the conjugation of the magnetic beads, figure 29 shows the FACS results of the beads conjugated to Tz. A population of 35.6% was measured to be positive for the conjugation to Tz, which aligns with previous experiments.

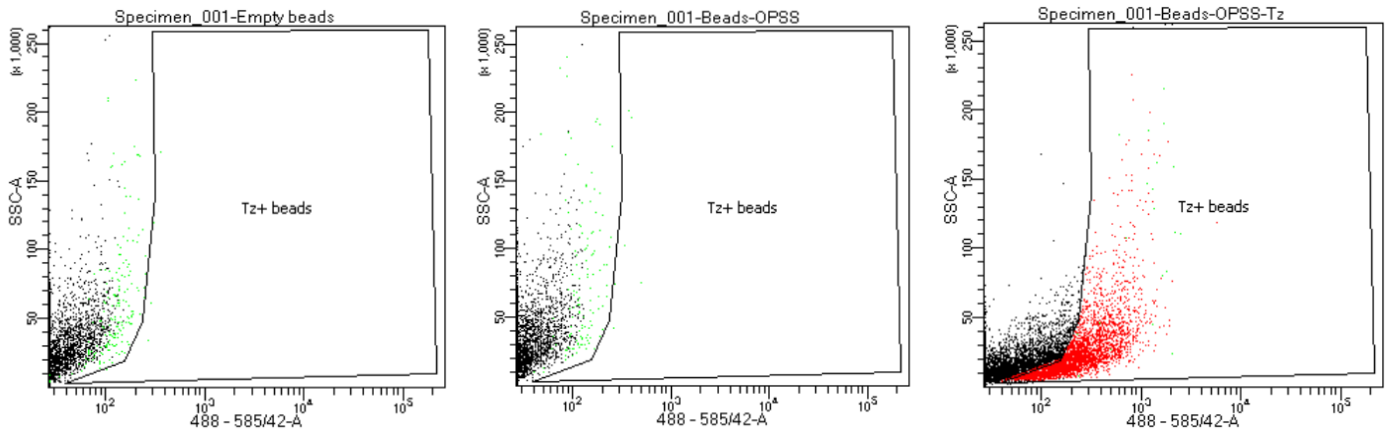

(a) *empty beads* **(b)** *beads-OPSS* **(c)** *beads-OPSS-Tz*

Figure 29: *FACS analysis of empty magnetic beads, beads bound to OPSS and beads conjugated to OPSS and Tz. The positive population (red) of fully conjugated beads is estimated to be 35.6%. The 488-585/42 channel shows the PE signal, in this case indicating the Tz binding. In addition, side scatter (SSC) informs about the complexity of the particles.*

Next, samples were compared that were prepared with different incubation steps described in table 10. Figure 30 shows FACS results of samples that contained EV spiked serum and PBS samples that were incubated overnight with the EpCAM-TCO and bead-OPSS-Tz complexes (protocol A, table 10). The FITC signal in the 488-530/30 channel, which is assumed to be the signal from the Calcein-AM stained EVs, decreases with an increasing amount of serum in the sample.

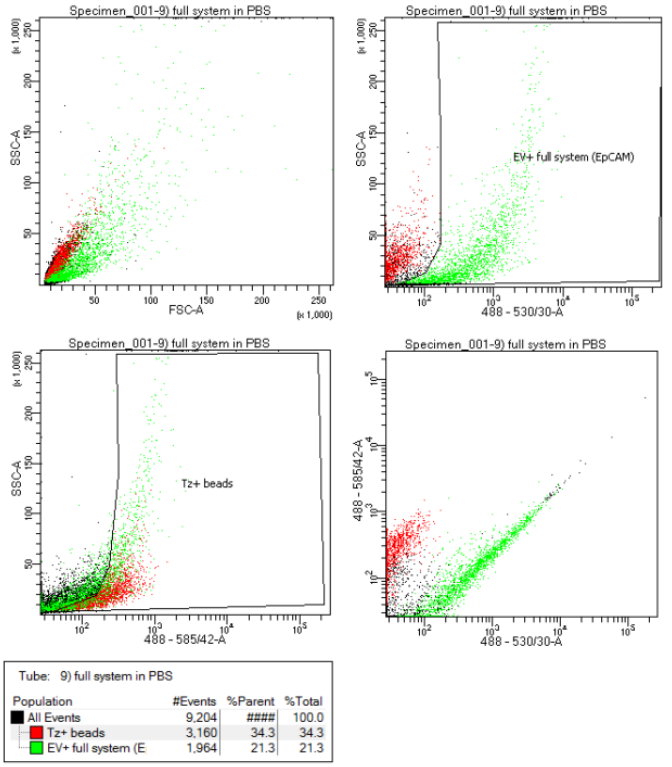

(a) *PBS spiked with EVs*

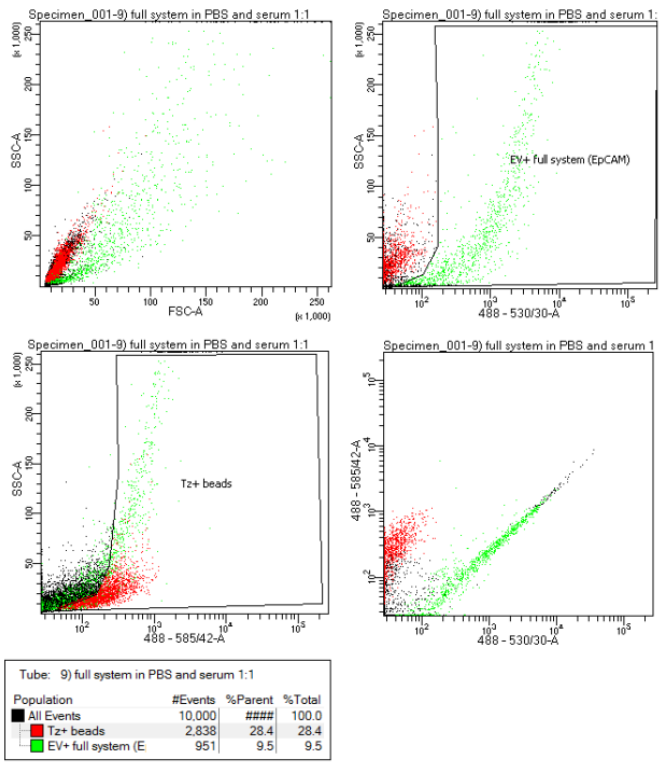

(b) *PBS and serum (1:1) spiked with EVs*

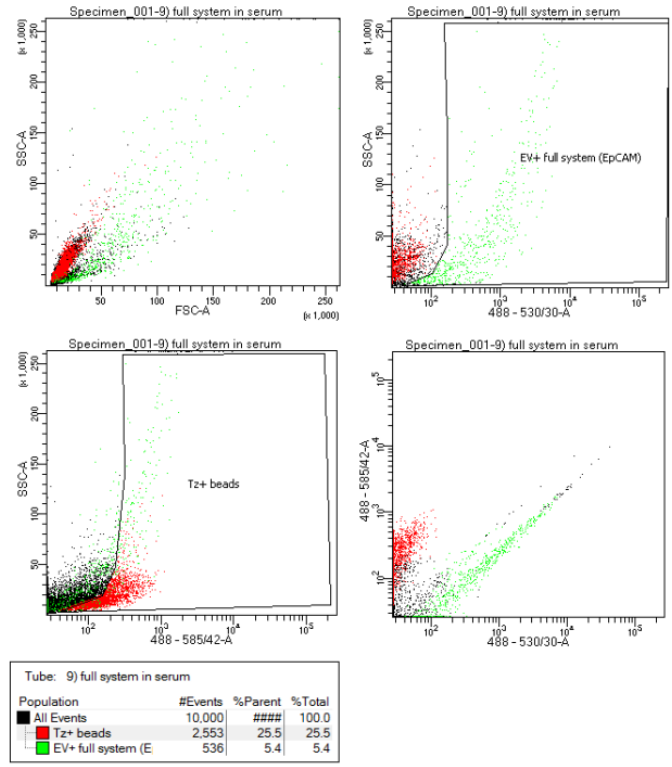

(c) *serum spiked with EVs*

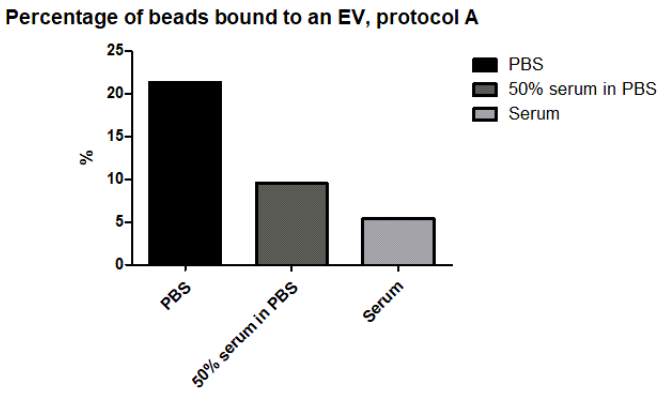

(d) *Histogram of the percentage of beads bound to an EV*

Figure 30: *Serum and PBS samples spiked with Calcein-AM EVs. Incubation was done overnight including the EpCAM-TCO and bead-OPSS-Tz complexes. The samples were analysed using FACS, including FITC (488-530/30 nm) and PE (488-585/42 nm) channels. In addition, forward scatter (FSC) informs about the size while side scatter (SSC) informs about the complexity.*

Figure 31 shows results from EV spiked serum and PBS samples that were incubated overnight con-

taining EpCAM-TCO. Afterwards, bead-OPSS-Tz was added which was followed by another incubation of 1 hour (protocol B, table 10). The figure shows that once again, the FITC signal of the Calcein-AM stained EVs decreases with the increasing amount of serum.

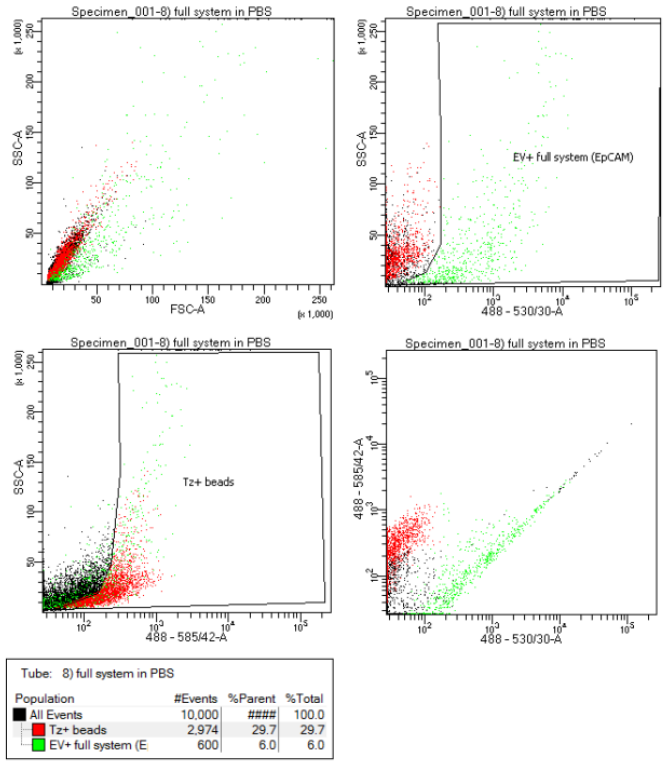

(a) *PBS spiked with EVs*

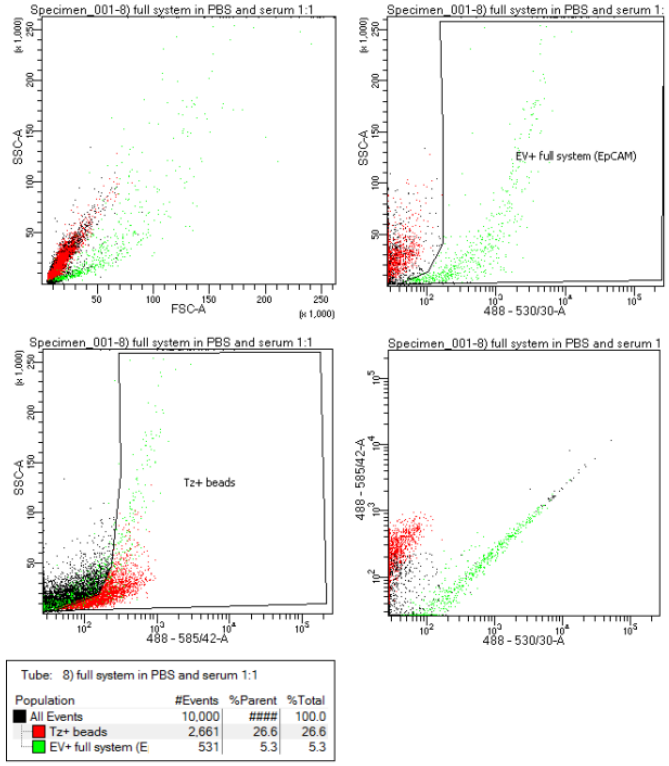

(b) *PBS and serum (1:1) spiked with EVs*

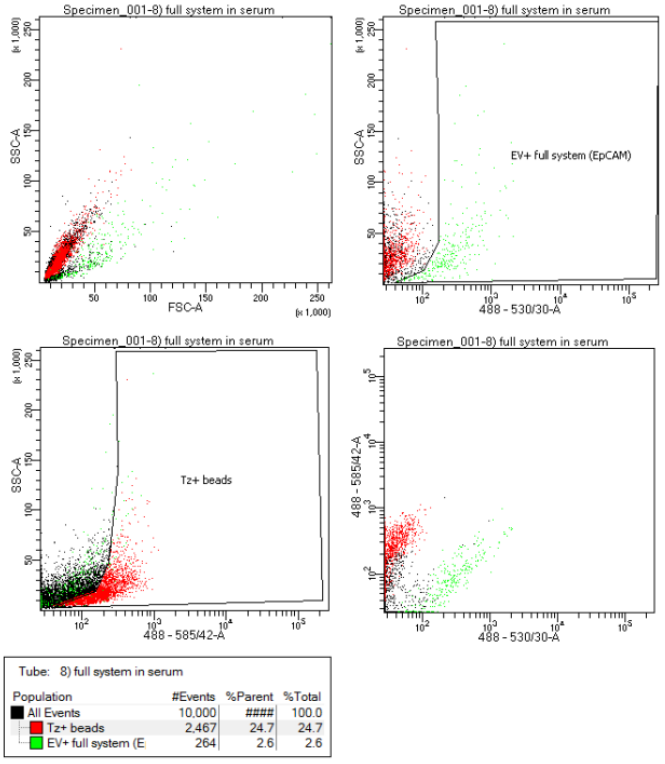

(c) *serum spiked with EVs*

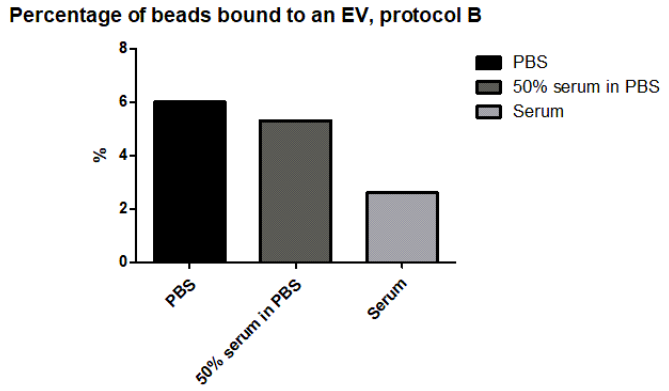

(d) *Histogram of the percentage of beads bound to an EV*

Figure 31: *Serum and PBS samples spiked with Calcein-AM EVs. Incubation was done overnight including the EpCAM-TCO complex. Afterwards, beads-OPSS-Tz was added followed by an incubation of 1 hour. The samples were analysed using FACS, including FITC (488-530/30 nm) and PE (488-585/42 nm) channels. In addition, forward scatter (FSC) informs about the size while side scatter (SSC) informs about the complexity.*

The experiment was also performed with incubation steps similar to those of earlier experiments. This included a 1 hour incubation after the addition of the EpCAM-TCO to the EV spiked serum/PBS sample, followed by another 1 hour incubation after the addition of the beads-OPSS-Tz (protocol C, table 10). Results are shown in figure 32. Again, fewer EVs seem to be captured in the serum sample.

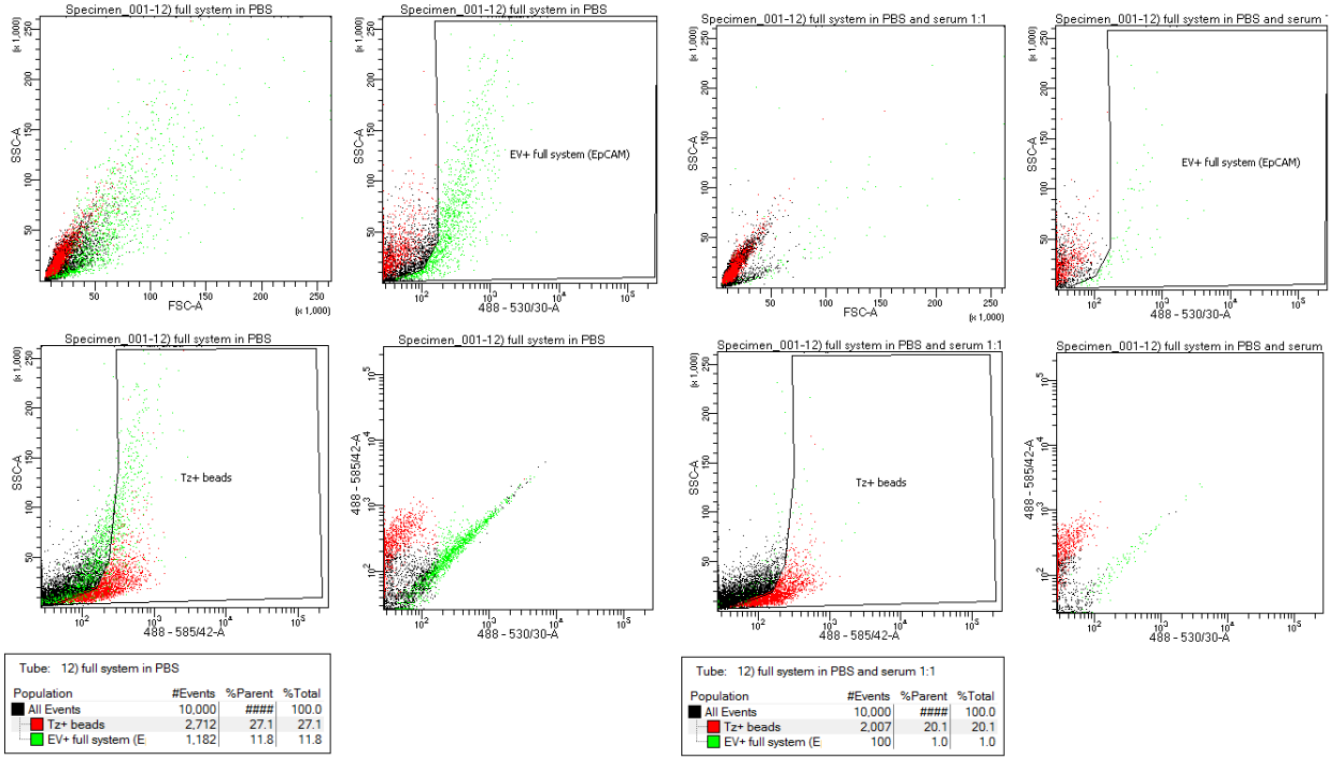

(a) *PBS spiked with EVs* **(b)** *PBS and serum (1:1) spiked with EVs*

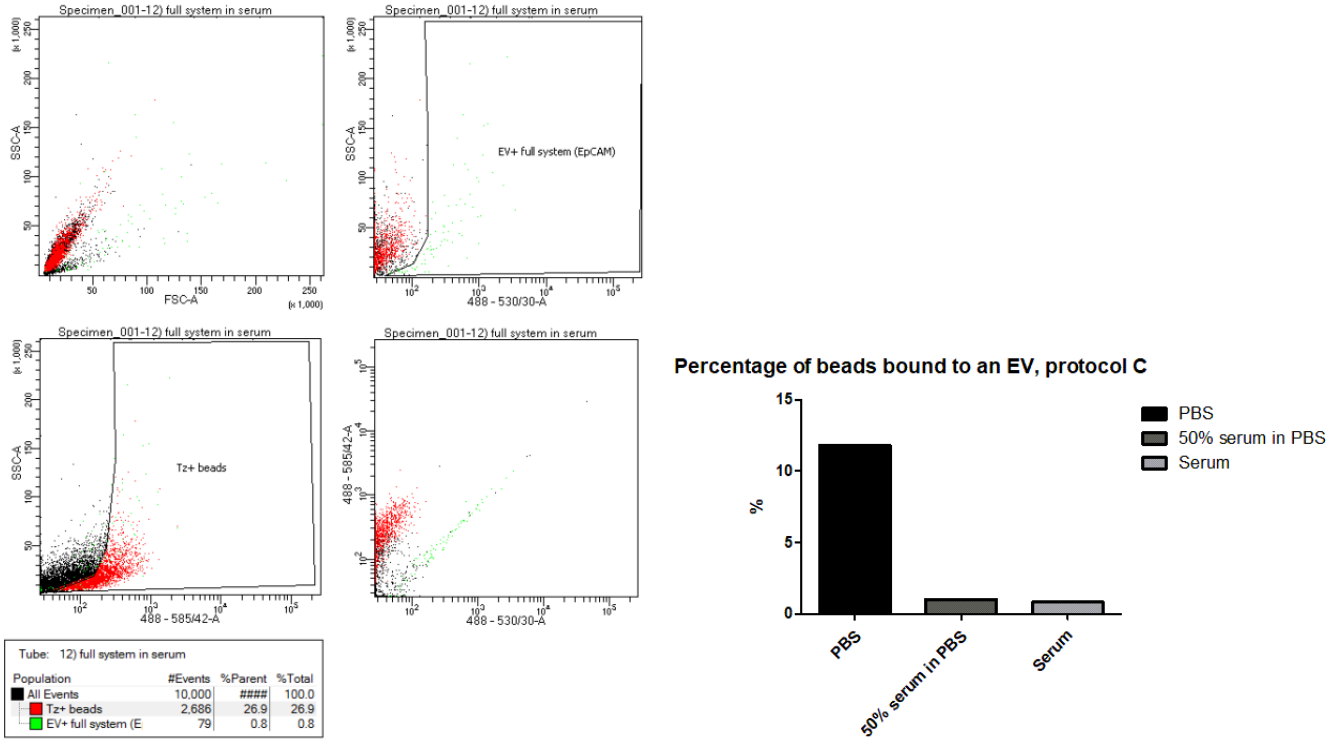

(c) *serum spiked with EVs* **(d)** *Histogram of the percentage of beads bound to an EV*

Figure 32: *Serum and PBS samples spiked with Calcein-AM EVs. Incubation consisted of 1 hour after adding the EpCAM-TCO complex, followed by 1 hour after the addition of the beads-OPSS-Tz. The samples were analysed using FACS, including FITC (488-530/30 nm) and PE (488-585/42 nm) channels. In addition, forward scatter (FSC) informs about the size while side scatter (SSC) informs about the complexity.*

Figures 30-32 are compared in figure 33. This figure showns how the incubation of the EpCAM-TCO

and the beads-OPSS-Tz overnight yields the best results in capturing the EVs. Incubation of merely 1 hour of the EpCAM-TCO in the sample and 1 hour of the beads-OPSS-Tz added to the sample does not seem sufficient enough for the binding of the EVs to the EpCAM in a sample that contains complex contaminants such as serum.

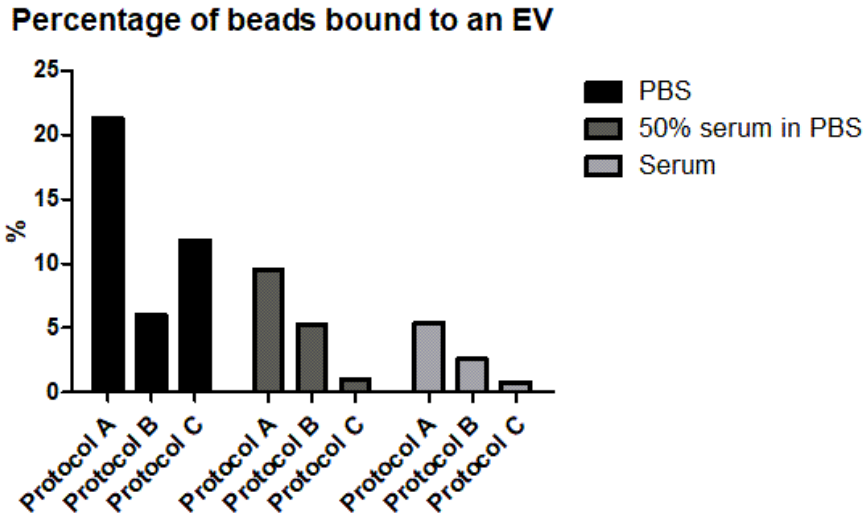

Figure 33: *Comparison of the three incubation protocols used to conjugate HepG2-derived EVs to magnetic beads in EV spiked PBS, serum and PBS (1:1) and serum. Protocol A consisted of an overnight incubation of the EpCAM-TCO and conjugated beads, protocol B of an overnight incubation of the EpCAM-TCO followed by a 1 hour incubation of the conjugated beads and lastly, protocol C consisted of a 1 hour incubation of the EpCAM-TCO and a 1 hour incubation of the conjugated beads.*

To further validate the experiment, the Calcein-AM staining of the EVs was compared, to see if the signal of the staining holds up overnight. Figure 34 shows a comparison between unstained and stained EVs. The Calcein-AM stained EVs that were over 24h old showed a better distinctive signal (41.0%) in the FITC channel compared to the newly stained EVs (18.8%). This indicates that the signal from the stained EVs is indeed sufficient for an overnight incubation of the samples. In addition, it seems it improves the signal.

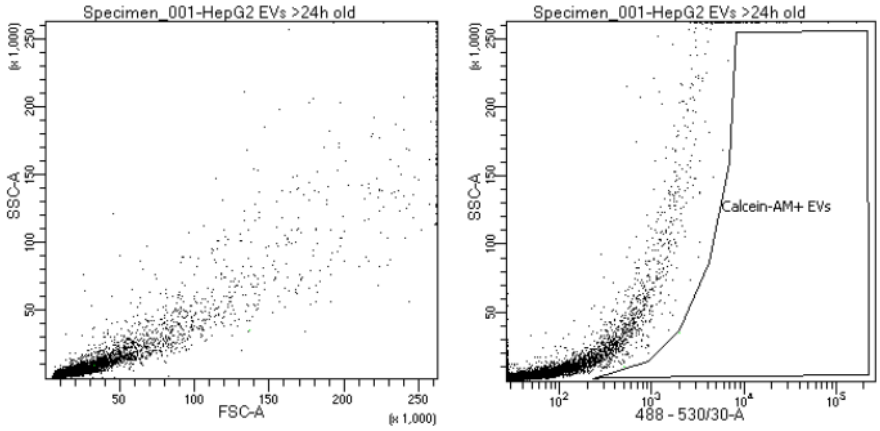

(a) *Unstained HepG2-derived EVs*

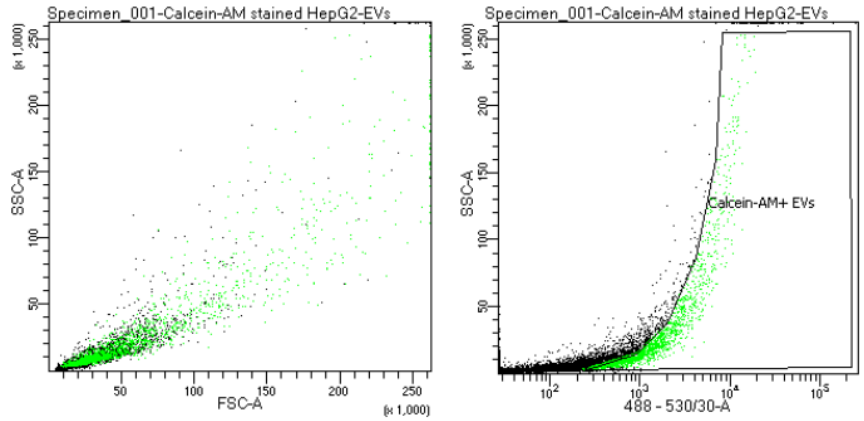

(b) *Calcein-AM stained HepG2-derived EVs*

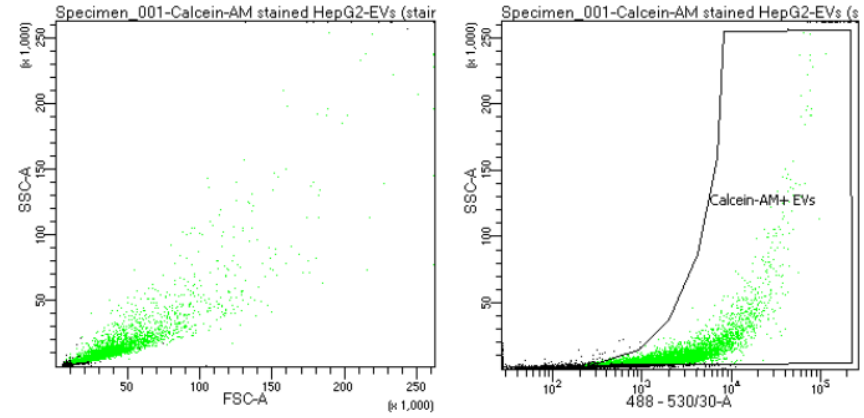

(c) *Calcein-AM stained HepG2-derived EVs, 24h old*

Figure 34: *FACS analysis of unstained and Calcein-AM stained HepG2-derived EVs. The newly stained EVs showed 18.8% positive in the FITC channel compared to the unstained EVs. Whereas the over 24h old stained EVs showed 41.0% positive. The Calcein-AM shows up in the FITC channel (488-530/30). In addition, side scatter (SSC) informs about the complexity of the particles.*

8.4 Ellman's reagent

Results of the Ellman's assay performed on the conjugated beads are shown in figure 35. It is visible how the decrease in the concentration of beads samples leads to a decrease in absorbance by the formed TNB, which suggests that the fewer beads are present in the wells, the fewer free thiol groups are detected. However, the difference between the beads, beads-OPSS and beads-OPSS-Tz is not significant in most

cases. It seems that the beads-OPSS have a slightly higher absorbance, however, this was not expected. It is suspected that the few slight differences that can be seen might be due to differences in the precise concentrations of the beads in the used samples.

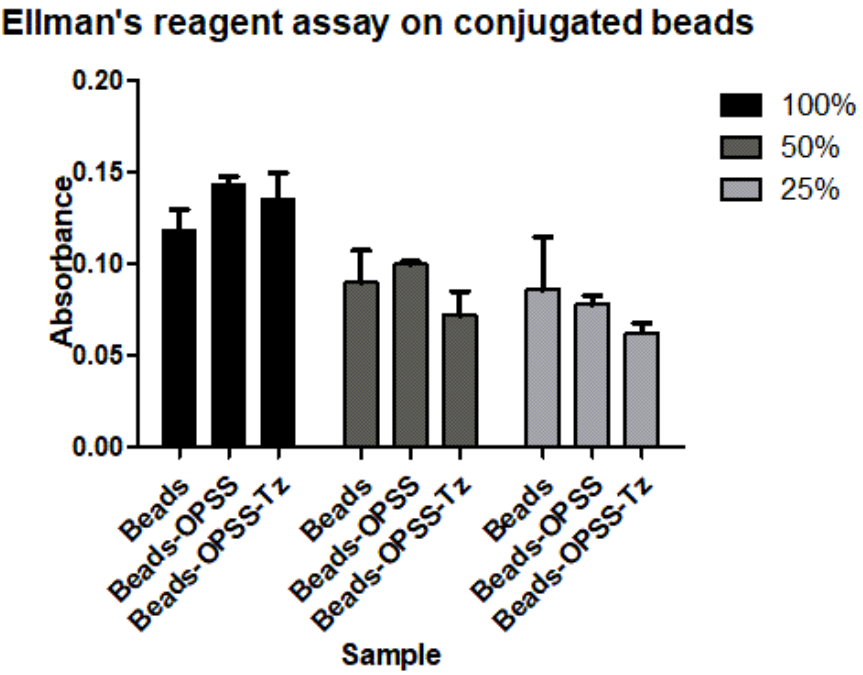

Figure 35: *Ellman's protocol performed on samples containing empty beads, beads-OPSS and beads-OPSS-Tz. Absorbance is corrected for the background signal of a Tris buffer control. All measurements were performed in duplo.*

After making changes to the protocol of the Ellman's reagent experiment, it was performed once more with samples including more beads and in comparison less DTNB. The results are shown in figure 36. It seems the differences between samples are not significant enough compared to the standard deviation of the duplo measurements. Again, the question is raised whether the concentrations of the beads are equal in the samples.

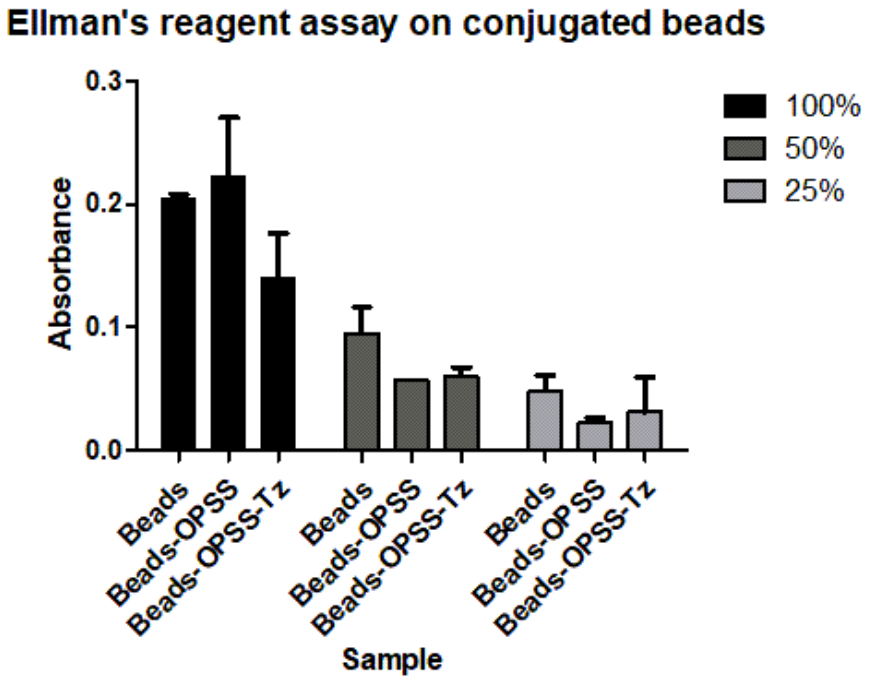

Figure 36: *Ellman's protocol performed on samples containing empty beads, beads-OPSS and beads-OPSS-Tz. Absorbance is corrected for the background signal of a Tris buffer control. All measurements were performed in duplo.*

The Ellman's assay was performed once more. This time, the empty bead sample was washed alongside the bead-OPSS sample to account for the beads that are lost while performing the washing step. The results are shown in figure 37.

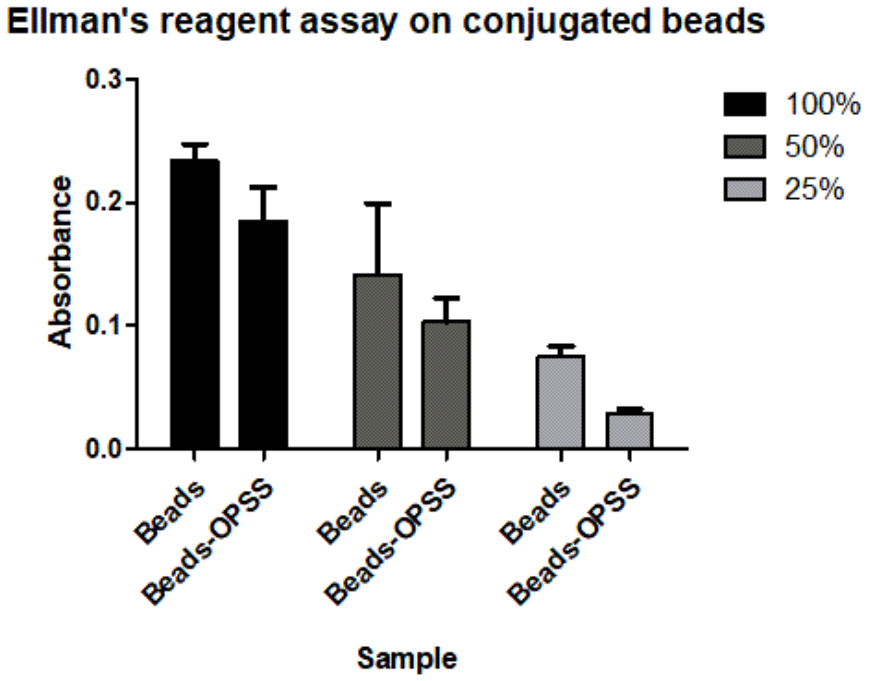

Figure 37: *Ellman's protocol performed on samples containing empty beads and beads-OPSS. Absorbance is corrected for the background signal of a Tris buffer control. All measurements were performed in duplo.*

As shown in the figure, the beads-OPSS samples caused a lower absorbance for all dilutions of the

sample. This indicates that there are fewer free thiol groups present, which have likely bound to the OPSS. The decline of absorbance of the beads-OPSS sample was expected since OPSS has bound to thiol groups, however the standard deviations are still too large to draw reliable conclusions.

In addition, a cysteine hydrochloride monohydrate calibration curve was prepared and analysed in the spectrometer. The results are shown in figure 38

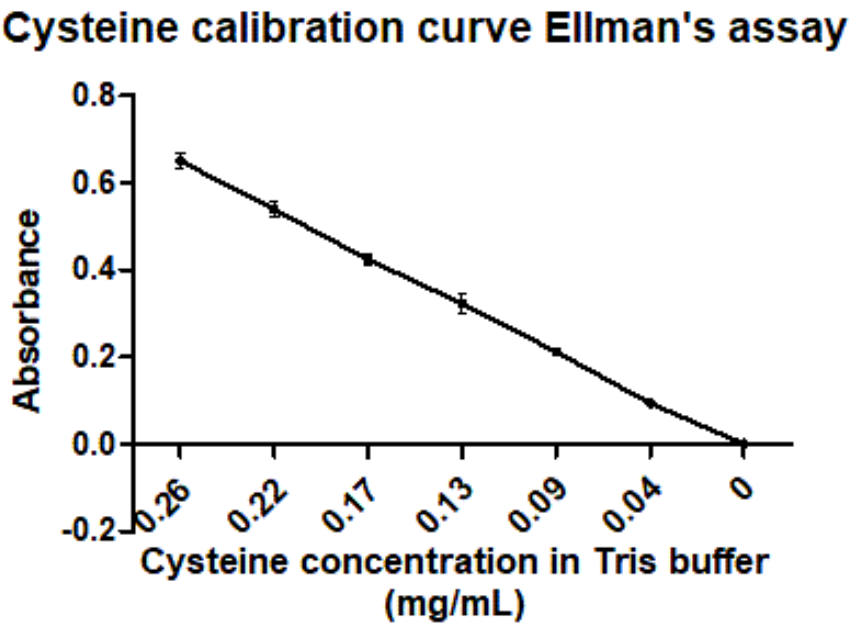

Figure 38: *Ellman's protocol performed on cysteine hydrochloride monohydrate dilutions to form a calibration curve. Absorbance is corrected for the background signal of a Tris buffer control. All measurements were performed in duplo. Samples of cysteine were diluted in Tris buffer (pH 8.0)*

The amount of cysteine present in the sample and the measured absorbance seem to be linearly connected. Using this line, the amount of free thiol groups is calculated for each sample of beads. The results are shown in table 11 and the percentage of thiol groups that have bound to OPSS are shown more clearly in figure 39.

Table 11: *Calculated amount of free thiol for each sample of beads(-OPSS)*

Sample	Dilution (in Tris buffer, pH 8.0)	Amount of free thiol groups (mmol) per 100μg beads	Percentage of thiol groups bound (presumably to OPSS)
Beads	100%	0.651	-
	50%	0.400	-
	25%	0.222	-
Beads-OPSS	100%	0.519	20.29%
	50%	0.299	25.27%
	25%	0.097	56.15%

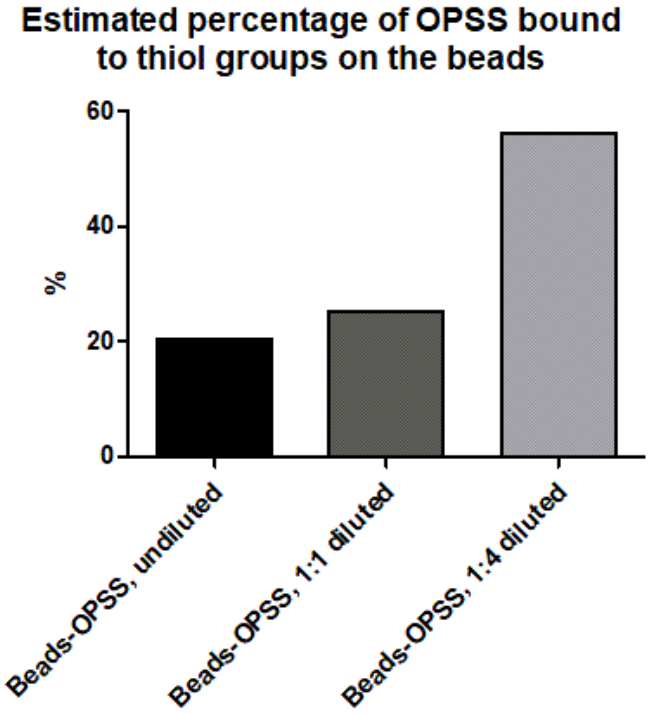

Figure 39: *Estimated percentage of thiol groups that have bound to OPSS on the magnetic beads. Calculated using the cysteine curve and the ellman's assay. Samples of different dilutions of the magnetic beads were used.*

9 Discussion and future recommendations

9.1 Fluorescence microscopy

In figures 13, 14 and 15, EpCAM and Calcein-AM stainings were evaluated using fluorescence microscopy. These figures show how both stainings were successful. EpCAM especially stained the cell membrane showing how the transmembrane glycoprotein is present on the cells.

9.2 Flow cytometry

This was confirmed by FACS results in figure 16 showing a population of 91.4% positive for EpCAM. FACS analysis in figure 18 showed a 43.3% population of live cells that express ASGR1 and 15.5% of fixed cells. In literature, the expression of ASGR1 is much higher, according to Li et al, 95.1 $\pm$ 2.6 % in the HepG2 cell line [71]. The reasons for this significant difference are not clear. It could be a difference in specific antibodies but the experiment will have to be repeated to draw more reliable conclusions. The ASGR1 expression in figure 18 of the cultured HepG2 cells not only shows how EpCAM is expressed more on the cells than ASGR1 but also that an analysis of the expression of antibodies on cells is more accurate when live cells are stained and analysed compared to fixed cells while using flow cytometry. This is in line with literature, researchers describe how the fixation of cells influences the staining results negatively. However, this does seem to depend on fixation timing, the cell line and the antibody itself [72].

9.3 Dot blot HepG2-derived extracellular vesicles

Further research was performed to collect information on the antibodies present on the EVs using a dot blot. Results in figure 19 show a significant background signal that interferes with the results' interpretation. It is clear how the signal of the stained EVs decreases with a decreasing concentration of EVs and the control of culture medium is negative. Also, this is the case for all tested antibodies: CD9, EpCAM, CD63 and ASGR1, indicating they are all present on the EV lipid bilayer. Literature supports this, other studies have also found that the isolation of HepG2-derived EVs is possible using CD9, CD63 and EpCAM antibodies [73], [74]. However, no control of the secondary and tertiary antibodies was measured, leading to the question of whether the secondary and tertiary antibodies lead to any signal without the presence of the primary antibodies. It is suspected that the tertiary antibody caused unspecific binding due to an experiment (not included in this project) using the same protocol and only unspecific binding as a result. Also remarkable, is that the EpCAM antibody showed a higher expression using flow cytometry compared to the ASGR1 antibody. However, in the dot blot, the signal of the ASGR1 seems stronger. It is assumed that the flow cytometry results are more valid, due to the potentially unreliable signal from the dot blot and literature stating that flow cytometry is more reproducible compared to immunohistochemistry [75].

9.4 Dynamic light scattering

DLS measurements were performed on human blood serum samples. The intensity peaks in figure 21 show how, presumably, the viscosity changes caused by an increasing amount of serum in the samples cause an increase in the number of peaks. The change in viscosity might also make the measurements less reliable. In addition, peaks at larger particle sizes are seen, which leads to the conclusion that serum contains larger particles than PBS samples. The addition of serum to the sample created peaks at 5.215-14.56 nm which could be exosomes or aggregated proteins. Also, peaks at 81.84-637.6 are measured, which falls within the microvesicle range. It is still unclear what particles are measured exactly because of the overlap between protein, protein aggregate and EV sizes. When comparing these values with literature, leads to the following conclusion. A study states that peaks found between approximately 3.8 and 9.6 nm were single molecules and peaks between 31 and 150 nm were molecular aggregates. During the study, a DLS measurement was performed on healthy and diseased blood serum samples [76]. The found peaks during

the addition of serum in this report match these values, however, also peaks with a much larger size were found. This is likely due to the viscosity changes. No strong conclusions can be drawn on the origin of the particles that were measured during the DLS measurement of human blood serum samples. HepG2-derived EV samples also underwent DLS measurements. Figures 22 and 23 compare EV samples from different cultured HepG2 cells and from varying times after isolation and concentration of the samples. It can be said that the HepG2-derived EVs have sizes ranging from approximately 13.60 to 343.1 nm in diameter on the day of isolation. The peaks at 13.60-27.64 nm fall within the range for exosomes while the peaks at 202.2-343.1 fall in the range for microvesicles. Whether these particles are indeed EVs, is unclear. They fall within the size ranges but it is possible they include for instance protein aggregates. Researchers have previously found a mean HepG2-derived EV diameter of 91.2 ± 1.3 nm. Most measured EVs in the articles also fell within microvesicle range [77]. When EV samples are left at $4°C$ after isolation, peaks appear at larger sizes, suggesting the EVs have aggregated. The smaller peaks that fell within the exosome range are not present anymore and a very large peak at 4 555 nm is measured. Since the measurements were performed on the exact same sample, it is likely the particles have aggregated and therefore caused the presence of larger particle sizes.

9.5 Magnetic bead conjugation

When evaluating the conjugation of the magnetic beads to the Tz, figures 24 and 29 show a population of 29.6% and 35.6% positive for Tz, making the link between the beads and Tz successful. Results in figures 24 and 27 show that the population positive for Tz seems to decrease when performing measurements on the full system (beads-OPSS-Tz + EpCAM-TCO). This could be due to the click reaction between Tz and TCO. Researchers have found that once the reaction has occurred, the fluorescence of Tz reaches its maximum after 20 minutes and only recovers its signal after several days. This could lead to less fluorescent signal while measuring the sample in the Pe (488-585/42) channel and therefore a seemingly lower Tz positive population while in reality, the bond to TCO makes the Tz lose fluorescence. The fluorescent signal of the Tz-TCO complex can be recovered through oxidation [78]. In future research, it could be useful to evaluate the Tz fluorescence over time when binding the Tz to TCO. However, when comparing the Tz percentages in figures 30, 31 and 32, this decline is less prominent and not constant across the different protocols and samples. Therefore it is difficult to draw definite conclusions on this phenomenon.

Figure 25 shows a successful conjugation of the beads to the EVs with an estimated population of beads of 19.9% positive for a Calcein-AM stained HepG2-derived EV. When testing the same system on activated LX2 and LX2-derived EVs, the isolation was unsuccessful with only 2.5% and 1.5% respectively. This shows how the EpCAM conjugated magnetic beads are specific for HepG2-derived EVs among the tested EV populations.

The conjugation experiment of the HepG2-derived EVs spiked in serum samples, has been performed according to 3 different incubation protocols. These are compared in figure 33. It can be concluded that EV isolation is more difficult in serum samples than in PBS samples, as can be seen from the decreasing amount of beads positive for Calcein-AM stained EVs. This was true for all 3 variations of the protocol and could be due to the amount of large and complex molecules that can aggregate with EVs, such as lipoproteins and plasma proteins. In addition, the 3 incubation variations can be compared. The overnight incubation of EpCAM-TCO and the Beads-OPSS-Tz complexes with the EV spiked serum/PBS samples (protocol A, table 10) led to the best capturing ability of the system, with 21.3%, 9.5% and 5.4% beads positive for a Calcein-AM stained EV for the increasing amount of serum in the respective samples. For an overnight incubation of only the EpCAM-TCO (protocol B, 10) positive populations of 6.0%, 5.3% and 2.6% for the respective serum/PBS samples were measured. Incubation of merely an hour for the EpCAM-TCO and an hour for the beads-OPSS-Tz seems too short when looking at the results in figure 32 (protocol C, table 10). The populations positive for Calcein-AM EVs were only 11.8%, 1.0% and 0.8% for the respective serum/PBS concentrations. Especially for the serum samples these percentages were very

low compared to the other two protocols, indicating once again how EV isolation in serum is more complex than for PBS samples. Therefore, it is concluded that when isolating EVs from human blood serum, an overnight incubation of the entire system is necessary for good capture efficiency. It can be assumed that due to the short incubation of the EpCAM-TCO, the samples of protocol B have not undergone the reaction between Tz (on the beads) and TCO (on the antibody) properly. Since this is a highly efficient click reaction, it can be assumed that the molecules simply have not come into contact with each other enough due to the complex contaminants in the serum samples. This is supported by the fact that the capture of EVs in the PBS samples is relatively higher compared to the serum samples for protocols A and C. For protocol C, the EVs and the EpCAM antibody also did not have enough time to properly bind, in addition to the Tz and TCO. In literature, researchers also often use an overnight incubation at $4°C$ when performing immuno-based isolation of EVs in serum using magnetic beads [79], [80]. When PBS samples of protocols B and C are compared, the result is remarkable. Although in protocol B the EVs and EpCAM-TCO have incubated overnight, in protocol C they were incubated for only 1 hour. Still, the capture of EVs was significantly higher for samples that followed protocol C. This could be due to the instability of the antibody. Earlier during this project, it was found that the production of the antibody-TCO complex cannot be done in advance, to avoid the loss of reactivity of the antibody leading to an extremely low capture efficiency. According to these results, it seems that the EpCAM-TCO stability declines while it is unbound during the overnight incubation. However, when it is bound to the EV, like in protocol A, it remains stable enough.

The experiment also contained a control of anti-EpCAM ferrofluids to confirm the capture of EVs from the PBS and serum samples. The results shown in figure 28 show differences between the samples that were spiked with EVs and the control sample with no EVs, however, since the flow cytometer did not measure enough events for the control due to the small size of the ferrofluid particles, no strong conclusions can be drawn.

Furthermore, the Calcein-AM staining was tested to see if the overnight incubation may influence the signal. Figure 34 shows how the stained EVs that were left for over 24 hours show a more distinctive signal from the unstained EVs compared to the freshly stained EVs. This shows how the Calcein-Am staining should hold up during overnight incubation of the serum/PBS samples. When comparing the signal, it is seen that the fluorescence of the Calcein-AM stained EVs is even brighter after 24 hours. This could be due to the fact that the sample of EVs and Calcein-AM was essentially left to incubate for 24 hours and therefore allowing the Calcein-AM more time to enter the vesicles and be cleaved by esterases. Once the Calcein-AM is turned into the fluorescent Calcein inside the vesicles, it is likely that the signal will be measurable for several hours to days. How long the Calcein fluorescence is measurable depends on experimental conditions and cell type. According to Miles et al, who tested several cell types, the Calcein fluorescence reaches a peak at about 30 minutes but is still present until 36 hours after labelling [81]. However, during these experiments, the samples were washed using PBS after a 30-minute incubation with Calcein-AM. During the experiments of this project, the EVs were left in the Calcein-AM dilution.

Important to keep in mind, is that while adding the stained EVs to the serum sample, Calcein-AM left in the EV sample was also added to the serum. This means that EVs already present in the serum could have been stained with Calcein-AM as well. In combination with the unspecific EpCAM antibody that was used, this could have led to misleading results. For future research, it is recommended to use a different method of distinguishing the EVs that are spiked from other EVs present in the blood serum. One way could be to use HCC-derived EVs from a male donor, containing the sex-determining region of Y gene (SRY gene), and spike these in blood serum from a female donor. An analysis of genetic material in the isolated sample can then provide information on the capture of the HCC-derived EVs [74].

As discussed, the used EpCAM antibody was not specific for the HepG2-derived EVs. EpCAM is an adhesion molecule that is expressed in many human epithelial tissues. It can only be assumed it may also be present in the EVs derived from these tissues. Expression of EpCAM is also closely related to the proliferation of the cell. Healthy adult hepatocytes are negative for EpCAM (except for bile duct epithelium cells). Regeneration in cases of cirrhosis shows an increase in EpCAM expression and while

EpCAM is often present in cancerous tissues, it is not always expressed in HCC tumours [82]. Only about 35% of HCC cases express EpCAM, even though HCC cells are epithelial in origin [83]. Research also shows that EpCAM is expressed in many different cancers, according to Went et al. in 98 out of 131 researched tumour categories [84]. Although EpCAM is not specific for HCC-derived EVs and is not expressed in all HCC tumours, it was expressed in the cultured HepG2 cells and HepG2-derived EVs in during this research. EpCAM may not form a good diagnostic marker on its own, but it can form a way of isolating EVs derived from tumours after which (PCR) analysis of the EV contents can provide more information on the origin of the isolated EVs and the possible presence of HCC tumours. During this research, EpCAM antibodies made the isolation of HepG2-derived EVs from blood serum samples possible. However, it is important to remember that other EVs that are already present in the serum before spiking may have bound to the EpCAM antibody on the beads and therefore reduce the binding ability of the HepG2-EVs to bind to the antibody. Such EVs could for instance be EpCAM-positive intestinal EVs [85]. In future research, it is important to develop an appropriate antibody cocktail to create a more specific capturing system for the HCC-derived EVs. This cocktail could consist of EpCAM, ASGR1 and Glypican 3 (GPC3) to achieve liver specificity from the ASGR1 and GPC3 antibodies[74], [86]. GPC3 in particular is said to be a highly specific marker, research shows it is expressed in 63.3% of HCC cases [87]. GPC3 is a type of heparan sulfate proteoglycan which can be present in malignant hepatic tissue but has been proven to be absent in healthy liver tissues [88]. In addition, when testing on patient samples, ASGR1 could provide good HCC specificity, researchers have found 75.2% of the researched HCC tumours stained positive for ASGR1 [89]. However, in the HepG2 cells in this study, it was expressed by only 43.3% of the cells. Therefore, during further research using the HepG2-derived EVs, other antibodies are recommended.

During this research, EVs were concentrated through TFF, however, they were never quantified. Therefore, the amount of EVs that was added to samples most likely was not constant for the different experiments. This could be improved by quantifying the number of EVs in the concentrated sample before adding them to the beads. In addition, this could enable the calculation of the capture efficiency. Currently, this report shows the phenomenon of fewer EVs captured in blood serum samples compared to PBS samples, however, this is not quantified in the form of a decreased capture efficiency. Quantification of the EVs before and after capture could be a solution. Quantification can be achieved through nanoparticle tracking analysis (NTA). This is a technique that uses the Brownian motion of individual particles in a solution that is tracked under a laser beam. Calculations using the displacement of the particles can lead to the calculation of hydrodynamic diameters using the Stokes-Einstein model. Research has shown how NTA provides not only a way to measure size distributions of particles and their quantity, but it can also provide quantitative information on the binding of nanoparticles to vesicles [90].

In addition, it is unclear whether multiple EVs bind to a single magnetic bead. Since the beads are much larger (1-5 μm) than the EVs (approximately 10-300 nm, based on DLS), it is likely multiple EVs will attach to one bead. However, the flow cytometer will count this as one event which therefore makes any future calculations of captured EVs difficult. Malys et al. have shown how multiple beads attach to one EV while using gold nanoparticles of 15 nm [91]. During their study the EVs were much larger than the nanoparticles whereas during this study, the reverse is true.

9.6 Ellman's reagent

After improving upon the Ellman's reagent protocol by analysing results in figures 35 and 36, the result in figure 37 was achieved. It is important to note that all values were already corrected for background signal using the absorbance of a Tris buffer control. Using the calibration curve in figure 38, calculations were performed leading to the values in table 11. The histogram shows the reduction of free thiol with decreasing concentrations of beads, which was expected. Also, the differences between empty magnetic beads and beads bound to OPSS (and Tz) show a reduction in free thiol groups when the beads are bound to OPSS. However, these differences do not seem significant. Further research will be necessary to increase the number of measurements to be able to draw more reliable conclusions. The calculated percentages of

OPSS bound to the beads in table 11 of 20.29%, 25.27% and 56.15% (for bead concentrations of 100%, 50% and 25% respectively) can be compared with FACS results that were measured in figures 24 and 29. The 100% and 50% bead concentrations yield comparable results to the FACS, indicating their reliability. However, the 56.15% of beads bound to OPSS for the 25% concentration of beads shows how the lowest concentration values in the histogram in figure 37 are not reliable enough. In addition, the absorbance of the samples that led to the calculation of 56.15%, was already very low which means they could be out of the quantifiable range. Currently, the magnetic beads that are used are quantified by weight. For each experiment, a set volume of beads is used at a concentration of 10mg/mL. However, it is unknown how many beads are in such a sample. This makes the quantification of the free thiol groups available per bead impossible. Therefore, in this report, the number of thiol groups is calculated per 100μg of beads.

9.7 Future recommendations

This project has shown that HepG2-EV isolation from human blood serum is possible using the magnetic bead and click chemistry system. For future research, it is important to investigate if these results are reproducible. To potentially improve the capture efficiency in blood serum samples, SEC could be used on the spiked serum sample to attempt to remove a bulk of the contaminants by using the principle of size differences in the sample. Researchers document no damage to the EVs caused by SEC and relatively little sample loss while it is successful in removing HDLs [21], [34], [38]. Furthermore, it is important to see if the magnetic beads attached to the EVs can be separated without inflicting too much damage on the EVs and their cargo. For this purpose, 1,4-dithiothreitol (DTT) can be used [74]. Furthermore, analysis of the EV cargo can result in information on the exact EV subpopulation that is isolated. It can then be determined if the system is targeting the correct EVs for it to have a diagnostic value. Once the system is optimized further and while using the appropriate antibodies, it can be useful to test it on different blood serum samples of healthy and diseased patients. By performing such an experiment, it can be determined if the system can distinguish HCC serum from healthy serum. In addition, it is also crucial that the distinction between other (liver) diseases such as NAFLD and HCC can be made. Finally, experiments should be performed to quantify either the number of isolated EVs or the genetic material found inside the isolated EVs to create guidelines or thresholds for the surveillance of patients that are at risk of developing HCC. Ultimately, the specificity and sensitivity of the system should be determined.

10 Conclusion

HepG2-derived EVs were successfully isolated using click chemistry and magnetic beads from both cell culture and blood serum samples. During these experiments, magnetic beads with free thiol groups were bound to an OPSS and Tz link. This then underwent a click reaction with a TCO-conjugated EpCAM antibody. Before isolation experiments were performed, antibodies were confirmed on the surface of the cells and EVs. EpCAM was present on the cells with a positive population of 91.4% while the ASGR1 antibody was positive for 43.3% of the HepG2 cells. EpCAM expression was also confirmed on the EV lipid bilayer through fluorescence microscopy. The free thiol groups on the beads were quantified through an Ellman's assay. Empty beads were estimated to contain 0.400-0.651 mmol free thiol groups per 100 μg of beads. In addition, it was estimated that about 20.29-25.27% of those free thiol groups have bound to OPSS after following the conjugation protocol. Results from the calculations using the lowest concentration of beads were not taken into account due to the low absorbance levels which are too close to the background signal.

Finally, the capture of the HepG2-derived EVs was estimated using flow cytometry. A value of 19.9% of beads positive for an EV was obtained for the isolation from culture medium. When spiking PBS and blood serum samples, 3 incubation protocols were tested and evaluated. The protocol with an overnight incubation of the EpCAM-TCO complex and the conjugated beads resulted in the highest capture efficiency of the Calcein-AM stained HepG2-derived EVs. A population of beads scoring positive for an EV was estimated to be 21.3% for isolation from PBS, 9.5% from 50% serum diluted in PBS and 5.4% from 100% serum.

To conclude, HepG2-derived EVs were successfully isolated from human blood serum samples. As excepted, the capture efficiency was significantly lower compared to isolating from culture medium samples, likely due to the complex contaminants found in a serum sample. Further research is needed to quantify the EVs and beads to calculate the exact capture efficiency of the system.

Overall, the click chemistry-based conjugation of magnetic beads to antibodies is a system that holds a promising future in the field of HCC diagnostics and surveillance. After optimizing the current system further, it can form a new way of isolating HCC-derived EVs from liquid biopsies such as human blood plasma. The used immuno-isolation ensures no/few contaminants will end up in the eventual sample, allowing for precise and reliable analysis of the captured EVs and their cargo. By profiling the genetic signatures found in the mRNA contents of the EVs through PCR experiments, the hope is to use genetic signatures to distinguish HCC patients from healthy or cirrhotic patients who are at risk for HCC. The developed system will allow for easy and quick analysis of the HCC development with minimal risks for the patient, making it an ideal substitute and improvement on the current surveillance techniques, consisting of AFP and ultrasound analysis. In conclusion, the system is a promising new way of improving the early diagnosis of HCC, hopefully improving the patients' survival chances.

References

[1] Rumgay H, Arnold M, Ferlay J, Lesi O, Cabasag CJ, Vignat J, et al. Global burden of primary liver cancer in 2020 and predictions to 2040. J Hepatol. 2022 Dec;77(6):1598-606.

[2] Bray F, Ferlay J, Soerjomataram I, Siegel RL, Torre LA, Jemal A. Global cancer statistics 2018: GLOBOCAN estimates of incidence and mortality worldwide for 36 cancers in 185 countries. CA Cancer J Clin. 2018 Nov;68(6):394-424.

[3] Petrick JL, Florio AA, Znaor A, Ruggieri D, Laversanne M, Alvarez CS, et al. International trends in hepatocellular carcinoma incidence, 1978-2012. Int J Cancer. 2020 Jul;147(2):317.

[4] Ko CJ, Chien SY, Chou CT, Chen LS, Chen ML, Chen YL. Factors affecting the prognosis of small hepatocellular carcinoma in Taiwanese patients following hepatic resection. Can J Gastroenterol. 2011 Sep;25(9):485.

[5] Tsuchiya N, Sawada Y, Endo I, Saito K, Uemura Y, Nakatsura T. Biomarkers for the early diagnosis of hepatocellular carcinoma. World Journal of Gastroenterology : WJG. 2015 Oct;21(37):10573.

[6] Marrero JA, Kulik LM, Sirlin CB, Zhu AX, Finn RS, Abecassis MM, et al. Diagnosis, Staging, and Management of Hepatocellular Carcinoma: 2018 Practice Guidance by the American Association for the Study of Liver Diseases. Hepatology. 2018 Aug;68(2):723-50.

[7] Reig M, Forner A, Rimola J, Ferrer-Fàbrega J, Burrel M, Garcia-Criado Á, et al. BCLC strategy for prognosis prediction and treatment recommendation: The 2022 update. J Hepatol. 2022 Mar;76(3):681-93.

[8] White DL, Kanwal F, El-Serag HB. Non-Alcoholic Fatty Liver Disease and Hepatocellular Cancer: A Systematic Review. Clinical gastroenterology and hepatology : the official clinical practice journal of the American Gastroenterological Association. 2012 Dec;10(12):1342.

[9] Refolo MG, Messa C, Guerra V, Carr BI, D'Alessandro R. Inflammatory Mechanisms of HCC Development. Cancers. 2020 Mar;12(3):641.

[10] Chidambaranathan-Reghupaty S, Fisher PB, Sarkar D. Hepatocellular carcinoma (HCC): Epidemiology, etiology and molecular classification. Adv Cancer Res. 2021;149:1.

[11] Couri T, Pillai A. Goals and targets for personalized therapy for HCC. Hepatol Int. 2019 Mar;13(2):125-37.

[12] Saito A, Toyoda H, Kobayashi M, Koiwa Y, Fujii H, Fujita K, et al. Prediction of early recurrence of hepatocellular carcinoma after resection using digital pathology images assessed by machine learning. Mod Pathol. 2021;34(2):417.

[13] Halazun KJ, Najjar M, Abdelmessih RM, Samstein B, Griesemer AD, Guarrera JV, et al. Recurrence After Liver Transplantation for Hepatocellular Carcinoma: A New MORAL to the Story. Ann Surg. 2017 Mar;265(3):557.

[14] Fitzmorris P, Singal AK. Surveillance and Diagnosis of Hepatocellular Carcinoma. Gastroenterology & Hepatology. 2015 Jan;11(1):38. Available from: `https://www.ncbi.nlm.nih.gov/pmc/articles/PMC4836577`.

[15] Sarasin FP, Giostra E, Hadengue A. Cost-effectiveness of screening for detection of small hepatocellular carcinoma in western patients with Child-Pugh class A cirrhosis. Am J Med. 1996 Oct;101(4):422-34.

[16] Esfeh JM, Hajifathalian K, Ansari-Gilani K. Sensitivity of ultrasound in detecting hepatocellular carcinoma in obese patients compared to explant pathology as the gold standard. Clinical and Molecular Hepatology. 2020 Jan;26(1):54-9.

[17] Bruix J, Sherman M. Management of Hepatocellular Carcinoma∗. Hepatology. 2005 Nov;42(5):1208.

[18] Jain D. Tissue Diagnosis of Hepatocellular Carcinoma. Journal of Clinical and Experimental Hepatology. 2014 Aug;4(Suppl 3):S67-73.

[19] Chang Y, Lee JH. Optimal Modalities for HCC Surveillance in a High-Incidence Region. Clinical Liver Disease. 2020 Dec;16(6):236.

[20] Wang J, Wang X, Zhang X, Shao T, Luo Y, Wang W, et al. Extracellular Vesicles and Hepatocellular Carcinoma: Opportunities and Challenges. Front Oncol. 2022 May;12:236-9.

[21] Abhange K, Makler A, Wen Y, Ramnauth N, Mao W, Asghar W, et al. Small extracellular vesicles in cancer. Bioact Mater. 2021 Nov;6(11):3705-43.

[22] Tan CY, Lai RC, Wong W, Dan YY, Lim SK, Ho HK. Mesenchymal stem cell-derived exosomes promote hepatic regeneration in drug-induced liver injury models. Stem Cell Res Ther. 2014 Sep;5(3):1-14.

[23] Yeung CLS, Yam JWP. Therapy-induced modulation of extracellular vesicles in hepatocellular carcinoma. Semin Cancer Biol. 2022 Nov;86:1088-101.

[24] Jiang B, Xie D, Wang S, Li X, Wu G. Advances in early detection methods for solid tumors. Front Genet. 2023 Feb;14:1091223.

[25] Schulze K, Gasch C, Staufer K, Nashan B, Lohse AW, Pantel K, et al. Presence of EpCAM-positive circulating tumor cells as biomarker for systemic disease strongly correlates to survival in patients with hepatocellular carcinoma. Int J Cancer. 2013 Nov;133(9):2165-71.

[26] Minciacchi VR, Freeman MR, Di Vizio D. Extracellular Vesicles in Cancer: Exosomes, Microvesicles and the Emerging Role of Large Oncosomes. Semin Cell Dev Biol. 2015 Apr;40:41.

[27] Ghosh S, Bhowmik S, Majumdar S, Goswami A, Chakraborty J, Gupta S, et al. The exosome encapsulated microRNAs as circulating diagnostic marker for hepatocellular carcinoma with low alpha-fetoprotein. Int J Cancer. 2020 Nov;147(10):2934-47.

[28] Kakazu E, Mauer AS, Yin M, Malhi H. Hepatocytes release ceramide-enriched pro-inflammatory extracellular vesicles in an IRE1α-dependent manner [S]. J Lipid Res. 2016 Feb;57(2):233-45.

[29] Li F, Zeng Z, Hamilton D, Zu Y, Li Z. EpCAM-Targeting Aptamer Radiotracer for Tumor-Specific PET Imaging. Bioconjugate Chem. 2021 Jun;32(6):1139-45.

[30] Johnsen KB, Gudbergsson JM, Andresen TL, Simonsen JB. What is the blood concentration of extracellular vesicles? Implications for the use of extracellular vesicles as blood-borne biomarkers of cancer. Biochimica et Biophysica Acta (BBA) - Reviews on Cancer. 2019 Jan;1871(1):109-16.

[31] Berckmans RJ, Lacroix R, Hau CM, Sturk A, Nieuwland R. Extracellular vesicles and coagulation in blood from healthy humans revisited. Journal of Extracellular Vesicles. 2019;8(1):1688936.

[32] Anderson NL, Anderson NG. The Human Plasma Proteome: History, Character, and Diagnostic Prospects∗. Mol Cell Proteomics. 2002 Nov;1(11):845-67.

[33] Buzás EI, Tóth EÁ, Sódar BW, Szabó-Taylor KÉ. Molecular interactions at the surface of extracellular vesicles. Seminars in Immunopathology. 2018;40(5):453.

[34] Holcar M, Kandušer M, Lenassi M. Blood Nanoparticles – Influence on Extracellular Vesicle Isolation and Characterization. Front Pharmacol. 2021 Nov;12.

[35] Karimi N, Cvjetkovic A, Jang SC, Crescitelli R, Feizi MAH, Nieuwland R, et al. Detailed analysis of the plasma extracellular vesicle proteome after separation from lipoproteins. Cell Mol Life Sci. 2018 Aug;75(15):2873-86.

[36] Tulkens J, De Wever O, Hendrix A. Analyzing bacterial extracellular vesicles in human body fluids by orthogonal biophysical separation and biochemical characterization. Nat Protoc. 2020 Jan;15(1):40-67.

[37] Sódar BW, Kovács Á, Visnovitz T, Pállinger É, Vékey K, Pocsfalvi G, et al. Best practice of identification and proteomic analysis of extracellular vesicles in human health and disease. Expert Rev Proteomics. 2017 Dec;14(12):1073-90.

[38] Baranyai T, Herczeg K, Onódi Z, Voszka I, Módos K, Marton N, et al. Isolation of Exosomes from Blood Plasma: Qualitative and Quantitative Comparison of Ultracentrifugation and Size Exclusion Chromatography Methods. PLoS One. 2015 Dec;10(12):e0145686.

[39] Doyle LM, Wang MZ. Overview of Extracellular Vesicles, Their Origin, Composition, Purpose, and Methods for Exosome Isolation and Analysis. Cells. 2019 Jul;8(7):727.

[40] Busatto S, Vilanilam G, Ticer T, Lin WL, Dickson DW, Shapiro S, et al. Tangential Flow Filtration for Highly Efficient Concentration of Extracellular Vesicles from Large Volumes of Fluid. Cells. 2018 Dec;7(12):237.

[41] Exosome Isolation and Detection; 2023. [Online; accessed 2. May 2023]. Available from: `https://www.novusbio.com/research-topics/cell-biology/exosome-isolation-and-detection`.

[42] Mørk M, Handberg A, Pedersen S, Jørgensen MM, Bæk R, Nielsen MK, et al. Prospects and limitations of antibody-mediated clearing of lipoproteins from blood plasma prior to nanoparticle tracking analysis of extracellular vesicles. J Extracell Vesicles. 2017 Apr;6(1):1308779.

[43] Veerman RE, Teeuwen L, Czarnewski P, Akpinar GG, Sandberg A, Cao X, et al. Molecular evaluation of five different isolation methods for extracellular vesicles reveals different clinical applicability and subcellular origin. J Extracell Vesicles. 2021 Jul;10(9):e12128.

[44] Dong L, Zieren RC, Horie K, Kim CJ, Mallick E, Jing Y, et al. Comprehensive evaluation of methods for small extracellular vesicles separation from human plasma, urine and cell culture medium. J Extracell Vesicles. 2020 Dec;10(2):e12044.

[45] Patel GK, Khan MA, Zubair H, Srivastava SK, Khushman M, Singh S, et al. Comparative analysis of exosome isolation methods using culture supernatant for optimum yield, purity and downstream applications. Sci Rep. 2019 Mar;9(5335):1-10.

[46] Böing AN, van der Pol E, Grootemaat AE, Coumans FAW, Sturk A, Nieuwland R. Single-step isolation of extracellular vesicles by size-exclusion chromatography. Journal of Extracellular Vesicles. 2014 Jan;3(1):23430.

[47] Vergauwen G, Dhondt B, Van Deun J, De Smedt E, Berx G, Timmerman E, et al. Confounding factors of ultrafiltration and protein analysis in extracellular vesicle research. Sci Rep. 2017 Jun;7(2704):1-12.

[48] Wu B, Chen X, Wang J, Qing X, Wang Z, Ding X, et al. Separation and characterization of extracellular vesicles from human plasma by asymmetrical flow field-flow fractionation. Anal Chim Acta. 2020 Aug;1127:234-45.

[49] Gandham S, Su X, Wood J, Nocera AL, Alli SC, Milane L, et al. Technologies and Standardization in Research on Extracellular Vesicles. Trends Biotechnol. 2020 Oct;38(10):1066-98.

[50] Holcar M, Ferdin J, Sitar S, Tušek-Žnidarič M, Dolžan V, Plemenitaš A, et al. Enrichment of plasma extracellular vesicles for reliable quantification of their size and concentration for biomarker discovery. Sci Rep. 2020 Dec;10(1):1-13.

[51] Tian Y, Gong M, Hu Y, Liu H, Zhang W, Zhang M, et al. Quality and efficiency assessment of six extracellular vesicle isolation methods by nano-flow cytometry. Journal of Extracellular Vesicles. 2020 Jan;9(1):1697028.

[52] Hassan PA, Rana S, Verma G. Making Sense of Brownian Motion: Colloid Characterization by Dynamic Light Scattering. Langmuir. 2015 Jan;31(1):3-12.

[53] Stott DI. Immunoblotting and dot blotting. J Immunol Methods. 1989 May;119(2):153-87.

[54] Krainer FW, Glieder A. An updated view on horseradish peroxidases: recombinant production and biotechnological applications. Appl Microbiol Biotechnol. 2015;99(4):1611.

[55] ECL western blotting substrates for horseradish peroxidase (HRP) detection. | Enhanced Luminol | Life Science Research | Bio-Rad; 2023. [Online; accessed 15. Jun. 2023]. Available from: `https://www.bio-rad.com/featured/en/ecl-western-blotting-substrates.html`.

[56] Hein CD, Liu XM, Wang D. Click chemistry, a powerful tool for pharmaceutical sciences. Pharm Res. 2008 Oct;25(10):2216-30.

[57] Kang K, Park J, Kim E. Tetrazine ligation for chemical proteomics. Proteome Sci. 2017 Jun;15:15.

[58] TCO – Tetrazine Ligation; 2019. [Online; accessed 28. Jun. 2023]. Available from: `https://clickchemistrytools.com/tco-tetrazine-ligation`.

[59] Khushman M, Bhardwaj A, Patel GK, Laurini JA, Roveda K, Tan MC, et al. Exosomal Markers (CD63 and CD9) Expression Pattern Using Immunohistochemistry in Resected Malignant and Nonmalignant Pancreatic Specimens. Pancreas. 2017 Jul;46(6):782-8.

[60] Peters DT, Henderson CA, Warren CR, Friesen M, Xia F, Becker CE, et al. Asialoglycoprotein receptor 1 is a specific cell-surface marker for isolating hepatocytes derived from human pluripotent stem cells. Development (Cambridge, England). 2016 May;143(9):1475.

[61] Jiawei S, Zhi C, Kewei T, Xiaoping L. Magnetic bead-based adsorption strategy for exosome isolation. Front Bioeng Biotechnol;10:942077.

[62] Visan KS, Lobb RJ, Ham S, Lima LG, Palma C, Edna CPZ, et al. Comparative analysis of tangential flow filtration and ultracentrifugation, both combined with subsequent size exclusion chromatography, for the isolation of small extracellular vesicles. J Extracell Vesicles. 2022 Sep;11(9):e12266.

[63] McKinnon KM. Flow Cytometry: An Overview. Current protocols in immunology. 2018 Feb;120:5.1.1.

[64] Liao X, Makris M, Luo XM. Fluorescence-activated Cell Sorting for Purification of Plasmacytoid Dendritic Cells from the Mouse Bone Marrow. Journal of Visualized Experiments : JoVE. 2016 Nov;(117).

[65] Tenopoulou M, Kurz T, Doulias PT, Galaris D, Brunk UT. Does the calcein-AM method assay the total cellular 'labile iron pool' or only a fraction of it? Biochem J. 2007 Apr;403(Pt 2):261.

[66] Calcein AAT Bioquest; 2023. [Online; accessed 28. Jun. 2023]. Available from: `https://www.aatbio.com/resources/application-notes/calcein`.

[67] Raghupathi K, Thayumanavan S. Nano-Armoring of Enzymes: Rational Design of Polymer-Wrapped Enzymes. Methods Enzymol. 2017;590:381-411.

[68] Nieri P, Carpi S, Fogli S, Polini B, Podestà A. Cholinesterase-like organocatalysis by imidazole and imidazole-bearing molecules. Sci Rep. 2017 Apr;8(1):45760.

[69] Arzumanian VA, Kiseleva OI, Poverennaya EV. The Curious Case of the HepG2 Cell Line: 40 Years of Expertise. Int J Mol Sci. 2021 Dec;22(23).

[70] Sun L, Wang Hx, Zhu Xj, Wu Ph, Chen Wq, Zou P, et al. Serum deprivation elevates the levels of microvesicles with different size distributions and selectively enriched proteins in human myeloma cells in vitro. Acta Pharmacol Sin. 2014 Mar;35(3):381.

[71] Li J, Chen L, Zhang X, Zhang Y, Liu H, Sun B, et al. Detection of Circulating Tumor Cells in Hepatocellular Carcinoma Using Antibodies against Asialoglycoprotein Receptor, Carbamoyl Phosphate Synthetase 1 and Pan-Cytokeratin. PLoS One. 2014 Apr;9(4):e96185.

[72] Yamashita-Kashima Y, Shu S, Yorozu K, Iwai T, Hashizume K, Fujimoto-Ouchi K, et al. P1-005 - Effect of Formalin Fixation on Immunohistochemical Staining for HER2. Ann Oncol. 2012 Oct;23:xi132.

[73] Breitwieser K, Koch LF, Tertel T, Proestler E, Burgers LD, Lipps C, et al. Detailed Characterization of Small Extracellular Vesicles from Different Cell Types Based on Tetraspanin Composition by ExoView R100 Platform. Int J Mol Sci. 2022 Aug;23(15):8544.

[74] Sun N, Lee YT, Zhang RY, Kao R, Teng PC, Yang Y, et al. Purification of HCC-specific extracellular vesicles on nanosubstrates for early HCC detection by digital scoring. Nat Commun. 2020 Sep;11(4489):1-12.

[75] Diederichsen AC, Hansen TP, Nielsen O, Fenger C, Jensenius JC, Christensen PB, et al. A comparison of flow cytometry and immunohistochemistry in human colorectal cancers. APMIS. 1998 May;106(5):562-70.

[76] Velichko E, Makarov S, Nepomnyashchaya E, Dong G. Molecular Aggregation in Immune System Activation Studied by Dynamic Light Scattering. Biology. 2020 Jun;9(6):123.

[77] Li X, Chen R, Kemper S, Brigstock DR. Extracellular Vesicles From Hepatocytes Are Therapeutic for Toxin-Mediated Fibrosis and Gene Expression in the Liver. Front Cell Dev Biol. 2020 Jan;7:368.

[78] Hild F, Werther P, Yserentant K, Wombacher R, Herten DP. A dark intermediate in the fluorogenic reaction between tetrazine fluorophores and trans-cyclooctene. Biophysical Reports. 2022 Dec;2(4):100084.

[79] Karimi N, Dalirfardouei R, Dias T, Lötvall J, Lässer C. Tetraspanins distinguish separate extracellular vesicle subpopulations in human serum and plasma - Contributions of platelet extracellular vesicles in plasma samples. J Extracell Vesicles. 2022 May;11(5):e12213.

[80] Inglis H, Norris P, Danesh A. Techniques for the analysis of extracellular vesicles using flow cytometry. J Vis Exp. 2015 Mar;97:52484.

[81] Miles FL, Lynch JE, Sikes RA. Cell-based assays using calcein acetoxymethyl ester show variation in fluorescence with treatment conditions. J Biol Methods. 2015;2(3):e29.

[82] de Boer CJ, van Krieken JHJM, Rhijn CMJv, Litvinov SV. Expression of Ep-CAM in normal, regenerating, metaplastic, and neoplastic liver. J Pathol. 1999 Jun;188(2):201-6.

[83] Yamashita T, Forgues M, Wang W, Kim JW, Ye Q, Jia H, et al. EpCAM and α-Fetoprotein Expression Defines Novel Prognostic Subtypes of Hepatocellular Carcinoma. Cancer Res. 2008 Mar;68(5):1451-61.

[84] Went PTH, Lugli A, Meier S, Bundi M, Mirlacher M, Sauter G, et al. Frequent EpCam protein expression in human carcinomas. Hum Pathol. 2004 Jan;35(1):122-8.

[85] Jiang L, Shen Y, Guo D, Yang D, Liu J, Fei X, et al. EpCAM-dependent extracellular vesicles from intestinal epithelial cells maintain intestinal tract immune balance. Nat Commun. 2016 Oct;7(13045):1-16.

[86] Julich-Haertel H, Urban SK, Krawczyk M, Willms A, Jankowski K, Patkowski W, et al. Cancer-associated circulating large extracellular vesicles in cholangiocarcinoma and hepatocellular carcinoma. J Hepatol. 2017 Aug;67(2):282-92.

[87] Baumhoer D, Tornillo L, Stadlmann S, Roncalli M, Diamantis EK, Terracciano LM. Glypican 3 expression in human nonneoplastic, preneoplastic, and neoplastic tissues: a tissue microarray analysis of 4,387 tissue samples. Am J Clin Pathol. 2008 Jun;129(6):899-906.

[88] Yamauchi N, Watanabe A, Hishinuma M, Ohashi Ki, Midorikawa Y, Morishita Y, et al. The glypican 3 oncofetal protein is a promising diagnostic marker for hepatocellular carcinoma. Mod Pathol. 2005 Dec;18(12):1591-8.

[89] Shi B, Abrams M, Sepp-Lorenzino L. Expression of Asialoglycoprotein Receptor 1 in Human Hepatocellular Carcinoma. J Histochem Cytochem. 2013 Aug;61(12):901-9.

[90] Foreman-Ortiz IU, Ma TF, Hoover BM, Wu M, Murphy CJ, Murphy RM, et al. Nanoparticle tracking analysis and statistical mixture distribution analysis to quantify nanoparticle-vesicle binding. J Colloid Interface Sci. 2022 Jun;615:50-8.

[91] Małys MSS, Aigner C, Schulz SMM, Schachner H, Rees AJJ, Kain R. Isolation of Small Extracellular Vesicles from Human Sera. Int J Mol Sci. 2021 Apr;22(9):4653.

11 Appendix

11.1 Appendix 1

Figure 40 shows profiles of the pixel intensities of the performed dot blot using HepG2-derived EVs. Antibodies CD9, EpCAM, CD63 and ASGR1 were tested in dilutions of only EVs, 1:1, 1:2, 1:5, 1:10 ratios of EVs : medium and only medium. This is described in section 7.2.4.

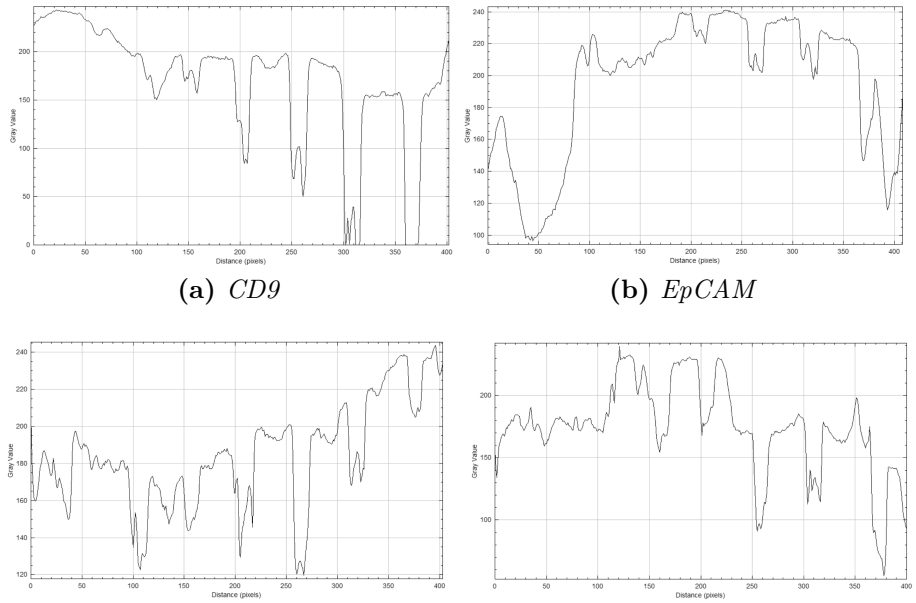

(a) *CD9* **(b)** *EpCAM*

(c) *CD63* **(d)** *ASGR1*

Figure 40: *CD9, EpCAM, CD63 and ASGR1 pixel intensity profiles of the performed HepG2-derived EV dot blot.*

11.2 Appendix 2

The conjugation of magnetic beads to EpCAM with a FITC label and to HepG2 cells is shown in figures 41 - 43. The Tz signal should be visible in the 488-585/42 (Pe) channel in figure 41 where 32.4 % of the beads are shown to be successfully conjugated to the Tz. However in figure 43 it is seen that either the Tz-TCO conjugation was unsuccessful or the binding of the HepG2 cells to the antibody. It is suspected that the fluorescent FITC label on the EpCAM antibody interfered with the binding of the cell to the EpCAM.

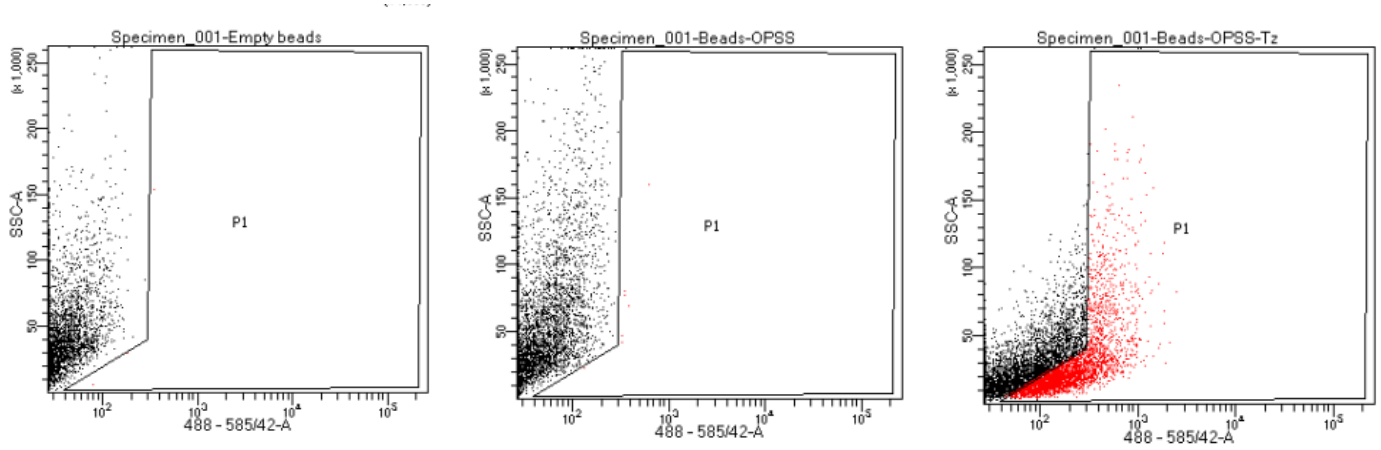

(a) *empty beads* **(b)** *beads-OPSS* **(c)** *beads-OPSS-Tz*

Figure 41: *FACS analysis of empty magnetic beads, beads bound to OPSS and beads conjugated to OPSS and Tz. The positive population (red) of fully conjugated beads is estimated to be 32.4%. The 488-585/42 channel shows the Pe signal, in this case indicating the Tz binding. In addition, side scatter (SSC) informs about the complexity of the particles.*

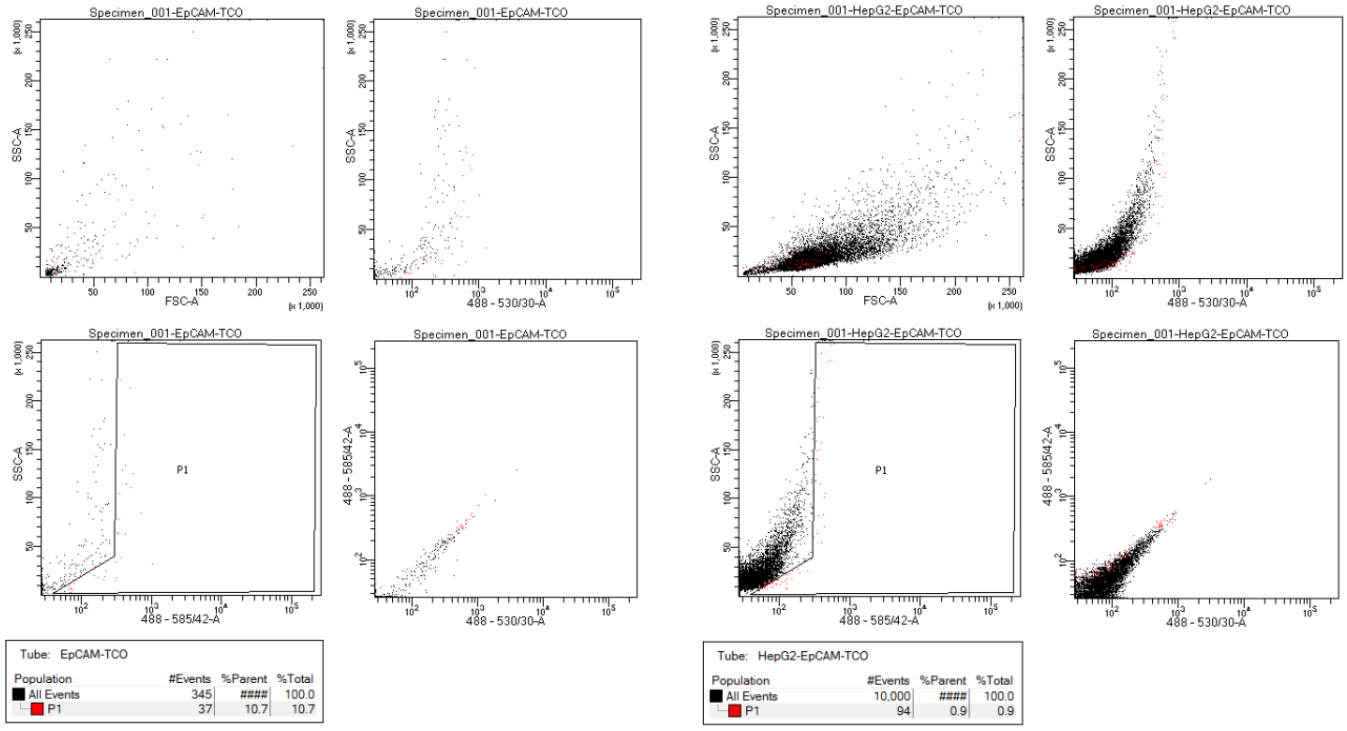

(a) *EpCAM-TCO* **(b)** *HepG2-EpCAM-TCO*

Figure 42: *EpCAM-TCO and HepG2-EpCAM-TCO analysed using FACS including FITC (488-530/30 nm) and Pe (488-585/42 nm) channels. In addition, forward scatter (FSC) informs about the size while side scatter (SSC) informs about the complexity.*

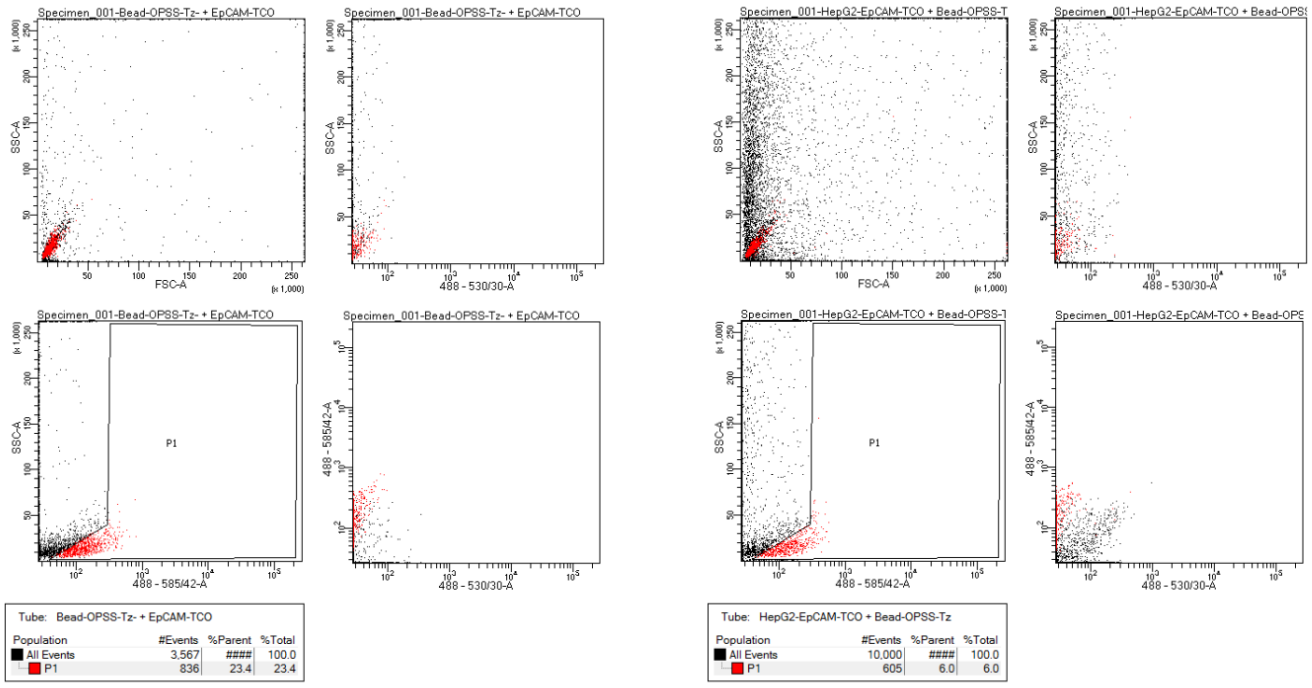

(a) *EpCAM-TCO + Beads-OPSS-Tz* **(b)** *HepG2-EpCAM-TCO + beads-OPSS-Tz*

Figure 43: *EpCAM-TCO + conjugated beads and HepG2-EpCAM-TCO + conjugated beads, analysed using FACS including FITC (488-530/30 nm) and Pe (488-585/42 nm) channels. In addition, forward scatter (FSC) informs about the size while side scatter (SSC) informs about the complexity.*

11.3 Appendix 3

Conjugation of the beads to antibodies and to EVs was attempted following a similar protocol as described in chapter 7. Non-fluorescent antibodies EpCAM, CD9 and ASGR1 were used. It was attempted to capture HepG2-derived EVs. The results of the conjugation of the beads are shown in figure 44. The percentage of successfully conjugated beads is estimated to be 23.5%.

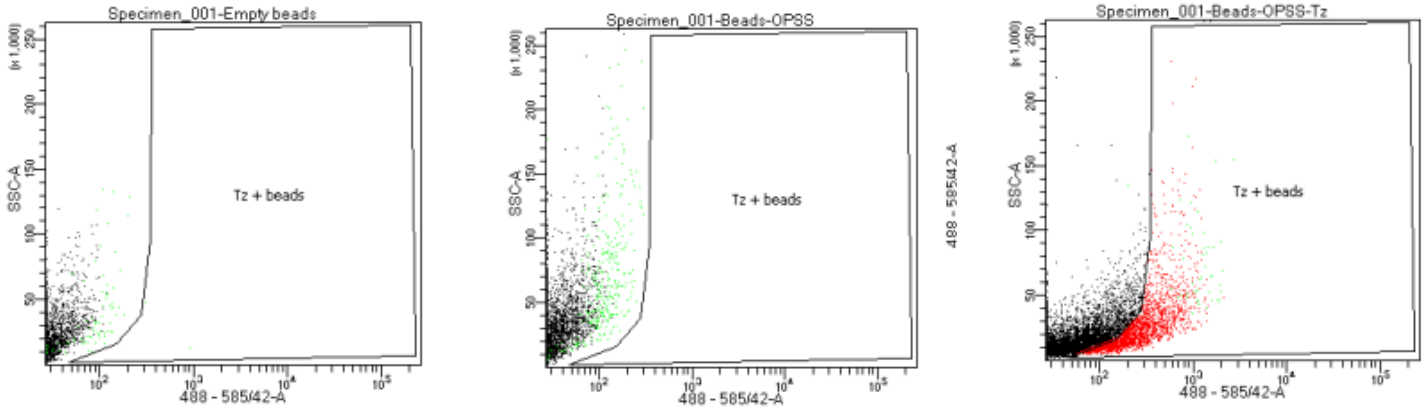

(a) *empty beads* **(b)** *beads-OPSS* **(c)** *beads-OPSS-Tz*

Figure 44: *FACS analysis of empty magnetic beads, beads bound to OPSS and beads conjugated to OPSS and Tz. The positive population (red) of fully conjugated beads is estimated to be 23.5%. The 488-585/42 channel shows the Pe signal, in this case indicating the Tz binding. In addition, side scatter (SSC) informs about the complexity of the particles.*

The comparison between the results of EpCAM-TCO + conjugated beads and the full system using EpCAM conjugated beads is shown in figure 45. It is estimated about 1.2% of the beads was positive for captured EVs. Most likely the 'positive' captured EVs are EVs that have not bound to the magnetic bead system. The conjugation has therefore most likely failed.

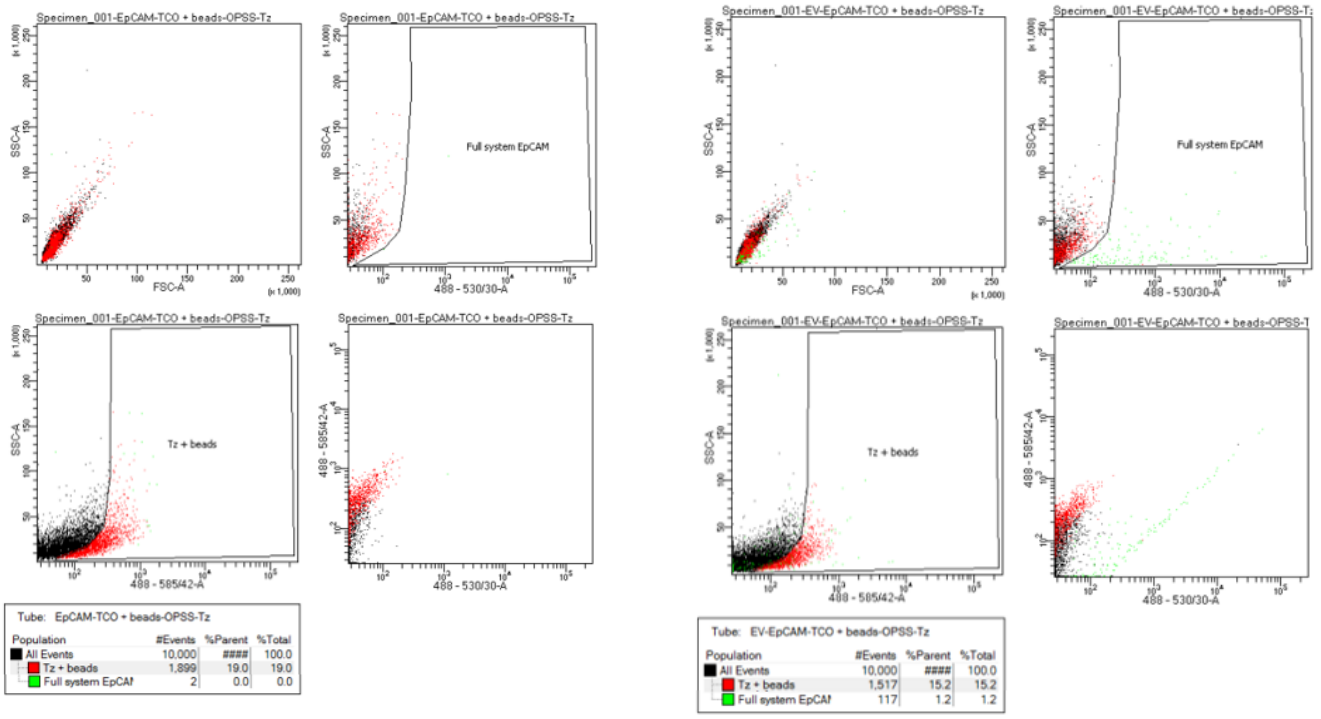

(a) *EpCAM-TCO + conjugated beads* **(b)** *EV-EpCAM-TCO + conjugated beads (full system)*

Figure 45: *FACS analysis of EpCAM conjugated magnetic beads using click chemistry and HepG2-derived EVs. The 488-585/42 channel shows the Pe signal, in this case indicating the Tz binding. The 488-530/30 channel shows the FITC signal, here the Calcein-AM-stained EVs. In addition, forward scatter (FSC) informs about the size while side scatter (SSC) informs about the complexity of the particles.*

The same was performed for CD9 conjugated magnetic beads, shown in figure 46. The population scoring positive for EVs is estimated to be 1.7%. Again, these EVs are likely to not have bound to the full system.

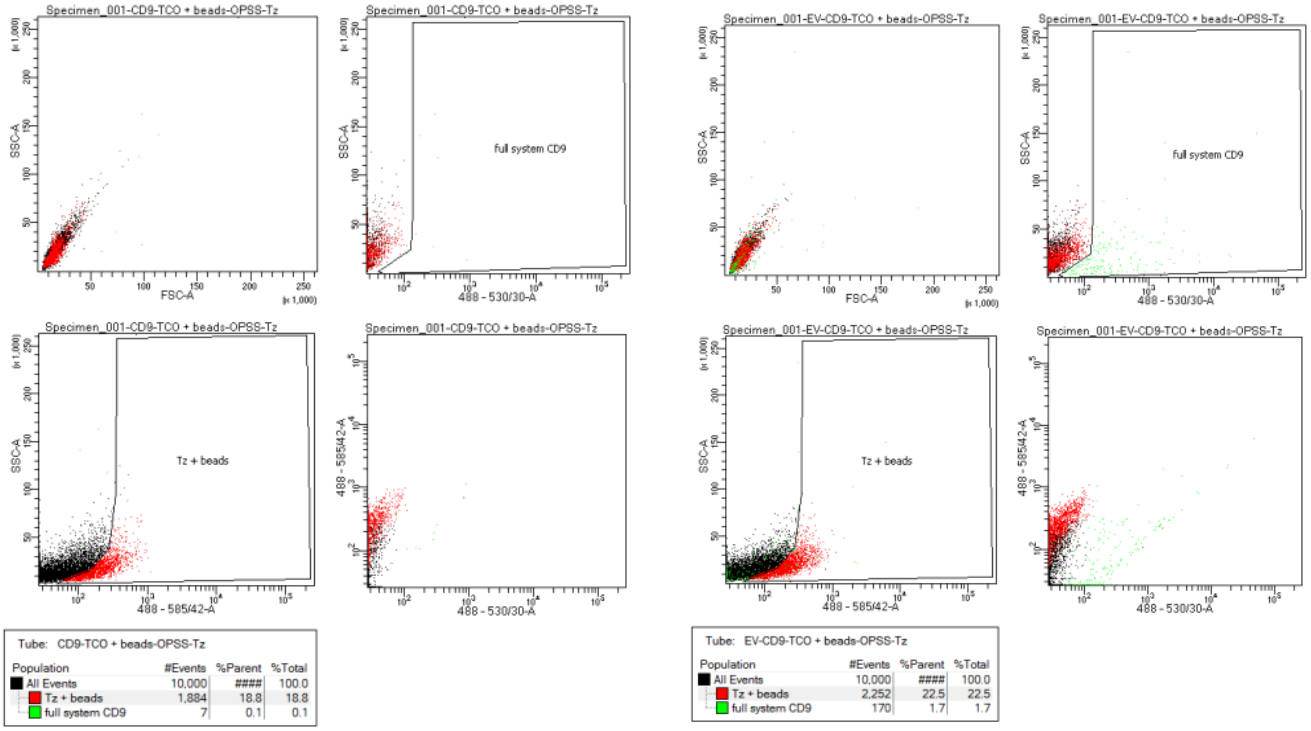

(a) *CD9-TCO + conjugated beads* **(b)** *EV-CD9-TCO + conjugated beads (full system)*

Figure 46: *FACS analysis of CD9 conjugated magnetic beads using click chemistry and HepG2-derived EVs. The 488-585/42 channel shows the Pe signal, in this case indicating the Tz binding. The 488-530/30 channel shows the FITC signal, here the Calcein-AM-stained EVs. In addition, forward scatter (FSC) informs about the size while side scatter (SSC) informs about the complexity of the particles.*

Finally, the experiment was performed with the ASGR1 antibody. As shown in figure 47, the EV-positive population is estimated to be 1%, these are assumed to be loose, unbound EVs.

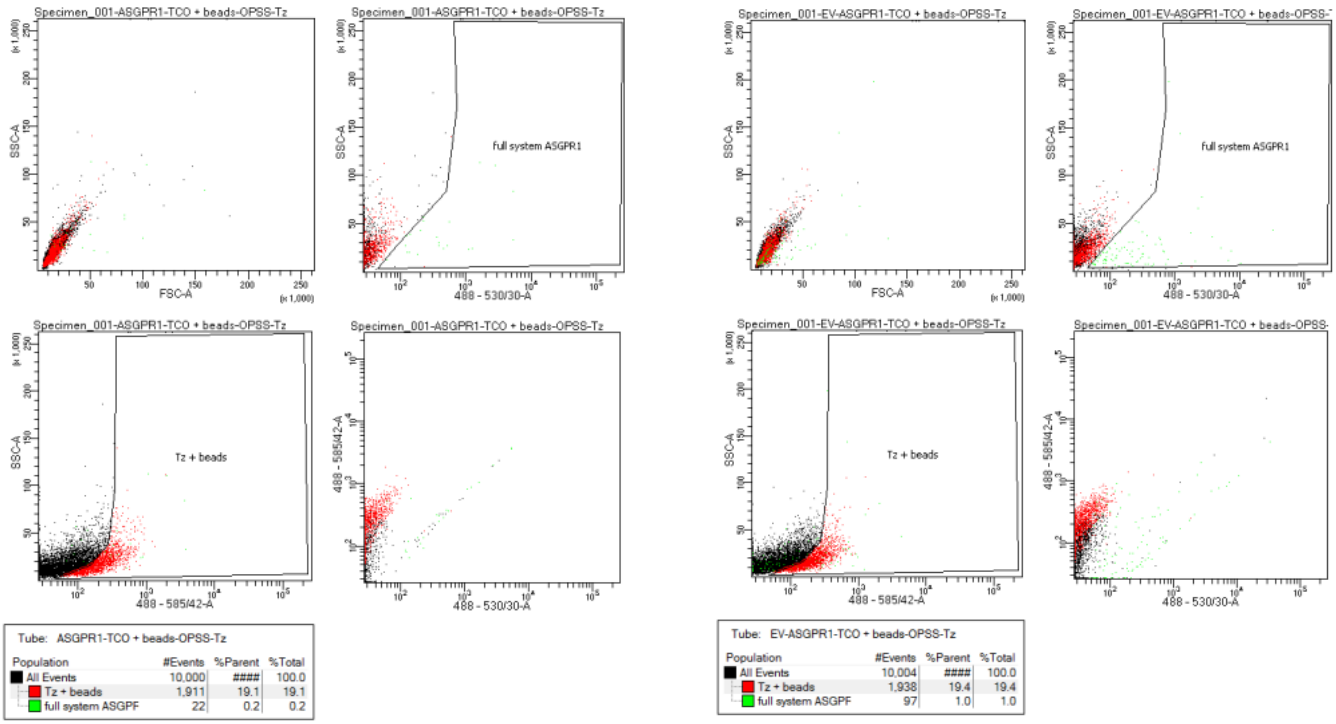

(a) *ASGR1-TCO + conjugated beads* **(b)** *EV-ASGR1-TCO + conjugated beads (full system)*

Figure 47: *FACS analysis of ASGR1 conjugated magnetic beads using click chemistry and HepG2-derived EVs. The 488-585/42 channel shows the Pe signal, in this case indicating the Tz binding. The 488-530/30 channel shows the FITC signal, here the Calcein-AM-stained EVs. In addition, forward scatter (FSC) informs about the size while side scatter (SSC) informs about the complexity of the particles.*

11.4 Appendix 4

The conjugation experiment was repeated with an increased (approximately 20 times) antibody solution. Unfortunately, due to time constraints, the antibody-TCO solutions and EV concentration were performed 2 days before the conjugation to the beads and FACS analysis. This may have influenced the results. The results that were collected are shown in figures 48 - 50.

As shown in figure 48, the conjugation of the Tz to the magnetic beads was successful, 33.8% of the beads tested positive for Tz during FACS analysis.

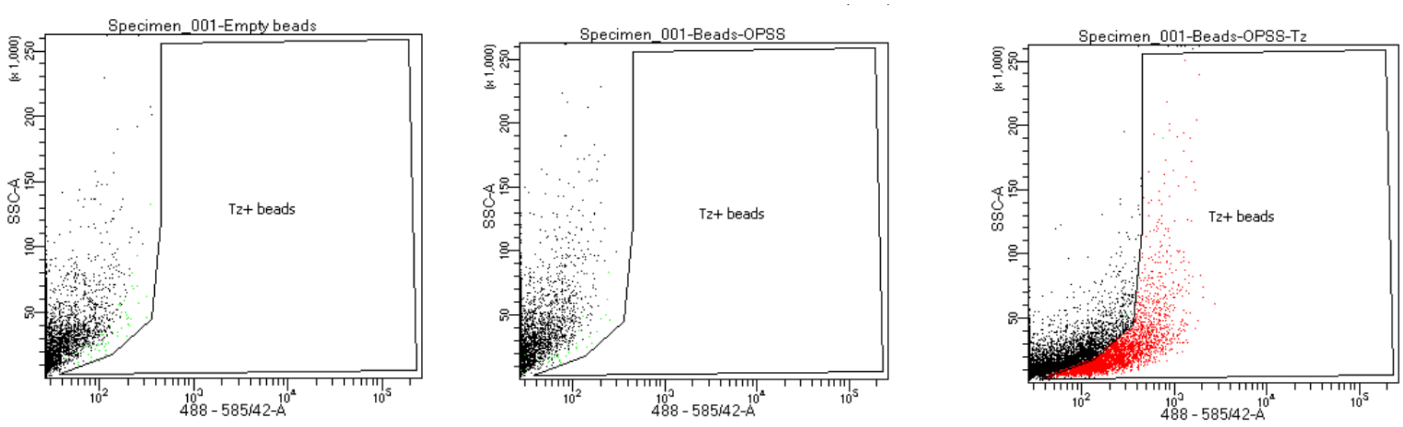

(a) *empty beads* **(b)** *beads-OPSS* **(c)** *beads-OPSS-Tz*

Figure 48: *FACS analysis of empty magnetic beads, beads bound to OPSS and beads conjugated to OPSS and Tz. The positive population (red) of fully conjugated beads is estimated to be 33.8%. The 488-585/42 channel shows the Pe signal, in this case indicating the Tz binding. In addition, side scatter (SSC) informs about the complexity of the particles.*

FACS analysis of the conjugation of EpCAM to EVs and the magnetic bead system is shown in figure 49. The conjugation of the Calcein-AM-stained EVs seems negative with only 0.2% positive in the 488-530/30 channel (FITC).

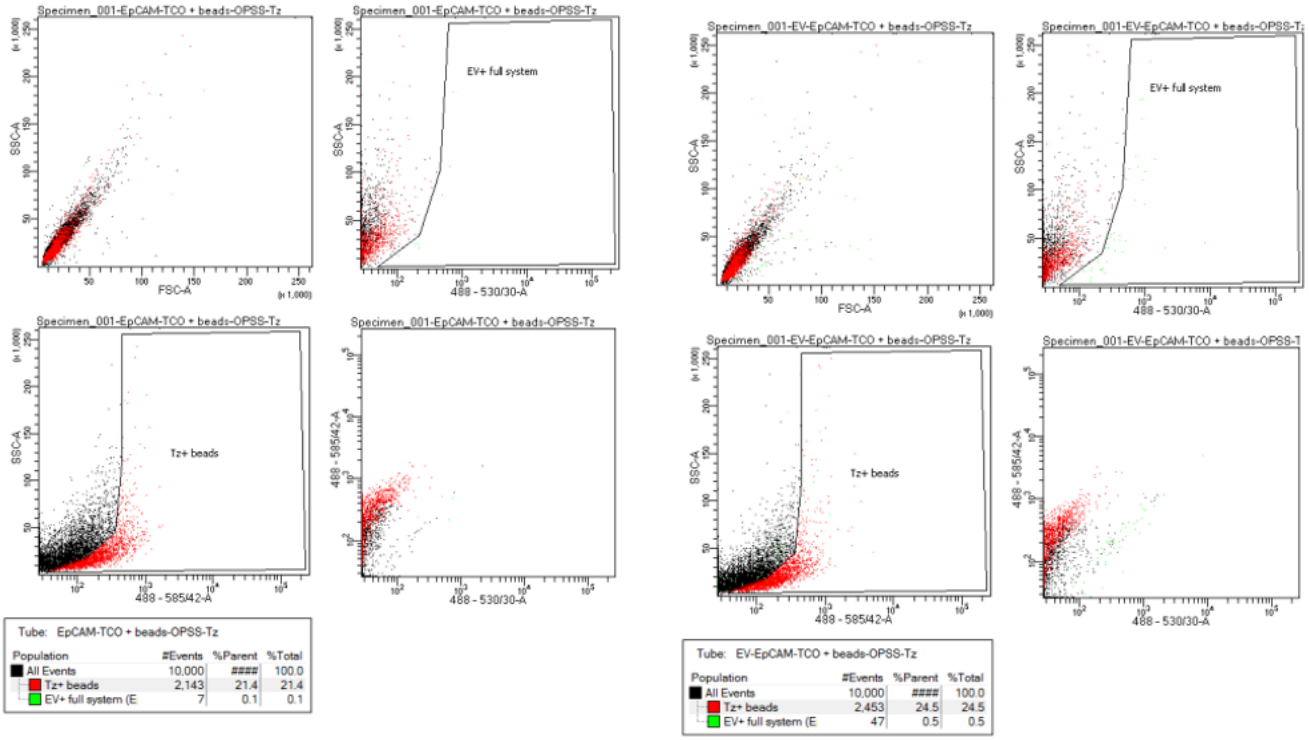

(a) *EpCAM-TCO + conjugated beads* **(b)** *EV-EpCAM-TCO + conjugated beads (full system)*

Figure 49: *FACS analysis of EpCAM conjugated magnetic beads using click chemistry and HepG2-derived EVs. The 488-585/42 channel shows the Pe signal, in this case indicating the Tz binding. The 488-530/30 channel shows the FITC signal, here the Calcein-AM-stained EVs. In addition, forward scatter (FSC) informs about the size while side scatter (SSC) informs about the complexity of the particles.*

The same was performed for the antibody ASGR1, shown in figure 50. Again, the conjugation of

Calcein-AM-stained EVs seems negative with only 1.2% scoring positive in the 488-530/30 channel (FITC).

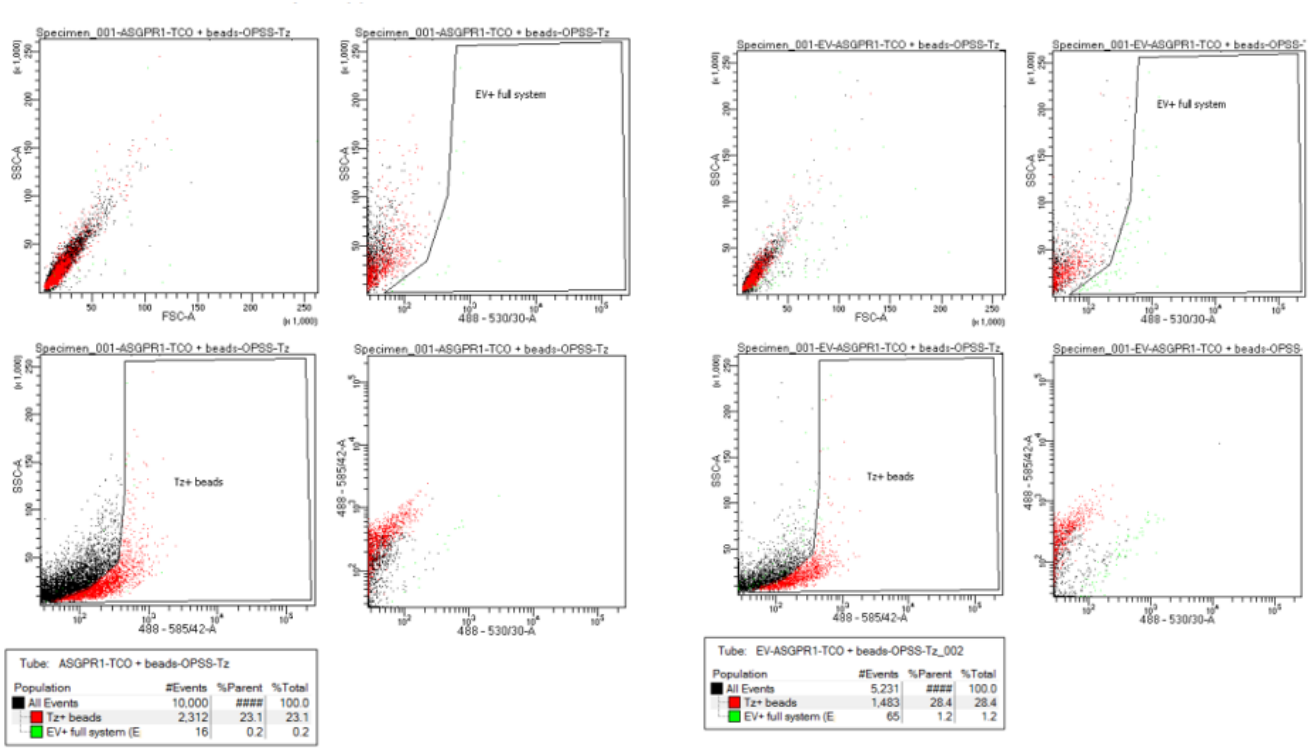

(a) *ASGR1-TCO + conjugated beads* **(b)** *EV-ASGR1-TCO + conjugated beads (full system)*

Figure 50: *FACS analysis of ASGR1 conjugated magnetic beads using click chemistry and HepG2-derived EVs. The 488-585/42 channel shows the Pe signal, in this case indicating the Tz binding. The 488-530/30 channel shows the FITC signal, here the Calcein-AM-stained EVs. In addition, forward scatter (FSC) informs about the size while side scatter (SSC) informs about the complexity of the particles.*

11.5 Appendix 5

The conjugation experiment was repeated with the EpCAM antibody. The concentration of the antibody solution which was used for the conjugation of the antibody to TCO was 10μg/mL. The results were similar to the results in the previous conjugation using the EpCAM antibody and the concentration of the antibody was increased.

The conjugation results of the beads to OPSS and Tz are shown in figure 51. The number of beads that were positive for Tz in the Pe channel was estimated to be 29.6%.

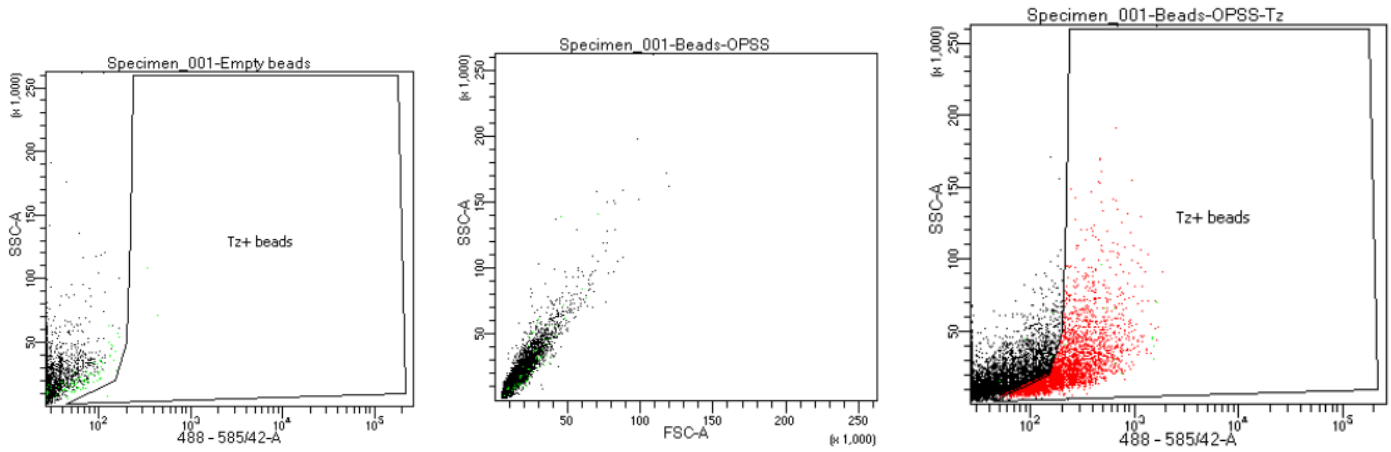

(a) *empty beads* **(b)** *beads-OPSS* **(c)** *beads-OPSS-Tz*

Figure 51: *FACS analysis of empty magnetic beads, beads bound to OPSS and beads conjugated to OPSS and Tz. The positive population (red) of fully conjugated beads is estimated to be 29.6%. The 488-585/42 channel shows the Pe signal, in this case indicating the Tz binding. In addition, side scatter (SSC) informs about the complexity of the particles.*

As shown in figure 52, the conjugation of EVs to the beads was estimated to be 9% successful. This is slightly lower than during the experiment that was performed before, in the same manner. Although this could also be due to the placement of the gates.

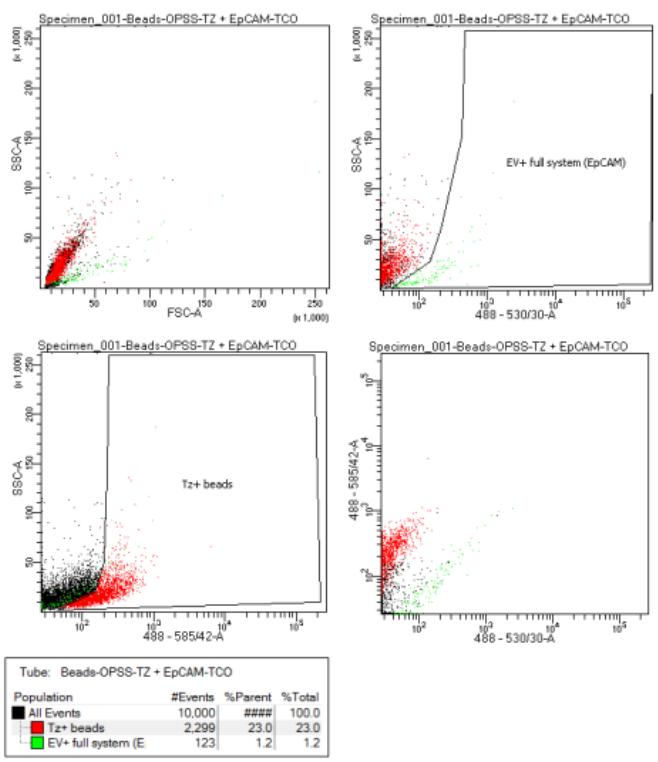

(a) *EpCAM-TCO + conjugated beads*

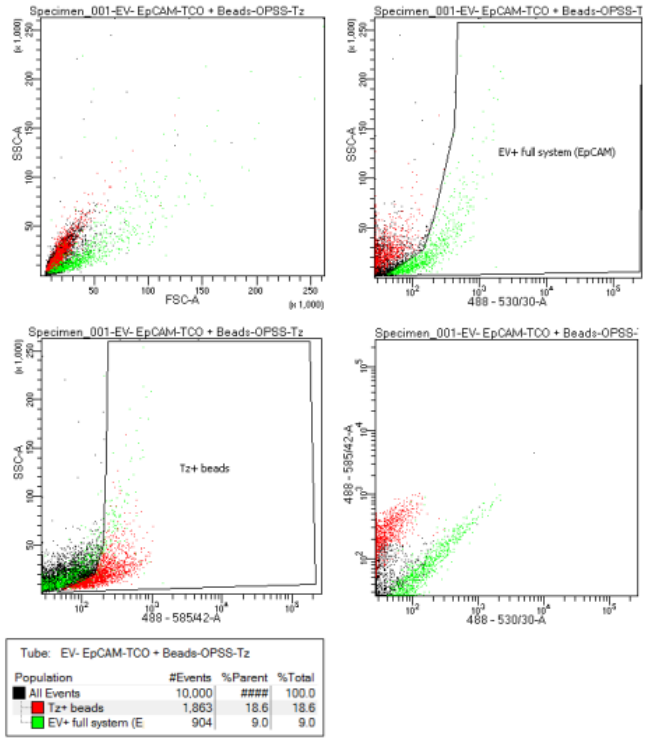

(b) *EV-EpCAM-TCO + conjugated beads (full system)*

Figure 52: *FACS analysis of EpCAM conjugated magnetic beads using click chemistry and HepG2-derived EVs. The used antibody concentration was 10µg/mL. The 488-585/42 channel shows the Pe signal, in this case indicating the Tz binding. The 488-530/30 channel shows the FITC signal, here the Calcein-AM-stained EVs. In addition, forward scatter (FSC) informs about the size while side scatter (SSC) informs about the complexity of the particles.*